The role of the monomeric GTPase RhoA

in cardiac fibroblasts

Dissertation
for the award of the degree
"Doctor rerum naturalium" (Dr.rer.nat.)
(alternatively: "Doctor of Philosophy" Ph.D. Division of Mathematics and Natural Sciences)
of the Georg-August-Universität Göttingen

within the doctoral program Chemistry
of the Georg-August University School of Science (GAUSS)

submitted by Aline Jatho

from Göttingen

Göttingen, 2014

Thesis Committee:

Prof. Claudia Steinem, Institute of Organic and Biomolecular Chemistry, Göttingen

Prof. Walter Stühmer, Max-Planck-Institute for Experimental Medicine, Göttingen

Members of the examination board:

Prof. Claudia Steinem, Institute of Organic and Biomolecular Chemistry, Göttingen

Prof. Walter Stühmer, Max-Planck-Institute for Experimental Medicine, Göttingen

Prof. Susanne Lutz, Institute of Pharmacology, Göttingen

Further members of the examination board:

Prof. Dörthe Katschinski, Department of Cardiovascular Physiology, Göttingen

PD Kaomei Guan-Schmidt, Department of Cardiology and Pneumology, Göttingen

Prof. Jörg Großhans, Institute of Biochemistry and Molecular Cell Biology, Göttingen

Date of the oral examination: 03.07.2014

Thank you!

The last four years were an exciting and educational journey for me. I learned so much about the basic science of cardiovascular diseases, myself and from others that it is not a hard job at all to fill the "Acknowledgements" paragraph.

I would like to thank my thesis committee Prof. Claudia Steinem and Prof. Walter Stühmer for participating and the interesting questions and discussions during my progress report presentations.

Many thanks go also to the other members of the examination board to agree on this position and participating in my oral examination.

Thank you, Prof. Zimmermann, for giving me the opportunity to work on my thesis in the institute of pharmacology, to be a member of the heart center and to become a young scientist of the DZHK.

But of course I am most grateful for the support and the supervision of my group leader Susanne Lutz. I moved to pharmacology from a whole different area of research and had a long way to go when I started in the institute four years ago. You helped me from the start with every small question, taught me methods, proper presentations, scientific writing, not believing everything I see and how I can still improve my performance in all these aspects. You encouraged me to present my data on congresses and supported me every day with advice, reasonable doubt and new ideas for this exciting project you assigned me to.

I would like also to thank my workgroup, the old and new members: Anita, Christina, Kerstin, Naim, Sebastian and Svenja for chat, advice and punctual lunch breaks. In particular I want to thank Beate to jump in, when I ran out of time, for strong coffee when it was needed and the constant reminder of positive thinking.

Finally, I would like to thank the whole institute of pharmacology. It was a great time and I will miss you all.

Ahmad, thank you for supporting me all this time with a helping hand, with sympathy and just for always being there for me.

I Table of Contents

II List of Abbreviations

2D	Two-dimensional
3D	Three-dimensional
A	Adenine
ADP	Adenosine triphosphate
Ang II	Angiotensin II
ANF	Atrial natriuretic factor
ANP	Atrial natriuretic protein
APS	Ammonium persulfate
AT_1R	Angiotensin II-type 1 receptor
BDM	2,3-Butanedione monoxime
β-MHC	β-Myosin heavy chain
BNP	Brain natriuretic protein
BSA	Bovine serum albumin
C	Cytosine
C3T	*Clostridium botulinum* C3 transferase
CBFHH	Calcium and bicarbonate-free Hanks' solution with HEPES
CEE	Chicken embryo extract
CO_2	Carbon dioxide
CTGF	Connective tissue growth factor
Cx	Connexin
DAPI	4′,6-Diamidino-2-phenylindole
DH	Dbl-homology
DMEM	Dulbecco´s modified eagle medium
DMSO	Dimethyl sulfoxide
DNA	Deoxyribonucleic acid
dNTP	Deoxyribonucleoside triphosphate
ECM	Extracellular matrix
EDTA	Ethylenediaminetetraacetic acid
EGF	Epidermal growth factor

EGFP	Enhanced green fluorescent protein
EHM	Engineered heart muscle
EMT	Epithelial-mesenchymal transition
ET-1	Endothelin-1
ET-R	Endothelin-1 receptor
FAK	Focal adhesion kinase
FCS	Fetal calf serum
FITC	Fluorescein isothiocyanate
G	Guanine
G1 phase	Gap 1 phase
G2 phase	Gap 2 phase
GAP	GTPase-activating protein
GDI	Guanine nucleotide dissociation inhibitor
GDP	Guanosine diphosphate
GEF	Guanine nucleotide exchange factor
GFP	Green fluorescent protein
GOI	Gene of interest
GPCR	G-protein-coupled receptors
GTP	Guanosine triphosphate
GTPγS	Guanosine 5'-O-[gamma-thio]triphosphate
H_2O	Water
HBSS	Hanks´-buffered salt solution
H1152P	(S)-(+)-2-methyl-1-[(4-methyl-5-isoquinolynyl)sulfonyl]homopiperazine dihydrochloride
HCl	Hydrogen chloride
HDAC6	Histone deacetylase 6
HEK293A	Human embryonic kidney 293A cells
HEPES	4-(2-hydroxyethyl)-1-piperazineethanesulfonic acid
HIV-1	Human immunodeficiency virus type 1
HUVEC	Human umbilical vein endothelial cells

IL	Interleukin
KO	Knockout
LARG	Leukemia-associated RhoGEF
LatA	Latrunculin A
LB	Lysogeny broth
M_1R	Muscarinic M_1 acetylcholine receptor
MAL	Megakaryocytic acute leukemia
MEF	Mouse embryonic fibroblast
MI	Myocardial infarction
MMP	Matrix metalloproteinases
NADP(H)	Nicotinamide adenine dinucleotide phosphate
NaOH	Sodium hydroxide
NEAA	Non-essential amino acids
NHCF	Normal human cardiac fibroblast
NKM	Non-cardiomyocyte medium
NRCF	Neonatal rat cardiac fibroblast
NRCM	Neonatal rat cardiomyocyte
PBGD	Porphobilinogen deaminase
PBS	Phosphate-buffered saline
PCR	Polymerase chain reaction
PE	Phenylephrine
PenStrep	Penicillin/streptomycin
qRT-PCR	Quantitative real time polymerase chain reaction
RBD	Rho binding domain of rhotekin
RhoA	Ras homolog (gene) family member A
RNA	Ribonucleic acid
ROCK	Rho-associated kinase
S phase	Synthesis phase
S1PR	Sphingosine-1-phosphate receptor
SAM	S-adenosyl methionine

SDS	Sodium dodecyl sulfate
SEM	Standard error of the mean
SRF	Serum response factor
T	Thymine
TBS	Tris-buffered saline
TBST	Tris-buffered saline with Tween 20
TEMED	Tetramethylethylendiamine
TGF-β	Transforming growth factor-β
TNF-α	Tumor necrosis factor-α
TPPP1	Tubulin polymerization promoting protein 1
Tris	Tris(hydroxymethyl)aminomethane
TRITC	Tetramethylrhodamine
TubA	Tubastatin A

Symbols and units

α	Alpha
β	Beta
γ	Gamma
°C	Degree Celsius
Da	Dalton
g	Gram
h	Hour
Hz	Hertz
k	Kilo (10^3)
kb	Kilo basepairs
L	Liter
μ	Micro (10^{-6})
m	Milli (10^{-3})
min	Minute
M	Molar concentration

II List of Abbreviations

n	Nano (10^{-9})
%	Percent
V	Volt

III List of Figures

IV List of Tables

1   Summary

The specific knockdown of RhoA in neonatal cardiac fibroblasts led on a molecular level to a decreased expression of the myofibroblast marker α-smooth muscle actin and an increase in the modified acetylated tubulin. On the subcellular level a loss of stress fibers and actin structures of higher order as well as a more compact Golgi apparatus were found. In addition, focal adhesion sites were smaller and randomly distributed implicating a loss in cell polarity. On a cellular level, the knockdown of RhoA led to an increase in cell area but not in cell volume. The functional outcomes of these changes were a faster adhesion independent of the substrate, a reduction in the migration capacity on a focal plane and, in contrast, an increase in the invasive migration through pores. Moreover, the mitogenic response to serum was strongly reduced without a change in cell viability. The expression and secretion of the fibrosis-associated CTGF in starved cells was significantly reduced by a lower expression of RhoA, which was however circumvented in the presence of serum. On a heterogeneous multicellular level, the knockdown of RhoA in NRCF impaired the contractile function of engineered cardiac tissue under calcium stimulation which was accompanied by a decreased expression of α-smooth muscle actin and calsequestrin. By using specific inhibitors for the RhoA-dependent kinases (ROCK) and HDAC6 several of these changes could be imitated and thus these downstream effectors assigned to certain functions. By using the ROCK inhibitor fasudil the morphological changes and the impaired migration capacity could be mimicked in wild type fibroblasts whereas the decrease in cell proliferation was detected after treatment with the HDAC6 inhibitor tubastatin A.

1.1. Zusammenfassung

Der spezifische Knockdown von RhoA in neonatalen kardialen Rattenfibroblasten führte auf molekularem Level zu einer Reduktion des Myofibroblastenmarkers α-Glattmuskelaktin und zu einem Anstieg im modifizierten acetylierten Tubulin. Auf subzellulärer Ebene konnte ein Verlust von Stressfasern, Aktinstrukturen höherer Ordnung und eine erhöhte Dichte des Golgi-Apparats beobachtet werden. Außerdem waren die Fokaladhäsionen kürzer und zufällig verteilt, was auf einen Verlust der Zellpolarität hinweist. Auf dem zellulären Level erhöhte der Knockdown von RhoA die Zellfläche aber nicht das Volumen. Diese Veränderungen führten zu einer schnelleren Adhäsion unabhängig vom Substrat, eine Reduktion der Migration in 2D und im Gegensatz dazu eine verbesserte Migration durch eine

1   Summary

poröse Membran. Außerdem war die mitogene Antwort der Zellen auf einen Serumstimulus stark reduziert. Eine Veränderung in Zellviabilität konnte zudem nicht beobachtet werden. Die Expression und Sekretion des Fibrose-assoziierten Faktors CTGF war in gehungerten Zellen mit einer Reduktion in RhoA Expression signifikant vermindert, was jedoch in der Anwesenheit eines Serumstimulus aufgehoben werden konnte. Auf einer heterogenen multizellulären Ebene verringerte der Knockdown von RhoA die kontraktile Funktion von generierten künstlichen Herzgeweben unter Kalziumstimulation. Dies ging einher mit einer Reduktion der Expression von α-Glattmuskelaktin und Calsequestrin. Durch die Verwendung spezifischer Inhibitoren der Rho-assoziierten Kinase (ROCK) und HDAC6 konnten einige dieser zellulären Veränderungen imitiert und demensprechend einem Effektorprotein zugeordnet werden. Der ROCK Inhibitor Fasudil konnte die morphologischen Veränderungen und die reduzierte Migrationskapazität in Wildtyp-Fibroblasten abbilden, wobei eine Reduktion der Proliferation nach der Verwendung des HDAC6 Inhibitors Tubastatin A beobachtet wurde.

2   Introduction

2.1   Monomeric GTPases

The low molecular weight superfamily of monomeric guanosine triphosphatases (GTPases) ranging in size between 20 and 40 kDa consists of more than 150 known members in humans. All members share their function as binary molecular switches and as such they bind and hydrolyse guanosine triphosphate (GTP) with the help of accessory proteins similar to the α-subunits of heterotrimeric G-proteins.

Based on structural and functional similarities monomeric GTPases can be divided into five subfamilies which are Ras, Arf/Sar1, Rab, Ran and Rho. [1, 2] In the last decades distinct members of these five subgroups were identified showing involvement in a wide spectrum of cellular processes. Most of these proteins are still under investigation, some still poorly understood. The Ras family proteins are currently intensively investigated targets because of their role in human oncogenesis in that regard functioning as signaling nodes transferring extracellular stimuli to multiple downstream effectors and influencing cell differentiation, survival and proliferation [1]. Arf1, the name giving and best characterized protein of this subfamily was found to be involved in vesicle coating processes and transport whereas another group member, Arf6, was identifies as a regulator of actin structures in cell membrane ruffles [3]. A very similar function was found for the members of the Rab GTPases, which represent the largest subgroup. These proteins were found to be involved in vesicle formation, actin- and tubulin-dependent vesicle movement, and membrane fusion [4]. A completely different function was identified for Ran, who is known to be involved in nuclear transport processes mediated by importins as well as in cell cycle regulation [5]. The latter is also true for some of the Rho GTPases which were furthermore found to be strong regulators of the actin cytoskeleton [6].

2.2   Rho GTPases

2.2.1   Structure of Rho GTPases

To date, the subfamily of Rho GTPases consists of 20 members in humans with many of them ubiquitously expressed. Evolutionary research of the branches´ origin revealed that the

monomeric GTPase Rac is the founder and the oldest known protein of this structure found in *mycetozoans* evolving over one billion years ago [7]. Rho family members share up to 95% homology within their own subgroup [6] and display 30% identity with other members of the Ras superfamily. However, classical proteins of the Rho family (see Figure 2.1, blue) can be distinguished from other monomeric GTPases by their specific Rho insert domain [8] located between the fifth β-strand and the fourth a-helix.
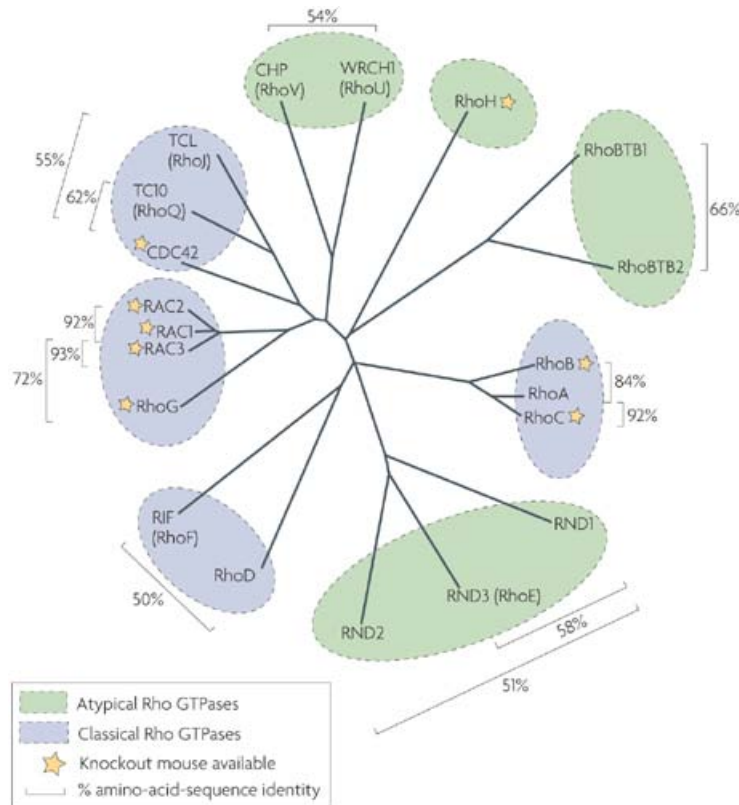
Figure 2.1: Rho GTPases phylogenetic tree, homologies and mouse models *Figure adapted from Heasman et al. 2008. Shown are the Rho family GTPases grouped based on sequence analysis with ClustalW.*

Within the Rho family distinct differences could be identified, e.g. classical members like RhoA, Rac1 and Cdc42 count 250 amino acids maximum while atypical members (Figure 2.1, green) can count more than 700. Apart from that all Rho GTPases share a similar GTP-binding site and two switch regions, which can differ in substitutions of single amino acids in different members (Figure 2.2.). In addition, most Rho GTPases are post-translationally modified at the C-terminus by an isoprenoid lipid which serves as an anchor to membranes of cell compartments after GTPase activation or as a binding moiety for guanine nucleotide dissociation inhibitors (RhoGDIs) [9-11]. The lipid residues vary with respect to the type of

different Rho GTPases, however, the most prominent motifs are geranylgeranyl- and farnesyl-residues covalently bound to the last cysteine in the proteins.
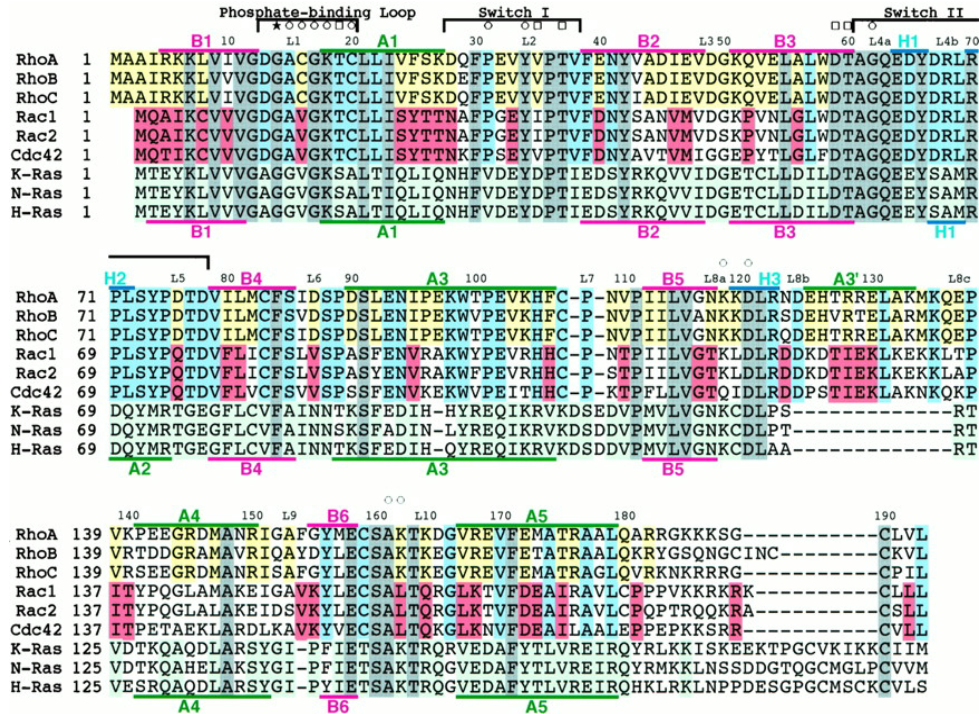
Figure 2.2: Amino acid sequence comparison of human Rho GTPases *Figure adapted from Ihara et al. 1998. The Figure shows the aligned sequences of RhoA-C including members of the Ras, Rac and Cdc42 family. Areas in yellow, red, green and blue are conserved regions, phosphate binding site and switch regions shown in black.*

2.2.2   Mechanism of Rho GTPase activation

As mentioned above, all monomeric GTPases serve as binary molecular switches cycling between an inactive GDP- and an active GTP-bound state [13]. This nucleotide exchange is tightly regulated and involves a number of factors. Every GTPase can be activated by one or more of the 60 known guanine nucleotide exchange factors (RhoGEFs) which promote the slow intrinsic exchange activity of GDP with GTP [12, 13]. RhoGEFs bind to the GDP-bound GTPase and the protein complex formed promotes the dissociation of GDP from the GTPase leaving an empty binding pocket. As soon as this binding site is filled with a GTP molecule the GEF detaches from the GTPase. In many cases, the activated GTPase then translocate to the cell membrane where it interacts with downstream effectors [14].
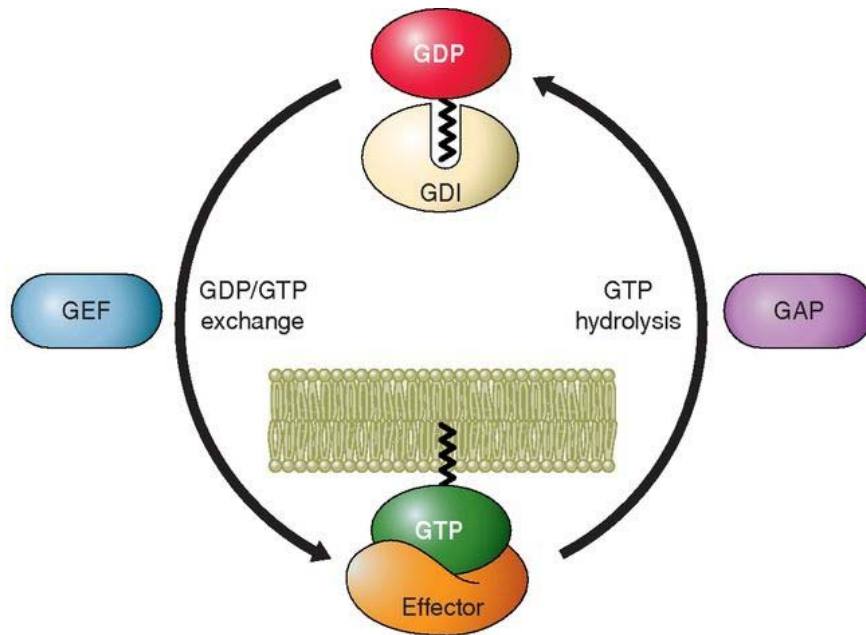
Figure 2.3: Activation cycle of GTPases *Figure adapted from Cherfils et al. 2013. Shown is the schematic activation by a guanine nucleotide exchange factor (GEF) with the translocation to the membrane and deactivation by a GTPase-activating protein (GAP) of GTP family proteins.*

To terminate the signaling event GTPase-activating proteins (RhoGAPs) bind to the activated monomeric GTPases and stimulate the intrinsic GTP hydrolytic activity. RhoGAPs lower the transition state energy of the hydrolysis reaction using an arginine-rich side chain to neutralize developing charges inside the catalytic pocket and activate water molecules inside to promote an in-line nucleophilic attack on the γ-phosphate of GTP [15, 16]. Upon hydrolysis of the GTP to GDP inside the catalytic pocket the protein is inactive again [17].

With respect to signaling processes a number of RhoGEFs and RhoGAPs could be identified to be involved in specific cascades while others activate and deactivate a variety of GTPases and therefore causing an even wider spectrum of cellular responses [17].

To inhibit the proteins participation in signaling events the GTPases can be kept in an inactive state bound by RhoGDIs which cap their isoprenoid rest with a lipid binding pocket and therefore prevent the GTPases from binding to the cell membrane in their active state [18]. The signals for binding and releasing GTPases are believed to be protein typical phosphorylation patterns, however, these mechanisms are still under investigation [15].

2.2.3   Functions of Rho GTPases

Rho GTPases are known to be involved in a wide variety of cellular processes. RhoA, Rac1, Cdc42, TC10, TLC and Rnd1 were found to influence remodeling and turnover of the actin cytoskeleton, while RhoB, RhoC, Rac1b and Rac3 participate in tumor growth and metastasis [19]. Rac1 and Rac2 were identified to be part of NADPH complex and to induce the superoxide production in many cells [20, 21]. Other members of the Rho GTPase family, like RhoD or RhoH, are not well investigated. RhoD was solely shown to be involved in the transport of early endosomes as well as in the disruption of focal adhesion sites [6] and RhoH antagonizes the signaling of Rac1 [22].

Most of the functional information gathered around the Rho family and their impact on the cytoskeleton was obtained by studying RhoA, Rac1 and Cdc42. In various cell types it was shown that while RhoA regulates the assembly of contractile actin structures, Rac1 and Cdc42 control the polymerization of peripheral lamellipodial and filopodial protrusions, respectively [23]. Apart from this many other functions were associated with these GTPases including the regulation of gene transcription [24-26]

2.3   RhoA-The Ras homolog family member A

The ubiquitously expressed Ras homolog family member A (RhoA) is a member of the monomeric GTPase protein subfamily of Rho-related proteins and approximately 21 kDa in size [27]. Since its identification in 1985 [28], two more mammalian isoforms were discovered: RhoB [29] and RhoC [30]. They both share 83% homology with RhoA and were also found to be involved in tumor invasion and metastasis [31, 32]. Alike all monomeric GTPases, RhoA is functioning as a molecular switch, which is activated and deactivated by the exchange of GDP and GTP and GTP hydrolysis, respectively [12]. After activation the geranylgeranyl-residue bound to the C-terminus of the protein enables RhoA to translocate and attach to the cell membrane. Therefore, it can be isolated from both membrane and cytosolic fractions [33].
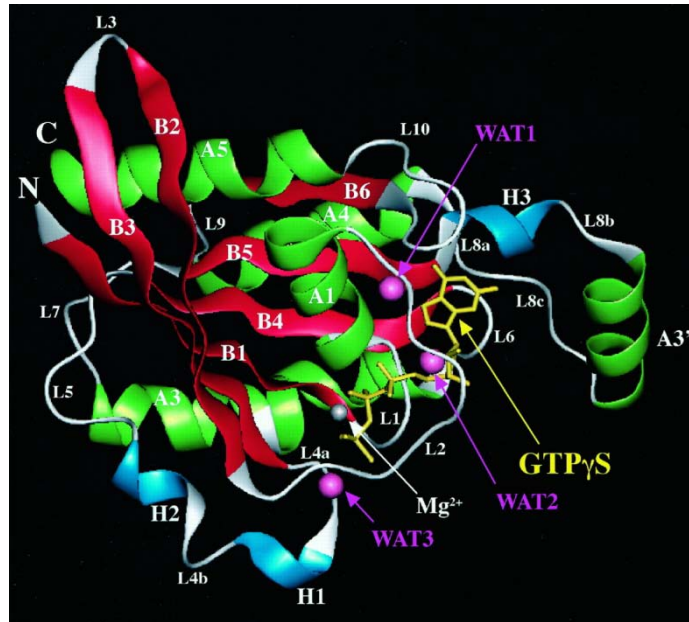
Figure 2.4: Crystal structure of RhoA-GTPγS *adapted from Ihara et al. 1998. RhoA was found in a crystal structure along with the Mg^{2+} ion and three water molecules.*

RhoA shows a major structural feature, that is also persistent in Ras proteins and which consists of a six-stranded β-sheet (red) surrounded by five α-helices (blue) and two 3_{10}-helices (green). When compared to Ras, a prominent structural difference in the crystal structure is the insert region which takes the form of a positively charged three turned helix and is specifically found in Rho-related GTPases. It is believed that this motif supports membrane binding of RhoA [34]. The ability of RhoA to exchange GDP to GTP is mediated by its two switch regions I and II, which undergo massive conformational changes upon guanine nucleotide binding. In addition, switch I was found to be involved into effector binding processes. Switch I was also shown to be exposed to the solvent and highly isolated within the Rho-related but not Ras-related proteins [35]. Moreover, both switch regions interact with the dbl-homology (DH) domain of GEFs, thereby contributing to the formation of the GTPase-RhoGEF complex and the GDP/GTP exchange [36].

2.4   Activation of RhoA

RhoA was shown to be activated by diverse upstream signals. Amongst them many G-protein-coupled receptors (GPCR) which can be activated by a wide spectrum of hormones and growth factors were identified like the sphingosine-1-phosphate receptor (S1PR) in cardiomyocytes [37], the angiotensin II-type 1 receptor (AT_1R) in smooth muscle cells [7] and muscarinic M_1 acetylcholine receptor (M_1R) in embryonic neural crest cells [38].

GPCRs signal via heterotrimeric G proteins, which consist of an α- and β/γ-subunit. After receptor activation, the G proteins dissociate in the α-subunit and the β/γ-dimer each interacting with different downstream effectors which includes certain RhoGEFs. Especially, the subfamily of $G_{12/13}$ proteins has been shown to activate RhoA and regulate via these pathways the cytoskeletal remodeling, proliferation, migration and invasion of cells [39, 40]. Mechanistically, $G\alpha_{12/13}$-subunits activate RhoA by direct binding and stimulation of three distinct RhoGEFs: p115RhoGEF, PDZ-RhoGEF and the leukemia-associated RhoGEF (LARG) that were found to affect gastrulation, actin remodeling and gene expression via the serum response factor (SRF) [41-43]. In addition, G proteins of the $G_{q/11}$ subfamily on the other hand were found to be involved in smooth muscle contraction not only by increasing the intracellular calcium levels, but also by activating RhoA. $G\alpha_{q/11}$-subunits activate RhoA through e.g. p63RhoGEF that was shown to mediate Ang II- and endothelin-1-dependent proliferation and contraction of rat aortic smooth muscle cells as well as the contractile properties of isolated vessels [17, 44].

Another receptor family mediating RhoA signaling are receptor tyrosine kinases. These autophosphorylating transmembrane receptors have been shown to affect the actin cytoskeleton via RhoA activation in several cell types [45, 46]. For example, stimulation of the epidermal growth factor (EGF)-receptor has been shown to induce RhoA activation in cancer squamous cell carcinoma cells and thereby leading to the formation of stress fibers. This could be blocked by the inhibition of the Rho-effectors Rho-dependent kinases (ROCK) [47]. The EGF-receptor itself on the other hand can be activated independently from its ligands. By forming protein complexes with integrins, EGF-receptor signaling can also be induced by changes in extracellular matrix (ECM) composition or in focal adhesion turnover [48]. As a consequence this leads to a change in cofilin phosphorylation levels and therefore in actin polymerization dynamics [49]. EGF-receptor was found to influence RhoA activation in combination with β1-integrins via regulation of p190RhoGAP in a mouse epithelial gland cell line. Downstream signaling of the p190GAP pathway was observed to be involved in cell-cell- and cell-matrix contacts involved in migration and metastasis [50]. Besides EGF-receptor signaling RhoA can also directly be activated by changes in the ECM via integrins. These receptors connect the actin cytoskeleton to the extracellular scaffold and were identified as part of focal adhesion complexes containing also RhoA [51].

2.5   Downstream effects of RhoA signaling

Inside the cell, RhoA has a wide variety of functions mostly connected to and mediated by the actin and tubulin cytoskeleton.

2.5.1   Effect of RhoA on the actin cytoskeleton

The actin cytoskeleton controls many processes in the cell like motility, secretion, proliferation and endocytosis. A tight spatial-temporal regulation of actin turnover is necessary to maintain these functions. In cells with a prominent cytoskeleton as for instance fibroblasts cell integrity is maintained by the cortical actin network and stress fibers [52, 53]. By microinjections of a constitutively active RhoA it was shown that RhoA can induce stress fibers in these cells, thereby identifying RhoA as a prominent regulator of the actin cytoskeleton [54]. Physiologically, this function plays a role in the regulation of cellular contraction of different cell types including smooth-muscle cells, but also of non-muscle cells [55]. Mechanistically, in smooth muscle cells RhoA activates ROCK which phosphorylates the myosin light chain phosphatase and thereby inhibits its activity. This consequently increases the phosphorylation of the myosin light chain which then results in the contraction of actin-myosin-containing fibers. At the same time the activation of ROCK activates LIM-kinase which directly induces cofilin phosphorylation and therefore inhibits actin depolymerization and fiber disassembly [56].
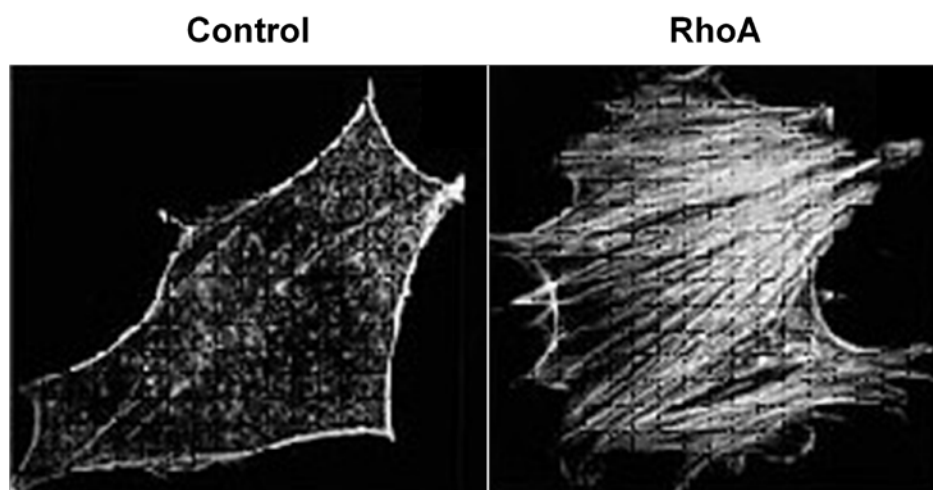
Figure 2.5: Effect of RhoA overexpression on the actin cytoskeleton *Figure adapted from Hall et al. 1995. Shown is an actin staining of control Swiss 3T3 fibroblasts and cells overexpressing RhoA wild type protein.*

Another pathway controlling the formation of actin fibers involves the formin mDia1 activation by RhoA. Formins can not only control polymerization speed, but also redirect g-actin to the plus-end of actin fibers and thus RhoA controls the formation of stress fibers and at the same time the actin turnover [57].

In addition, RhoA was found to be involved in the focal adhesion complex located at the stress fiber tip. These protein complexes, consisting of clusters of integrin receptors, vinculin, talin, paxilin as well as diverse signal mediators like RhoA which control the actin cytoskeleton dependent on the available extracellular substrate [58]. For example, in vascular smooth muscle cells it has been demonstrated that upon stress fiber formation induced by RhoA, the total number of focal adhesion sites increased, improving the cell contact to the substrate and the cytoskeletal contractility [59]. With respect to the heart muscle, the ECM is mostly composed of collagen I and III, laminin and fibronectin. Integrin receptors have been found to interact intensively with these matrix proteins. With a change in ECM elasticity, which is caused by a change in composition, RhoA was found to be activated by integrin receptor mediated signals [51].

Controlling the remodeling of the actin cytoskeleton and the focal adhesion turnover makes RhoA also a strong regulator of migratory and invasive processes. Moreover, in various cell types it was found that RhoA contributes to the cell polarity and therefore to the direction of the movement by retracting the rear of the migrating cell [23]. Other studies report that RhoA can be found in the leading edge of migrating tumor cells. It was discovered that advanced carcinomas do not form thick stress fibers but thinner contractile filaments which can be observed after formin activation by RhoA with simultaneous ROCK pathway inhibition [60]. Later mDia2 was identified as the regulating factor activated by RhoA to mediate invasive migration in relevant 3D models [61].

Furthermore, actin fibers are also necessary to break cell symmetry and polarize it for division. The contractile ring formed in the anaphase is induced by microtubule-mediated activation of the RhoA-ROCK pathway. The recruitment of actin and myosin fibers creates the ring at the cell cortex which separates the two daughter cells by contraction. In addition, it was found that inhibition of the actin polymerization hinders the effective separation of the centrosomes concluding that the remodeling and turnover of actin is necessary for this essential mechanism [62].

2.5.2   Effects of RhoA on microtubule structure

Very similar to actin fibers, microtubules are filaments shaped by constant turnover of subunit polymerization and depolymerization. Built-up by heterodimeric α- and β-tubulin forming a hollow tube with a pack of 13 strands, microtubules are a prominent structure-giving component of the cytoskeleton involved in cell division and vesicle trafficking [63]. Throughout the cell, different populations of microtubules can be found. Microtubules that differ in turnover speed are mostly found on the leading edge of a migrating cell [64]. Stable structures on the other hand are located in the perinuclear region where the microtubules organizing center is located [65]. α-tubulin, one of both monomers of microtubules, can be modified post-translationally by attachment and removal of i.e. tyrosine and acetyl residues. These modifications differ between stable and unstable populations of microtubules, which can be distinguished by their slow or fast depolymerization rate, respectively. However, role of these modifications in cellular processes is still under investigation [66]. For tubulin acetylation, which is the only modification occurring in the lumen of the microtubule, it has been shown that this modification stabilizes the microtubule [67].

Within single studies the impact of RhoA on microtubule turnover and stability mediated via the formin mDia1 was investigated [68, 69]. This pathway was found to be involved in microtubule reorganization, however, the details of this mechanism still remain obscure. Nevertheless, a subset of microtubules, which showed an increased loss of tyrosine residues (Glu-tubulin), were involved in cell migration and could be connected to RhoA activation by heterotrimeric G-proteins and GEFs [69]. Another study investigated the connection between focal adhesion sites and stable microtubules at the leading edge of migrating cells. It was hypothesized that integrin-mediated activation of the focal adhesion kinase (FAK) is able to activate the RhoA-mDia pathway, thereby increasing the fraction of local detyrosinated tubulin [70]. With regards to tubulin acetylation a RhoA-mDia2 mediated pathway was identified influencing the activity of the histone deacetylase 6 (HDAC6). HDAC6 is by 80% found in the cytosol and catalyses amongst others the deacetylation of tubulin and cortactin [71]. In osteoclasts it was observed that the overexpression of wild type RhoA or of the formin mDia2 activate the deacetylase activity of HDAC6 leading to a decrease in tubulin acetylation [72]. In addition it was found in bone osteosarcoma cells that the tubulin polymerization promoting protein 1 (TPPP1) can be phosphorylated by ROCK causing HDAC6 activation. Upon deacetylation of microtubules by the activated HDAC6, a faster microtubules turnover can be observed [73]. Nevertheless, the effect of RhoA on HDAC6 and acetylated tubulin in fibroblasts is poorly investigated.

2.5.3 Effects of RhoA on gene transcription

In addition to its ability to modify the actin cytoskeleton, RhoA is also able to induce the transcription of cytoskeletal and ECM-associated genes like *ACTA2* (α-smooth muscle actin) or *COL1A2* (collagen I), respectively [74]. This occurs mainly indirectly through remodeling of actin fibers and changing the g/f-actin ratio which subsequently leads to the activation of the SRF [75]. This was supported by the finding that actin interfering drugs, which bind g-actin rather than promote actin polymerization, can activate SRF without Rho GTPase participation. Therefore, the level of free actin monomers is considered to create a feedback loop and in return activates regulatory mechanisms for the SRF [26]. This activation is mediated by the SRF co-activator megakaryocytic acute leukemia (MAL) which binds to g-actin in the cytosol. Upon actin polymerization MAL dissociates from g-actin and translocates into the nucleus where it binds to and activates the SRF. Both, RhoA effectors mDia1 and ROCK were shown to indirectly mediate the dissociation of MAL from g-actin [76].

2.5.4 Effects of RhoA on secretion

The packaging of proteins into vesicular vehicles and their transport within the cell or to the plasma membrane is an important function in secreting cells. Secreted factors are transported away from the Golgi apparatus to be released into the intercellular space. [77]. The actin and tubulin cytoskeleton is known to be involved in vesicular transport processes, the fusion of membranes and exocytosis. Therefore, it is not surprising that RhoA is connected to the secretory behavior in various cell types [78].

First, it could be shown in mast cells that an inactivation of RhoA using the *clostridium botulinum* C3 transferase (C3T) which inhibits the GDP/GTP exchange in RhoA/B/C by ADP-ribosylation impairs the secretion [79]. On the other hand, stimulation of the RhoA pathway in keloid fibroblasts by TGF-β increased the secretion of the connective tissue growth factor (CTGF) and collagen I [80]. In addition, vesicles coated with an f-actin structure were identified in alveolar type II cells that can release their content solely by actin contraction. In secretion assays no release of any surfactant from these actin-coated vesicles could be measured when the cells were treated with the actin monomer binding toxin latrunculin A (LatA). In this study, it was additionally shown that when active RhoA was inhibited by C3T no vesicle budding, vesicle actin coating or exocytosis occurred [81].The importance of the regulation of actin structures for the fusion of vesicles with the membrane and for stabilization of the vesicle-membrane connection were also shown in different other cell types [82]. Moreover, it was found in HeLa cells that the translocation of the exocyst complex

after its activation by GEF-H1 is mediated by RhoA. Inhibition of the exocyst complex translocation led to a reduction in exocytosis and therefore to an accumulation of vesicles inside the cells [83].

In the heart muscle and in cardiac cells including cardiac fibroblasts, RhoA is implied to control the secretion of matrix metalloproteinases (MMP) which degrade the extracellular matrix (ECM) but also activate apoptotic ligands and influence cell-cell contacts [84]. Most studies discussing this topic show, that an inhibition of RhoA signaling using HMG-CoA-reductase inhibitors (statins) affect RhoA activation and hence MMP secretion. This effect functions mainly via disabling the geranylgeranyl lipid residue synthesis [85]. The outcome of MMP secretion has been shown for example in a tumor cell model, here MMPs support the invasion into the tissue by degrading scaffold proteins and enhance the migration potential [86] In hepatocellular carcinoma models a reduction in tumor size, an increased tumor apoptosis rate and a decreased metastasis could be observed after the treatment of mice with the ROCK inhibitor Y-276323. Similar as describe for cardiac fibroblasts, RhoA could be linked to MMP secretion in this study. This led to the hypothesis that ROCK inhibition could be a possible target in anticancer therapy [87].

2.5.5   Effect of RhoA in proliferation

The actin cytoskeleton and microtubule structures are equally involved and important in cell proliferation. While microtubules separate chromosomes during the anaphase, actin forms a part of the contractile ring that is essential for cytokinesis [88].

In a number of publications the effect of RhoA, which has been shown to translocate to the cell cortex during ana-telophase in mitosis was investigated. In this context RhoA, which is activated by the RhoGEF ECT2 is mandatory for the formation of the contractile ring and thus for cytokinesis [89]. In addition, the stress fiber formation induced by RhoA was found to be involved in G1-S phase transition and mitotic cell rounding in *Xenopus* epithelial kidney cells [90]. The disruption of actin structures by LatA led in the same cell type from a different species to a G1 phase arrest and failure in centrosome separation. These effects were also induced by the inhibition of ROCK using Y27632 [91].

During mitosis microtubules were found to stabilize an area at the furrow region. This area is then supporting the cortical ring where active RhoA is concentrated during cytokinesis. A pharmacological manipulation of microtubule structures led to a diffusion of active RhoA from

the already formed cortical ring or to a suppression of translocation to the forming cortical in star fish oocytes [92]. RhoA can also regulate the turnover of microtubules and therefore influence mitosis e.g. via ROCK and HDAC6. ROCK had been shown to phosphorylate TPPP1 which blocked its ability to inhibit HDAC6. This led to a rapid deacetylation of microtubules which enabled human osteosarcoma cells to progress through the cell cycle. In G2 phase TPPP1 was dephosphorylated and the resulting inhibition of HDAC6 allowed the stable mitotic apparatus to form [73].

With respect to the heart, just a few studies were published investigating the impact of RhoA on cell proliferation. It was found that in atrial fibroblasts RhoA influences the process of serum-driven proliferation. Upon treatment with simvastatin, which reduced the level of active RhoA at the membrane, the cells showed a decrease in proliferation rate by 50 to 70% [93]. Furthermore, for neonatal rat cardiac fibroblasts, it has been demonstrated that the induction of proliferation by Ang II or TGF-β could be almost completely blocked by the co-application of the ROCK inhibitor GSK-576371 [94].

2.6   Pathological cardiac remodeling

Heart remodeling can occur under physiological and pathological conditions. Physiological remodeling, which is in most cases a reversible process, develops during pregnancy or in the athletes´ heart and is characterized by a growth of cardiomyocytes in order to improve the contractile function and fulfill the body's demand [95, 96]. In contrast, pathological remodeling which can be a consequence of genetic predisposition and diverse processes like persistent hypertension, valve malfunctions and infections causes mainly irreversible changes including cardiac hypertrophy, fibrosis and often later on cardiac dilation. As a consequence the contractile function of the heart is impaired and heart failure occurs [97, 98].

During the progress of dysfunction, the heart muscle changes in shape, cellular composition and performance [99]. Initially, a thickening of the heart muscle by an increase in cardiomyocyte size is developed to compensate for the additional work load. Then, due to the high energy expenditure and the decreased perfusion of the heart cardiomyocytes undergo apoptosis [100] and the spaces are filled with extracellular matrix. Cardiac fibrosis occurs, which cannot be reversed. In this process cardiac fibroblasts are thought to be the mayor source of excessive ECM proteins and other factors working auto- or paracrine in the tissue [101].
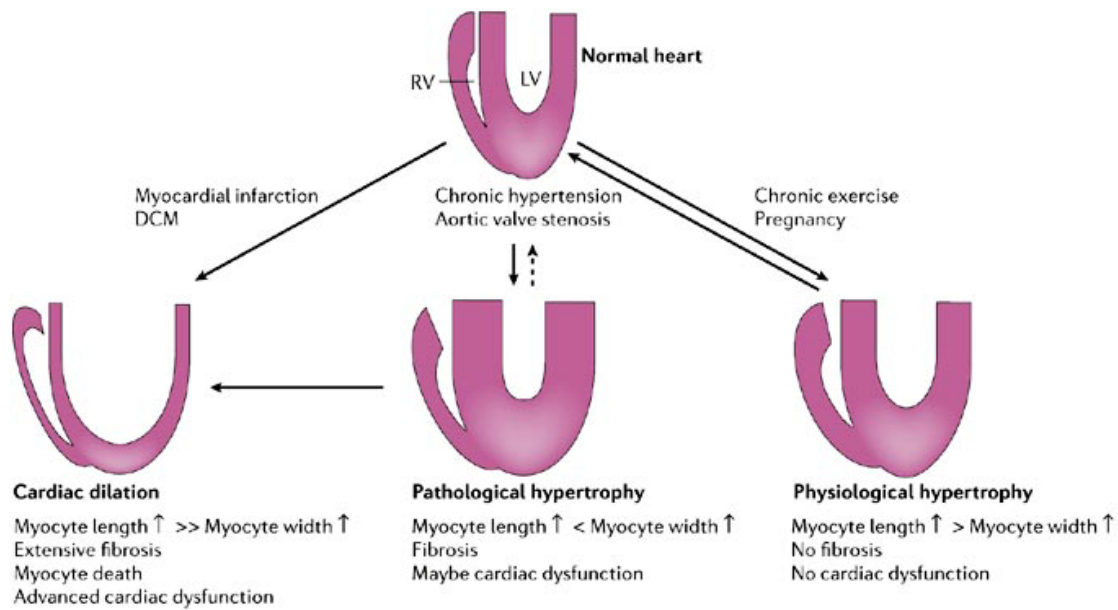
Figure 2.6: Different cases of remodeling in cardiac myopathies *Figure adapted from Heineke et al. 2006. Shown is a schematic picture of changes in ventricle size and wall thickness during reversible and irreversible remodeling processes.*

2.7   The cardiac fibroblast

Fibroblasts in general can be found amongst others in the lung, heart, skin and kidney. They are vimentin expressing cells with mesenchymal origin whose function during embryogenesis is yet not fully understood. In adulthood, one of the most important roles of fibroblasts is to maintain the homeostasis of the extracellular matrix [102]. Most fibroblasts show certain common characteristics like a spindle shaped cell body in culture, the absence of a basal membrane and a prominent Golgi apparatus [103]. This is also in part true for cardiac fibroblasts which can make up to 70% of the whole heart cell content dependent on the species [104]. Cardiac fibroblasts are no homogenous cell population, they e.g. can originate from epithelial cells from the epicardium or evolve out of cardiac endothelial cell that undergo endothelial-to-mesenchymal transition like this has been shown for valvular fibroblasts [105]. In addition, there are also other sources like fibrocytes, which are bone marrow-derived cells [106]. The complexity of different origins of the cardiac fibroblasts also explains why there is no clear characterization possible by specific markers as the gene expression patterns of different fibroblast cultures tested were found to be highly divers [107].

Electron microscopy revealed that cardiac fibroblasts are located within a three-dimensional network of extracellular proteins between cardiomyocytes. There, they contribute to the

structural, mechanical and electric properties in the healthy heart by regulating the ECM and probably functioning as conducting units. To maintain ECM homeostasis cardiac fibroblasts secrete components of the ECM, especially collagen I, III and fibronectin to create a scaffold for other cell types [108]. On the other hand they express and secret MMPs to maintain the balance of matrix synthesis and degradation [109]. Within this scaffold cardiac fibroblasts were shown to connect tightly to contracting groups of cardiomyocytes via gap junctions made of connexin (Cx) 43 and 45 and as well as to the ECM via integrins [110, 111]. Due to this network provided, fibroblasts support the distribution of contractile forces throughout the heart tissue [108]. In addition, cardiac fibroblasts possess a high membrane resistance which makes them good conductors inside the ECM which itself has more the characteristics of an insulator [112, 113]. It was shown in a co-culture model of rat ventricular cells that cardiac fibroblasts respond to the contraction of neighbor cardiomyocytes by changing their membrane potential and that they can even synchronize the contraction rhythm of two distinct cardiomyocyte populations [114]. As mentioned above, fibroblasts connect to contracting myocytes via ion-permeable gap junctions. In an *in vivo* model it was observed that fibroblasts express different patterns of connexins dependent on the cell-cell type interaction. While fibroblasts connected to each other were found to express more Cx 40, fibroblasts connected to cardiomyocytes expressed more Cx 45 and 43 in the rabbit sinoatrial node [110].

2.8   The activated fibroblasts - myofibroblasts

Cardiac fibroblasts embedded in a healthy tissue are considered quiescent. Although the cells secrete factors at all times and participate in electric coupling their potential to migrate or proliferate is very low. Nevertheless, fibroblasts become activated by external stimuli like the overactivated renin-angiotensin-aldosterone system in heart failure or an increased cyclic tensile stress [105, 115, 116]. Upon activation cardiac fibroblasts start to display features of smooth muscle differentiation and were found to contribute to repair and remodeling processes in the diseased heart. After a myocardial infarct these cells can also be found in the scar area [117]

Where these transformed fibroblasts, also called myofibroblasts due to their smooth muscle characteristics, originate from is still not clear. By fate-mapping experiments they were shown to originate out of quiescent fibroblasts but also out of epithelial-like cell undergoing epithelial-mesenchymal transition (EMT) [118]. Another source are leukocytes, in particular

fibrocytes from the bone marrow, as well as endothelial cells from blood vessels and pericytes which are α-sm-actin positive cells [119].
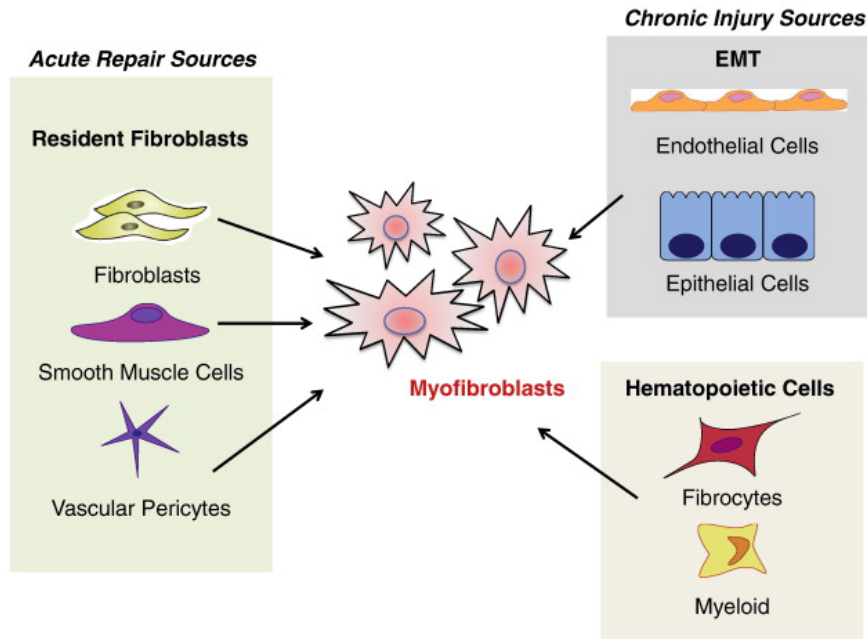
Figure 2.7: Sources of myofibroblasts *Figure adapted from Davis et al. 2014. Shown are sources of myofibroblasts which are mobilized during acute remodeling (left box) and during chronic injury (right boxes).*

In the scenario of a myocardial infarction cardiac fibroblasts were found to transform in two steps: first a proto-myofibroblast is created which develops strong stress fibers. In addition, they show a fast focal adhesion site turnover which makes it easier for the activated fibroblast to migrate towards the damaged area [120]. As soon as the cells arrive at the damaged area, they initiate the second phase secreting ECM proteins and inflammatory factors. To built-up a scar tissue the cells start to express α-sm-actin to support stress fibers and develop a strong contractile phenotype that is important for closing the wound and preventing the rupture of the ventricular wall [120]. In addition, the activated fibroblasts increase the secretion of collagen I and III and also of ECM-degrading MMPs [121]. The secretion of MMPs enables the myofibroblasts to migrate within the scar tissue to the side of repair by degrading ECM proteins in their path [83]. The deposition of collagens leads to a stiffening of the tissue at the site of repair supporting the closed wound and thus to reparative fibrosis. The equilibrium of constant matrix deposition and degradation that exists in a healthy heart is therefore shifted in pathological remodeling by myofibroblasts towards the production of ECM components [122].

Besides secreting MMPs and key proteins of the ECM, fibroblasts are also a source of bioactive molecules in the heart. After injury, a pro-inflammatory environment is generated by

the secretion of cytokines and interleukins and by the recruitment of neutrophils and macrophages that clear the area from dead cells and debris [123]. The tumor necrosis factor-α (TNF-α), interleukins like IL-1β and IL-6 and the transforming growth factor-β (TGF-β) were found to be secreted by activated cardiac fibroblasts upon acute remodeling. These factors were shown to act in a paracrine and autocrine fashion [124]. TNF-α not only induced myofibroblast invasion, MMP secretion and proliferation but also the secretion of IL-1β and IL-6 [125]. Cardiomyocytes were found to respond to IL-6 secreted by myofibroblasts as a paracrine stimulus that contributed to hypertrophic cardiomyocyte growth [126]. TGF-β was identified as a locally generated cytokine that induces the transformation of quiescent fibroblasts into myofibroblasts and therefore promotes proliferation, migration, apoptosis as well as ECM production [124]. The induction of fibroblast transformation by TGF-β in the early stages of MI have been proven to be beneficial. However, a continuously high level of this cytokine in the scar area contributed to an excessive deposition of ECM components [115]. In general, the increase in ECM deposition leads to an impaired contractile performance of the heart by stiffening of the ventricular wall, irreversible fibrosis and increases the risk of arrhythmias [127].

After scar maturation an unknown number of myofibroblasts undergoes apoptosis while some still stay located in the collagen-rich network they produced [128]. The fate of these activated cells inside the scar long after maturation is not well investigated. It is believed that the remaining cells continue to reinforce the tissue with further collagen deposition as an adaptive response to further hemodynamic stress [129]

2.9 RhoA and its effectors in the heart

A variety of *in vitro* and *in vivo* studies have been performed to investigate the role of RhoA, its activators, inhibitors and effectors in the heart with the main focus on cardiomyocytes. On a cellular level RhoA was initially connected to a hypertrophic response in these cells induced by factors like endothelin-1, Ang II and the α_1-adrenoceptor agonist phenylephrine [130-132]. Early studies showed that the inhibition of RhoA and ROCK reduced the expression of hypertrophy-associated proteins like of the atrial natriuretic factor (ANF) and of the α-myosin heavy chain [133, 134].
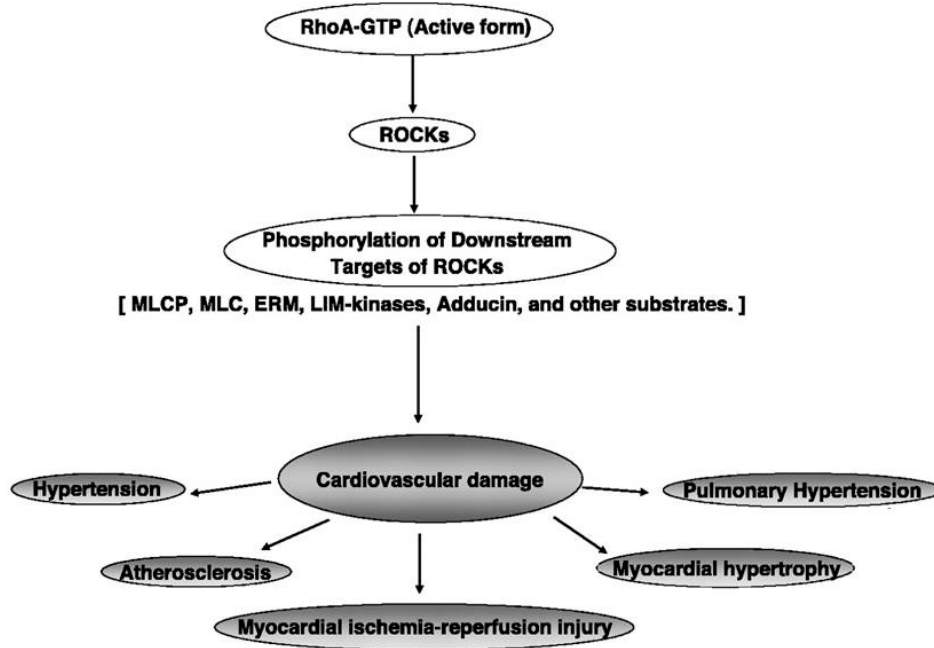
Figure 2.8: Role of Rho-associated kinases (ROCKs) in cardiovascular diseases
Scheme modified from Noma et al. 2006. Cardiovascular diseases which involve the RhoA-ROCK pathway are depicted.

In vivo the RhoA pathway was found to be activated in a number of cardiac disease models. For example, after transverse aortic constriction (TAC) RhoA was shown to be strongly activated shortly after surgery in mice [135]. In a rat model of diabetic cardiomyopathy it could be demonstrated that not only the activation of RhoA was increased but also its expression [136], and in a rat model of hypertension-induced heart failure ROCK2 was found to be increased in the membrane fraction of the heart [137]. Most of these models suggest that an induction of the RhoA/ROCK pathway is detrimental for the heart as the inhibition of RhoA activation e.g. by statins [33, 138] or the inhibition of ROCK [139] could prevent the remodeling of the hearts. In line with this idea of a disease-driving pathway were also the results of most studies with genetic RhoA/ROCK models. Sah and colleagues demonstrated in 1999 that the cardiomyocyte-specific overexpression of wild type RhoA had a clear negative influence on the performance of the heart. These hearts did not show a hypertrophic phenotype as hypothesized from *in vitro* data, but a strong interstitial fibrosis and ventricular dilation. In electrocardiography, bradycardia, and atrioventricular blocks were observed. Overall the mice had severe edema and the survival was strongly impaired [140]. In accordance, it has been shown that in haplodeficient ROCK1(+/-) mice the degree of cardiac fibrosis was reduced after Ang II-infusion, TAC and myocardial infarction [141]. A

recent study, then again raised the idea of a contribution of this pathway in cardiac hypertrophy as the specific deletion of ROCK2 in cardiomyocytes resulted in a reduction in cardiomyocyte hypertrophy after Ang II infusion [142].

In contrast, other models support the hypothesis that the RhoA pathway has at least some beneficial aspects in heart diseases. By inhibiting the activation of RhoA, Rac1 and Cdc42 by a cardiomyocyte-specific overexpression of RhoGDI unexpectedly the same phenotype was found as in the RhoA-transgenic mice including the AV conduction defect [143]. This might be explained by the unselective inhibition of diverse GTPases. But in addition, a beneficial function of RhoA was shown in a model of ischemia/reperfusion in mice. The transgenic animals expressed a doxycycline-inducible, cardiomyocyte-specific, constitutively active form of RhoA. After ischemia caused by ligation of the left anterior descending artery the vessel was reopened again to induce reperfusion. Animals, expressing the active form of RhoA, showed in a comparable area at risk a reduction in infarct size by 70% compared to control. This data argues for a cardioprotective effect of RhoA in the heart [144].

Compared to cardiomyocytes only few data is available on the role of RhoA in cardiac fibroblasts, especially on its impact on myofibroblast characteristics. Recently, the differentiation into myofibroblasts, involving the secretion of fibrotic markers like collagen I, TGF-β and CTGF, as well as the migration performance were found reduced upon downregulation of RhoA in rat ventricular fibroblasts [53]. In addition, atrial fibroblasts with lower levels of active RhoA showed a decrease in their proliferation rate *in vitro* [93]. One of the main reasons for this lack of knowledge on RhoA in cardiac fibroblasts is that there is no genetic model available allowing the specific knockout or overexpression of a certain gene in this cell type.

3   Aim of the thesis

The aim of this thesis was to investigate the role of RhoA in cardiac fibroblasts. For this neonatal rat cardiac fibroblasts were isolated and RhoA expression reduced via lentiviral-mediated shRNA expression. Then, the impact on protein expression, cell morphology as well as adhesion velocity was studied. Furthermore, it was evaluated whether the knockdown of RhoA affects the typical myofibroblast characteristics like migration, proliferation and the secretion of profibrotic factors. Finally, engineered tissues were generated containing fibroblasts with reduced RhoA expression to investigate the impact on contractile properties. In parallel wild type cardiac fibroblasts were treated with inhibitors of the RhoA downstream effectors ROCK and HDAC6 and the outcome of these experiments was compared with the results obtained with the knockdown model.

4 Material and Methods

4.1 Material

4.1.1 Devices and plastic material

Device	Model	Company
Agarose gel chamber	Mini SUB Cell GT	Bio-Rad Laboratories
Bacteria incubator	Incubator	Sanyo/Panasonic
Blot imager	VersaDoc	Bio-Rad Laboratories
Blotting chamber	Mini Protean Tetra Cell	Bio-Rad Laboratories
Fluorescence microscope camera	XM-10	Olympus
Cell counter	Casy Counter	Roche
Cell culture centrifuge 1	Centrifuge 5804R	Eppendorf
Cell culture centrifuge 2	Megafuge 3.0R	Thermo Scientific
Combi table centrifuge with vortexer	Combispin FVL 2400 N	Peqlab
Contraction setup	IOA-5301	Föhr Medical Instruments
Gel imager	GelDoc	Bio-Rad Laboratories
Incubator	C200	Labotect, Göttingen
Large scale shaker	Innova 4300	Eppendorf
Multi-mode microplate reader	Flexstation 3	Molecular Devices
Microscope filter blue	350 DAPI	Olympus
Microscope filter red	575 TxRed	Olympus
Microscope filter green	485 FITC	Olympus
Microscope objective 4x	UPlanFLN4xPh	Olympus
Microscope objective 10x	UPlanFLN10xPh	Olympus
Microscope objective 20x	LUCPlanFLN20xPh	Olympus
Microscope objective 40x	LUCPlanFLN20xPh	Olympus

Multiparameter cell analyzer	Cellavista	SynenTec
Micro volume spectro-photometer	Nanodrop 1000	Peqlab
PCR machine	Mastercycler gradient	Eppendorf
pH meter	Inolab pH	Wtw
Power supply	Power PAC HD	Bio-Rad Laboratories
Real-time PCR system	Taqman 7900 HT	Life Technologies
Rocker	Diomax 1030	Heidolph
Rotation shaker	Reax 3	Heidolph
Rotor ultracentrifuge	SW27	Beckman Coulter
Scale	Portable	Sartorius
Shaker	3016	GFL
Shaker (4°C)	Vibramax 100	Heidolph
Special accuracy scale	Research	Sartorius
Sterile workbench	Telstar Bio II A	Prettl
Stimulator	STI 08 Current Stimulator	Föhr Medical Instruments
Table centrifuge	Centrifuge 5415D	Eppendorf
Thermomixer	Thermomixer compact	Eppendorf
Ultracentrifuge	L8 70M	Beckman Coulter
Vortexer	VF2	W. Krannich
Water bath	2764	Eppendorf

Table 4.1: Devices

Plastic material

	Type	Company
Cell culture bottles	T75, T175	Sarstedt
Cell culture plates	10 cm, 15 cm	Sarstedt
Filter tips	1000 mL, 100 mL,10 mL	Greiner Bio One
Multi tips	10 mL	Eppendorf
Pipette tips	1000 mL, 100 mL,10 mL	Sarstedt

Reaction tubes	50 mL, 15 mL, 2 mL, 1.5 mL, 0.5 mL, 0.2 mL	Sarstedt
384-well plates	MicroAmp optical 384-well reaction plate	Life Technologies
Centrifugation tubes	Polyallomer centrifugation tubes, 17 mL	Beckman

Table 4.2: Plastic material

4.1.2 Chemicals and media

Reagent	Company
Acetic acid	Carl Roth
Acrylamide solution rotiphorese gel 30	Carl Roth
Agar-agar	AppliChem
Ammonium persulfate (APS)	AppliChem
Angiotensin II (Ang II)	Sigma-Aldrich
Ascorbic acid	AppliChem
Bradford reagent (Roti-Quant)	Carl Roth
Bromophenol blue	Sigma-Aldrich
Carbenicillin	AppliChem
Chicken embryo extract (CEE)	Self made
Cesium chloride ($CsCl_2$)	AppliChem, Darmstadt
Collagen I (rat tail)	Self made
4′,6-Diamidin-2-phenylindol (DAPI)	Roche
DMEM (1 g/L glucose, $NaHCO_3$)	Biochrom
DMEM Glutamax (1 g/L glucose, pyruvic acid)	Life Technologies
DMEM Glutamax (4.5 g/L glucose)	Life Technologies
DMEM (powder)	BD Biosciences
DNAseI	Merck
Fetal calf serum (FCS)	Life Technologies

FGM-3 BulletKit	Lonza
Glycerol	Carl Roth
Glycin	AppliChem
HEPES-buffered saline	Lonza
Horse serum	Life Technologies
Igepal CA-630	Sigma-Aldrich
Kanamycin	Sigma-Aldrich
Lumi light	Roche
Matrigel	BD Biosciences
Methanol	Carl Roth
β-mercaptoethanol	AppliChem
Non-essential amino acids (NEAA) (100x)	Life Technologies
Paraformaldehyde (PFA)	Sigma-Aldrich
Phosphate-buffered saline (PBS)	Life Technologies
Penicillin/Streptomycin (PenStrep) (10000 units/mL and 10000 µg/mL)	Life Technologies
Polybrene	Sigma-Aldrich
Polyfect	Qiagen
PonceauS	Sigma-Aldrich
Puromycin	Life Technologies
Sodium dodecyl sulfate (SDS)	AppliChem
Super signal west femto	Thermo Scientific
Tetramethylethylenediamine (TEMED)	Merck
Tryptone	AppliChem
Triton-X 100	Carl Roth
Trypsin (powder)	BD Biosciences
Trypsin-EDTA 0.05%	Life Technologies
Trypsin/EDTA solution	Lonza
Trypsin neutralizing solution	Lonza

Tween-20	Carl Roth
Yeast extract	AppliChem

Table 4.3: Chemicals and media

4.1.3 Media

4.1.3.1 Media and buffers for cell culture

Growth medium	DMEM Glutamax (4.5 g/L glucose)
	10% FCS (active)
	1% PenStrep
	1% NEAA
Serum-reduced medium	DMEM Glutamax (4.5 g/L glucose)
	1% FCS (active)
	1% PenStrep
	1% NEAA
Non-cardiomyocyte medium (NKM)	DMEM Glutamax (1 g/L glucose, pyruvic acid)
	10% FCS
	(heat inactivated at 56°C for 30 min)
	1% PenStrep
HEK293/TSA201 growth medium	DMEM Glutamax (4.5 g/L glucose)
	10% FCS
	(heat inactivated at 56°C for 30 min)
	1% PenStrep
HEK293/TSA201 serum-reduced medium	DMEM Glutamax (4.5 g/L glucose)
	0.5% FCS
	(heat inactivated at 56°C for 30 min)
	1% PenStrep
10 x DMEM	13.3 mg DMEM (powder)

	ad 10 mL with distilled H_2O
	→ sterile filtered
2 x DMEM	1 mL 10 x DMEM
	1 mL Horse serum
	0.2 mL CEE
	0.1 mL PenStrep
	ad 5 mL with distilled H_2O
2.5 x DMEM	2.5 mL 10 x DMEM
	2.5 mL FCS (active)
	0.25 mL PenStrep
	ad 10 mL with distilled H_2O
	→ sterile filtered
EHM medium	DMEM (1 g/L glucose, $NaHCO_3$)
	11.6% Horse serum
	2.3% CEE
	1% PenStrep

Buffers for contraction measurements and cell isolation

$CaCl_2$ stock	165.57 g $CaCl_2$*2 H_2O
	ad 500 mL with distilled H_2O
$MgCl_2$ stock	106.38 g $MgCl_2$*6 H_2O
	ad 500 mL with distilled H_2O
Stock 1 (0.2 mM Ca^{2+})	175 g NaCl
	10 g KCl
	2.22 mL $CaCl_2$ stock

	25 mL $MgCl_2$ stock
	ad 1 L with distilled H_2O
Stock 2	50 g $NaHCO_3$
	ad 1 L with distilled H_2O
Stock 3	5.8 g NaH_2PO_4
	ad 1 L with distilled H_2O
Tyrode solution	40 mL Stock 1
	38 mL Stock 2
	10 mL Stock 3
	1 g Glucose
	100 mg Ascorbic acid
	ad 1L with distilled H_2O
HEPES stock	47.66 g HEPES
	ad 1 L with distilled H_2O
	pH 7.4 with NaOH
	$\rightarrow$ sterile filtered
Calcium and bicarbonate-free Hanks´ with HEPES (CBFHH)	40 mL NaCl stock (3.42 M)
	10 mL KCl stock (0.54 M)
	10 mL $MgSO_4$ stock (0.081 M)
	10 mL KH_2PO_4 stock (0.044 M)
	10 mL Na_2HPO_4*2 H_2O stock (0.034 M)
	10 mL glucose stock (0.56 M)
	100 mL HEPES stock
	$\rightarrow$ sterile filtered

4.1.3.2 Media for bacterial culture

LB medium	10 g Tryptone
	5 g NaCl
	5 g Yeast extract
	ad 1 L with distilled H_2O
	$\rightarrow$ autoclaved
SOB medium	20 g Tryptone
	5 g Yeast extract
	0.5 g NaCl
	ad 1 L with distilled H_2O
	$\rightarrow$ autoclaved
	10 mL $MgCl_2$ stock (10 mM)
	10 mL $MgSO_4$ stock (1 mM)
Agar plates	2.8 g Agar agar
	200 mL LB medium
	Antibiotics:
	50 µg/mL Carbenicillin
	or
	33 µg/mL Kanamycin

4.1.4 Buffers

Buffer for lentivirus purification

TNE buffer	0.3 g Tris
	0.3 g NaCl
	7.3 mg EDTA

	ad 15 mL with distilled H_2O
	pH 7.4 with HCl
	$\rightarrow$ sterile filtered

Buffer for adenovirus purification

10 x VSB	12.1 g Tris
	80 g NaCl
	3.7 g KCl
	0.95 g $MgCl_2$
	ad 1 L with distilled H_2O
	pH 7.4 with HCl
Cesium chloride „light stock"(ρ=1.209 g/mL)	11.02 g $CsCl_2$
	ad 50 g with 1x VSB Buffer
Cesium chloride „heavy stock"(ρ=1.459 g/mL)	21.1 g $CsCl_2$
	ad 50 g with 1 x VSB Buffer

Buffer for protein biochemical methods

10 x Tris-buffered saline (10 x TBS)	24.2 g Tris
	175.3 g NaCl
	ad 2 L with distilled H_2O
	pH 7.4 with HCl
1 x Tris-buffered saline with tween-20	200 mL TBS
(TBST)	2 mL Tween-20
	ad 2 L with distilled H_2O
5 x SDS-PAGE electrophoresis buffer	30.2 g Tris

	188 g Glycine
	10 g SDS (w/v)
	ad 2 L with distilled H_2O
	pH 8.3 with HCl
1 x Immunoblot buffer	6 g Tris
	28.8 g Glycine
	400 mL Methanol (v/v)
	ad 2 L with distilled H_2O
	pH 8.4
PonceauS	0.2 g PonceauS
	3 mL Acetic acid
	ad 100 mL with distilled H_2O
Lysis buffer (GST-Fish)	6 g Tris
	8.8 g NaCl
	0.4 g $MgCl_2$
	100 mL Glycerol (v/v)
	10 mL Igepal CA-630 (v/v)
	ad 1 L with distilled H_2O
	pH 7.4 with HCl
4 x SDS loading buffer (Laemmli buffer)	50 mL Glycerol
(with glycerol)	10 mL β-Mercaptoethanol
	3.6 g Tris
	5.7 g SDS
	0.2 g Bromophenol blue
	ad 100 mL with distilled H_2O

	pH 7.4 with HCl
4 x SDS Loading buffer (Laemmli buffer)	10 mL β-Mercaptoethanol
(without glycerol)	3.6 g Tris
	5.7 g SDS
	0.2 g Bromophenol blue
	ad 100 mL with distilled H_2O
	pH 7.4 with HCl

4.1.5 Antibodies

Primary antibodies for immunoblot (IB) and immunofluorescence (IF) analyses

Primary antibody	Dilution IB/IF	Clone/Type	Company
Acetylated tubulin	1:2000/1:500	6-11B-1	Sigma-Aldrich
β-actin	1:7500/-	AC-47	Sigma-Aldrich
β-actin	-/1:50	4C2F9H12	C. Chapponier Lab
γ-actin	-/1:50	2A3G8E2	C. Chapponier Lab
CTGF	1:200/1:50	L-20	Santa Cruz
HDAC6	1:1000/-	D21B10	Cell Signaling
α-smooth muscle actin	1:2500/1:500	1A4	Sigma-Aldrich
RhoA	1:200/-	26C4	Santa Cruz
RhoC	1:1000/-	D40E4	Cell Signaling
Tubulin	1:2000/1:500	B-5-1-2	Sigma-Aldrich
Tyrosinated tubulin	1:5000/1:200	Tub-1A2	Sigma-Aldrich

Vimentin	1:2000/1:100	V9	Sigma-Aldrich
Vinculin	1:2000/1:500	hVIN-1	Sigma-Aldrich

Table 4.4: Primary antibodies

Secondary antibodies for immunoblot analyses

Secondary antibody	Dilution	Lot no.	Company	Host
Anti-mouse-IgG-HRP	1:10000	031M4752	Sigma-Aldrich	rabbit
Anti-rabbit-IgG-HRP	1:40000	119K4815	Sigma-Aldrich	goat
Anti-goat-IgG-HRP	1:10000	sc-2020	Santa Cruz	donkey

Table 4.5: Secondary antibodies for immunoblot analyses

Secondary antibodies for immunofluorescence analyses

Secondary antibody	Dilution	Company	Host
Alexa Fluor 488-conjugated anti mouse	1:800	Jackson Immuno Research	goat
Cy3-conjugated anti mouse	1:800	Jackson Immuno Research	goat
Cy5.5-conjugated anti goat	1:50	Jackson Immuno Research	rabbit
IgG$_1$-FITC	1:50	SouthernBiotech	mouse
IgG$_{2b}$-TRITC	1:50	SouthernBiotech	mouse

Table 4.6: Secondary antibodies for immunofluorescence analyses

Fluorophore-conjugated phallotoxin and wheat germ agglutinin

Reagent	Stock concentration (in H_2O)	Dilution	Company
TRITC-phalloidin	0.5 mg/mL	1:1000	Sigma-Aldrich
Alexa Fluor 488-WGA	1 mg/mL	1:200	Life Technologies

Table 4.7: Fluorophore-conjugated phallotoxin and wheat germ agglutinin

4.1.6 Enzymes and Kits

Application	Name	Company
Total RNA preparation	RNeasy mini kit	Qiagen
Plasmid DNA preparation	Exprep mini kit	GeneAll
Plasmid DNA preparation	Plasmid midi kit	Qiagen
Apoptosis/necrosis staining	Annexin-V-FLUOS staining kit	Roche
PCR product purification	High Pure PCR Product Purification Kit	Roche
DNA ligation	Quick ligase kit	New England Biolabs

Table 4.8: Kits

PCR

Application	Name	Company
qRT-PCR	Quantifast RT-PCR SYBR mix	Qiagen
qRT-PCR	Hot FirePol Eva Green polymerase	Solis BioDyne
cDNA synthesis	RevertAid first strand cDNA synthesis kit	Thermo Scientific
Endpoint PCR	PrimeStar HS polymerase	TaKaRa

Table 4.9: PCR enzymes

Restriction enzymes

Enzyme	Supplements	Company
BamHI	-	New England Biolabs
EcoRI	-	New England Biolabs
BsgI	S-adenosyl methionine (SAM)	New England Biolabs
MfeI	-	New England Biolabs

Table 4.10: Restriction enzymes

4.1.7 Primer

All primer sequences are annotated in 5´→3´ orientation.

Protein		Sequence
RhoA	forward	gca gat att gaa gtg gac ggg
	reverse	tgg gat gtt ttc taa act atc agg g
RhoB	forward	cat cga ctc gca caa agc ag
	reverse	ata cga tgc acg gag tgt cg
PBGD	forward	cct gaa act ctg ctt cgc tg
	reverse	ctg gac cat ctt ctt gct gaa
CTGF	forward	ccg ggt tac caa tga caa ta
	reverse	cac acc cca cag aac tta gc
HDAC6	forward	agc gca gtc tta ttg atg gg
	reverse	cca tgc tca tag cgg tgg at
Venus N-terminus	forward	tta gga tcc atg gtg agc aag ggc gag
	reverse	agc gaa ttc ggc cat gat ata gac gtt gtg gct gt
RhoA-RBD	forward	gag caa ttg ctc gac tgg tcc ctg cta ga
	reverse	cga gaa ttc gcg gcc gcc acc aga ttt tt
Venus C-terminus	forward	gag gaa ttc gac aag cag aag aac ggc atc
	reverse	ctc gaa ttc tta ctt gta cag ctc gtc cat

Table 4.11: Primer

4.1.8 Plasmids

Plasmid	Company/Lab
pcDNA3.1(+)-Zeo	Invitrogen
FRET sensor pRaichu1298X (M. Matsuda Lab) [Yoshizaki et al, 2003, J. Cell. Bio.]	Venus, RhoA-Rho binding domain of rhotekin (RBD)

Table 4.12: Plasmids

4.1.9 Viruses

Lentivirus

Vectors derived from the human immunodeficiency virus-1 (HIV-1) are a preferred system for gene delivery into proliferative and non-proliferative cells. This system provides a stable long-term expression of the gene of interest by using the virus´ ability to transcribe its delivered RNA into DNA and randomly integrate in the cell genome. With cell division the integrated gene of interest is replicated and therefore inherited to the daughter cells [145].

To make this system particularly safe, three plasmids have to be cotransfected into host cells to produce lentiviral particles (table below). The first plasmid is coding for the gene of interest (GOI) and an antibiotic resistance gene. The second plasmid, psPAX.2, codes for the necessary lentiviral proteins involved in assembly of particles (Gag [146], virus replication and pathogenesis (Nef [147]) as well as virus DNA replication (Tat [148]). Finally, pMD2.G encodes for the glycoprotein G of the vesicular stomatitis virus and extends the spectrum of cell types that can be infected by the virus particles.

In this project the gene of interest plasmids code for shRNA which are specific for RhoA or control sequences. All plasmids encode in addition for a resistance gene allowing the selection of positive cell clones with puromycin.

Name	Plasmid	Coding for **shRNA sense highlighted**	Company
shRhoA	pLKO.1	CCGG**CCCAGACTAGATGTAGTATTT**CTCGAG**AAATACTACATCTAGTCTGG**GTTTTTG	Thermo Scientific

shControl	pLKO.1	CCGG<u>CGGAATGACGAGCACACGAGA</u>CTCG AG**<u>TCTCGTGTGCTCGTCATTCC</u>**GTTTTTG	Thermo Scientific
shScr	pLKO.1	shRNA, no fit to any mammal gene, **CCTAAGGTTAAGTCGCCCTCG**	Sigma-Aldrich
psPAX.2	psPAX.2	Lentiviral proteins (Gag, Rev, Tat)	D. Trono Lab
pMD2.G	pMD2.G	Glycoprotein of the human vesicular stomatitis virus	D. Trono Lab

Table 4.13: Lentivirus plasmids

Adenovirus

For live cell imaging the LifeAct GFP-tagged adenovirus provided by Ibidi was used.

The LifeAct fusion protein consists of a 17 amino acid actin binding domain fused to GFP and is described to have no interference with actin dynamics. Therefore it is highly suitable for live cell imaging [149].

4.1.10 Cells and bacteria

Cells

Name	Organism	Source, Note
Neonatal rat cardiac fibroblasts	rat	Heart ventricular tissue, primary cells
Normal human cardiac fibroblasts (NHCF-V)	human	Heart ventricular tissue Donor: male, 50 years, caucasian, no heart disease
HEK293A	human	Embryonic kidney, immortalized by an adenovirus serotype 5
Tsa201	human	Embryonic kidney, immortalized by SV40 large T-antigen

Table 4.14: Cells

Bacteria

For cloning chemically competent MAX Efficiency DH10B bacteria provided by Life Technologies were used.

Genotype: F⁻ [mcrA](#) Δ(*mrr-hsd*RMS-*mcr*BC) Φ80d*lacZ*ΔM15 Δ*lac*X74 *end*A1 *rec*A1 *deo*R Δ(*ara*,*leu*)7697 *ara*D139 *gal*U *gal*K *nup*G *rps*L λ⁻

4.1.11 Software

Analyses	Software
Immunoblot	Quantity One
Immunofluorescence/life cell imaging	Xcellence pro
Migration assay	ImageJ Plug-in: manual tracking, chemotaxis assay
Golgi size and density analyses	ImageJ Plug-in: analyze particles
qRT-PCR	SDS 2.4
Contraction measurement	BeMon32
Contraction measurement analyses	Amon32
Proliferation-DAPI-assay	CellaVista
Multi-mode microplate reader measurements	SoftMax Pro 5.4
Statistical evaluations	Graphpad Prism

Table 4.15: Software

4.2 Methods

4.2.1 Cell biological methods

4.2.1.1 Neonatal rat cardiac fibroblast isolation

Cardiac fibroblasts were isolated from neonatal rats (day 0 to 3) by using a modified cell isolation protocol established by Simpson et al.[110].

The complete hearts were taken out and the atria were removed. The ventricles were cut into pieces of 1-2 mm size and washed twice with CBFHH. The tissue was dissociated over 4 h by alternating treatments with trypsin and DNAseI solutions in CBFHH at room temperature during continuous agitation or gentle pipetting, respectively. The first supernatant was discarded, the ones of the following step after trypsin and DNAseI treatments were collected upon clouding of the supernatant (1-4 min) till no cells dissolved from the tissue anymore. After centrifugation at 60 g for 15 min at 4°C the cells were pooled and washed with ice-cold NKM. After one last DNAseI treatment the cells were centrifuged, pooled and strained with a mesh of stainless steel (250 μm pores). The cells were counted in trypan blue solution (1:1, 0.4%) to determine the cell number and the amount of cell death.

4.2.1.2 Cardiac fibroblast/cardiomyocyte separation

For cell separation 10^7 cells in suspension were seeded on a 15 cm cell culture dish in ice-cold NKM. After 60 min of incubation at 37°C, 5% CO_2, the NKM containing the majority of cardiomyocytes was collected and the medium was changed to prewarmed growth medium. For the next 6 days the medium was changed every day to wash off cell debris and unattached cardiomyocytes. The cardiac fibroblasts were cultures until they reached full confluency.

4.2.1.3 Cell cultivation and passaging

All cells were cultured in the respective growth medium in a water steam-saturated cell culture incubator at 37°C and 5% CO_2.

For passaging, NRCF were rinsed with an appropriate volume of prewarmed PBS and treated with trypsin (0.05%, trypsin-EDTA) for cell detachment. After 3-4 min incubation at 37°C, 5% CO_2, the detachment of the fibroblast was controlled with a light microscope. The trypsin was deactivated by adding 2 volumes of growth medium. The cells were harvested and centrifuged at 1000 g at 4°C for 2 min. The supernatant was discarded and the cells were resuspended in growth medium, then counted and seeded in the required density.

For TSA and HEK293 cells the same protocol was applied but incubation time of the trypsin step was shortened to 2 min at room temperature.

4.2.1.4 Lentivirus production

Tsa201 cells were cultured on 10 cm dishes in growth medium until confluency of 70% was reached. After washing with PBS the conditions were changed to serum-reduced medium.

Transfection was performed strictly according to the polyfect transfection reagent handbook provided by Qiagen.

Plasmid with GOI	3 µg
psPAX.2	3 µg
pMD2.G	2 µg
Medium without antibiotics or serum	300 µL
Polyfect	80 µL
Serum-reduced medium	620 µL
Serum-reduced medium to cells	7 mL
Total volume	8 mL

Table 4.16: Transfection mixture for 10 cm culture dish

After 48 and 72 h the virus particle-containing supernatants were harvested and if required fresh serum-reduced medium was added. The collected supernatants were pooled and filtered through a 45 μm syringe filter to remove cell debris.

4.2.1.5 Lentivirus purification

The concentration and purification of lentiviral particles reduces the possibility of contamination and removes the, for primary cells potentially harmful, host cell debris. Plus the lentiviral particles can be stored in solution at -80°C for month in a space-saving fashion.

The harvested supernatants containing lentiviral particles were filled in 17 mL plastic centrifuge tubes and carefully underlayed with 1 mL 20% sucrose solution in TNE buffer. After centrifugation for 4 h at 22000 g and 4°C the lentiviral particles were found in and on the sucrose cushions. The overlaying supernatants were discarded and the concentrated viruses were mixed, aliquoted, instantly frozen in liquid nitrogen, and stored at -80°C.

4.2.1.6 Lentiviral infection of NRCF

Wild type fibroblasts were passaged according to 4.2.1.3 and seeded in growth medium containing 8 µg/mL polybrene to improve the infection rate. Virus particles were thawed on ice and added to the medium in the culture vessel. After culturing the cells for 48 h at 37°C, 5% CO_2, the medium was changed to selection medium containing 1 µg/mL puromycin. The selection of the lentiviral-infected fibroblasts was performed for up to 12 days. Selection conditions were maintained also in case of further passaging. The RhoA knockdown was controlled by immunoblot.

4.2.1.7 Amplification of Adenoviruses

LifeAct adenoviral particles were purchased from Ibidi and then amplified as described in the following. HEK293A in serum-reduced medium were infected with adenovirus particles and incubated at 37°C, 5% CO_2 until cells show a clear GFP expression and start to detach. The cells were harvested, and for lysis the suspension was frozen in liquid nitrogen, then again thawed at 37°C in a water bath. This procedure was repeated three times. To pellet cell debris, the lysed cells were centrifuged at 1000 g for 5 min. The supernatant was then supplemented with serum-reduced medium and transferred to a new plate of 70% confluent HEK2983A cells. Starting from a 10 cm culture dish the virus was amplified up to 20 x 15 cm dishes. In the final step, the cells were harvested by gentle rinsing as soon as GFP expression was clearly detectable but no cell lysis was observed. The cells suspension was centrifuged at 1000 g for 5 min and the cell pellet was carefully washed with 50 mL PBS. After centrifugation at 1000 g for 5 min and resuspension in 10 mL PBS, the cells were lysed

as described above. The virus particles in the supernatant were separated from empty capsids and concentrated by cesium chloride gradient. To generate the cesium chloride gradient, 5 mL of the cesium chloride "light stock" was underlayed with 5 mL of the "heavy stock". The harvested and washed virus particles in PBS were pipette on top and the gradient was centrifuged in an ultracentrifuge for 20 h, at 22000 g and 4°C.

During centrifugation the virus particles manifested as a defined layer between the two cesium chloride phases and were harvested by puncturing the centrifuge tube wall with a needle. The obtained virus was frozen in 45% glycerol and stored at -20°C in aliquots.

4.2.1.8 Casting of engineered heart muscle (EHM)

A suspension of $2*10^6$ cardiac cells isolated as described in 4.2.1.1 was supplemented with $0.5*10^6$ lentiviral-infected and selected cardiac fibroblasts. The cells were mixed with collagen type I (rat tail) and a basement membrane protein mixture (Matrigel) to provide a scaffold in the condensed tissues.

Reagent	Volume
Collagen I (4.2 mg/mL)	847 µL
2 x DMEM	847 µL
NaOH (0.1 N)	184 µL
Matrigel	400 µL
Cell suspension ($2.5*10^6$ cells)	1722 µL
Total	1 mL/ mold

Table 4.17: Master mixture for 4 EHMs

The EHM mixtures were casted into silicon molds of 3.5 cm diameter and incubated at 37°C, 5% CO_2 for 1 h. The molds were then filled with EHM medium. The EHMs were cultured for 7 days with medium changes on day 1, 3 and 5 and then transferred onto a phasic stretcher. For 24 h the EHMs were stretched at 1 Hz, later at 2 Hz for 6 days. Contraction measurements were performed 14 days after casting.

4.2.1.9 Contraction measurements of engineered heart muscle

The contraction measurement setup was filled with tyrode solution containing 0.2 mM Ca^{2+} and the EHMs were mounted on hooks attached to the highly sensitive force meter in the organ baths. The calcium concentration was adjusted to 0.4 mM and the EHMs were paced at 2 Hz for synchronic contraction. To reach the maximal length (L_{max}) as defined by Frank Starling, the EHMs were stepwise equally stretched every 5 min. As soon as L_{max} was reached, the pacing was stopped, the buffer was changed and the rings were equilibrated for 30 min in tyrode solution. After systolic and diastolic forces reached back to the baseline the buffer was changed again. To determine contraction force at different calcium concentrations, a calcium chloride stock solution (0.2 M) was stepwise added to the organ baths. In intervals of 10 min the calcium concentration was elevated from 0.2 mM to a final concentration of 3.2 mM. The systolic and diastolic forces of the paced EHMs were documented. After measurement the EHMs were frozen in liquid nitrogen for protein isolation.

4.2.1.10 Protein isolation from EHMs

The deep-frozen EHM tissues were ground with a pestle in a liquid nitrogen-cooled metal block and transferred into 1.5 mL reaction tubes containing GST-Fish buffer (200 µL/tissue). After incubation on ice for 15 min the samples were mixed, centrifuged at 16000 g, 4°C, 10 min and the lysates separated from the particulate fractions for further analyses by immunoblot.

4.2.1.11 Annexin-V-FLUOS/propidium iodide staining

To identify apoptotic and necrotic cells in culture the Annexin-V-FLUOS staining kit from Roche was used. In brief, infected and selected fibroblasts were seeded on a 12-well plate at 30% confluency. The Annexin-V-FLUOS and propidium iodide solution were mixed in 2 mL incubation buffer according to the manufacturer's protocol. The growth medium was removed, the cells washed with prewarmed PBS and incubated with the staining solution for 15 min at room temperature in the dark. Then, the cells were imaged with an inverted fluorescence microscope and the percentage of green (apoptosis) and green/red (necrosis) cells were evaluated.

4.2.1.12 Phalloidin staining of the actin cytoskeleton

The infected and selected cells were fixed with 4% paraformaldehyde in PBS, washed twice with PBS, and the membranes were permeabilized with 0.05% Triton X-100 in PBS for 3 min. After 3 washing steps the fixed cells were incubated in a blocking solution (1x Immunoblock in distilled H_2O) for 1 h at room temperature. TRITC-tagged phalloidin was used at a concentration of 0.5 µg/mL in PBS and incubated for 1 h at room temperature in combination with 1 µg/mL DAPI in the dark. The cells were again washed twice with PBS and then stored protected from light at 4°C.

4.2.1.13 Immunofluorescence

The infected and selected cells were fixed, washed, permeabilized and blocked as described in 4.2.1.12. Then, the cells were incubated with the primary antibody solution at its corresponding concentration according to table 4.4 at 4°C overnight. Afterwards, the cells were washed with PBS and incubated with the fluorophore-tagged secondary antibody in the appropriate concentration for 1 h at room temperature in the dark. The cells were again washed twice with PBS, then stored protected from light at 4°.

4.2.1.14 Evaluation of Golgi size and density by ImageJ

High resolution grey-scale images of wheat germ agglutinin (WGA)-stained Golgi membranes were analyzed with the ImageJ particle analysis software. In brief, the images were transformed into an 8 bit format, inverted and the Golgi area encircled. In this region, the threshold was adjusted and a binary image of the Golgi membrane stacks was generated. From this the complete area containing Golgi stacks was determined and by using the command "Analyze Particles" the membrane fraction was also determined. The real sizes of both areas were then calculated with the help of the microscope settings and the camera chip characteristics.

4.2.1.15 Adhesion assay

The infected and selected cells were seeded in growth medium on uncoated 12-well plates or plates which were coated before with 1% rat tail collagen I in PBS. After every 15 min up to 1 h ten images per virus type were randomly taken. The adherent and non-adherent cells were counted and compared relative to the total cell number.

4.2.1.16 2D-Migration assay

Wild type or infected and selected fibroblasts were seeded on 24-well plates and infected with LifeAct adenovirus stock (around 5 μL, approx. multiplicity of infection 500) for 24 h, then incubated with the respective inhibitors at 37°C, 5% CO_2 or just kept in growth medium for another day. Imaging was performed in growth medium with an inverted fluorescence microscope equipped with a climate chamber at 37°C, 5% CO_2 for 24 h. Every 20 min the cells were imaged in the GFP channel. Cell tracking was performed with the manual tracking macro in ImageJ. The average velocities and the absolute distances were calculated using the chemotaxis plug-in for ImageJ provided by Ibidi.

4.2.1.17 Amoeboid migration assay

For amoeboid migration analysis, cell culture inserts with a porous membrane on the bottom with randomly distributed 8 μm pores were used from Greiner Bio One (thincerts).

Thincerts were inserted into a 24-well plate and filled with high serum or serum-reduced medium. Per cavity 5000 infected and selected cardiac fibroblasts or wild type cardiac fibroblasts with the respective inhibitors were seeded and incubated for 24 h at 37°C and 5% CO_2. The thincerts were then washed with PBS and the cells fixed for 15 min in 4% paraformaldehyde in PBS. After removing the paraformaldehyde and two washing steps with PBS, the remaining cells were carefully removed from the membrane surfaces using a cotton swap. The membrane was cut out of the plastic frame with a scalpel, placed on a microscope slide and incubated with 10 µg/mL Hoechst 33342 in PBS for 30 min. For evaluation, the cells found in the pores of the membrane were visualized by fluorescence microscopy and counted.

4.2.1.18 Proliferation-DAPI-assay

The proliferation of cells was determined over a time course of 4 days. In brief, the infected and selected cells were seeded on a 96-well plate with 5000 cells per cavity. For every time point cells were fixed with 4% paraformaldehyde in PBS and washed twice with PBS. The membranes were permeabilized with 0.05% Triton X-100 in PBS for 3 min and again washed three times. After incubation with 1 µg/mL DAPI in PBS for 30 min at room temperature in the dark the cell numbers were evaluated using the Cellavista system.

4.2.1.19 Rho activity binding assay-pulldown assay

The infected and selected fibroblasts were seeded on 10 cm cell culture dishes. After 24 h the medium was changes to low serum conditions for another day. Then, the cells were kept on a heating plate at 37°C and stimulated with 100 nM Angiotensin II for 30 seconds. Afterwards, the medium was immediately discarded and the plates were put on ice. From this step on, the complete assay was performed at 4°C in the cold room. The cells were lysed with 500 µL ice-cold GST-Fish buffer, scraped of the plate and the debris was pelletized by centrifugation for 2 min at 16000 g. To determine total RhoA expression 50 µL of the supernatants were stored separately on ice. The remaining lysate was incubated with the GST-Rho-binding domain of rhotekin (RBD)-fusion protein bound to glutathione sepharose which exclusively binds the active forms of RhoA-C. The mixture was then incubated for 1 h on ice in a rotating shaker. Then, the sepharose was separated from the lysates by centrifugation for 2 min at 16000 g. The supernatant was removed and the sepharose washed twice with GST-Fish buffer. The sepharose and the stored lysates were mixed with 4x loading buffer with and without glycerol, respectively. The samples were heated up to 95°C for 5 min. Analysis of the total and the activated amount of RhoA was then performed via immunoblot analyses.

4.2.2 Molecular biological methods

4.2.2.1 Quantitative real time PCR (qRT-PCR)

Total RNA was isolated from $1*10^6$ infected and selected fibroblasts using the RNeasy kit and dissolved in 50 µL RNAse-free H_2O. The concentration was determined using a micro

volume spectrophotometer. cDNA was synthesized from 150 ng of total RNA using the ReverseAid First Strand cDNA synthesis according to manufacturer's protocol. The cDNA was diluted 1:20 with RNAse-free H_2O for qRT-PCR analysis.

All runs of qRT-PCR were performed in a 384-well plate with the following reaction mixture composition:

Component	Volume
cDNA (diluted 1:20)	1 µL
Primer forward (10 µM)	1 µL
Primer reverse (10 µM)	1 µL
Quantifast RT-PCR SYBR Mix or Hot FirePol Eva Green Polymerase	5 µL or 4 µL
Nuclease-free water	2 µL /13 µL
Total	10 µL/20 µL

Table 4.18: qRT-PCR mixture

The following PCR conditions were used:

Cycle	Temperature	Time	Number of Cycles
Initial Denaturation	95°C	15 min	1
Denaturation	95°C	15 sec	40
Annealing	60°C	20 sec	40
Extension	72°C	40 sec	40
Denaturation	95°C	15 sec	1
Melting curve start Ramp rate: 1.6°C/s	60°C	15 sec	1
Melting curve end	95°C	15 sec	1

Table 4.19: qRT-PCR protocol

Samples were run in quadruplicates each using the primers listed above in table 4.11. The data was calculated using a standard curve with the following cDNA dilutions of a reference cDNA: 1:10, 1:30, 1:100, 1:300. The values were normalized to PBGD as a housekeeping gene.

4.2.2.2. End point polymerase chain reaction (PCR)

DNA amplification was performed using the proof reading, hot start Prime Star polymerase provided by TaKaRa.

Component	Volume
5 x Prime Star Buffer	10 µL
dNTP Mix (2.5 mM each)	4 µL
Primer start/end (10 µM)	1 µL each
Template DNA - pRaichu-1298X	100 ng
Prime Star Hot Start Polymerase	0.5 µL
Nuclease-free H_2O	Up to 50 µL

Table 4.20: PCR mixture

Cycle	Temperature	Time	Number of Cycles
Initial Denaturation	95°C	15 min	1
Denaturation	95°C	10 sec	30
Annealing	55°C	15 sec	30
Extension (1 min/kb)	72°C	25 sec	30
Final extension	72°C	10 min	1

Table 4.21: PCR protocol

4.2.2.3. Cloning strategy

The BiFC sensor fusion protein was generated in three cloning steps:
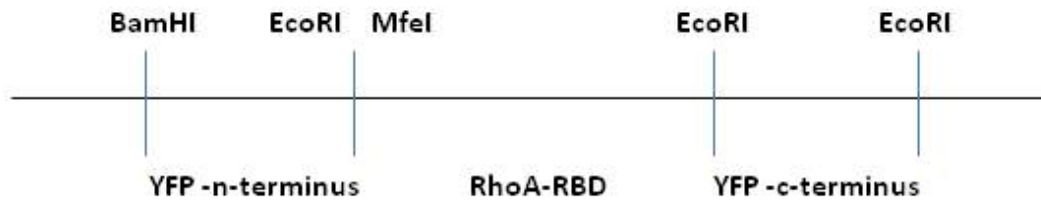
Strategy:

Figure 3.1: Cloning strategy

The N-terminus of Venus was amplified by PCR adding BamHI and EcoRI restriction sites at the end of the forward and reverse primers, respectively. The obtained fragment was then cloned in the pcDNA3.1(+)-Zeo vector. In the next step, the plasmid was reopened by restriction digest with EcoRI and ligated with the PCR-amplified RhoA-RBD insert. This insert contained additional MfeI and EcoRI restriction sites inserted by PCR at the 5' and 3' ends, respectively. The ligation of the MfeI and the EcoRI site disabled the EcoRI recognition sequence and allowed to reopen the plasmid again with EcoRI. In the last step the C-terminus of Venus was amplified with primers containing both EcoRI sites at the end and the resulting fragment was finally ligated in the plasmid.

4.2.2.4 Restriction Digest

The DNA was dissolved in distilled H_2O completed with the appropriate reaction buffer. After mixing with the restriction enzyme the solution was shortly centrifuged and incubated at 37°C for at least 2 h. Restriction enzymes were inactivated at 65°C for 20 min. The DNA was then purified using a high pure PCR product purification kit and eluted with 50 µL of H_2O.

4.2.2.5 Ligation

50 ng of linearized vector DNA in distilled H_2O was mixed with 150 ng of insert-DNA and adjusted with H_2O to 10 µL. Then 10 µL ligation buffer and T4 ligase (1 µL) were added, the solution was incubated for 1 h at room temperature, and stored at -20°C or transformed immediately.

4.2.2.6 Transformation

Chemically competent DH10B bacteria were thawed on ice and incubated with 7 µL of the ligation mixture for 30 min. The bacteria were then heat shocked in a thin wall 15 mL reaction tube at 42°C for 1 min and instantly put on ice for another 2 min. After mixing with 500 µL prewarmed SOB medium, the suspension was spread on a preheated agar plate and incubated overnight at 37°C.

4.2.2.7 DNA isolation

For DNA isolation single bacteria colonies from agar plates were picked and cultured in 3 mL or 150 mL of LB-medium overnight in a shaker at 37°C.

Small scale and medium scale plasmid preparation were performed with kits according to the manufacturer´s protocols. The DNA concentration was determined using a micro volume spectrophotometer.

4.2.3   Protein chemical methods

4.2.3.1. Preparation of protein samples for SDS-PAGE

Fibroblasts were washed with PBS, lysed and scraped off using an adequate volume of GST-Fish buffer. The homogenates were incubated on ice for 15 min, mixed and centrifuged at 4°C for 10 min at 16000 g. The supernatants containing the cell lysates were separated from the particulate fractions which were then frozen in liquid nitrogen and stored at -20°C. The lysates were kept on ice for determination of protein concentrations by Bradford assay. To prepare SDS-PAGE samples, 4x SDS loading buffer without glycerol was added to cell lysates and incubated at 95°C for 5 min for protein denaturation.

4.2.3.2. Bradford assay

The concentration of total protein in cell lysate samples was determined using a colorimetric protein assay by Bradford [150]

The relevant samples and a standard curve with increasing protein amounts (0, 0.4, 0.8, 1.2, 1.6, 2.0 µg BSA) were prepared in 50 µL distilled H$_2$O. Into every cavity 200 µL of 1x Bradford reagent (Coomassie Brilliant Blue-G250) in H$_2$O was added and incubated for 5 min at room temperature. The absorbance at 595 nm was detected with a microplate reader and the total protein concentrations of the samples were calculated.

4.2.3.3. Sodium dodecyl sulfate polyacrylamide gel electrophoresis (SDS-PAGE)

For analysis of protein expression in total cell lysates discontinuous SDS-PAGE was performed. Gels with Tris-HCl (pH 8.8), 10% SDS as well as ammonium persulfate (APS) and tetramethylethylenediamine (TEMED) polymerization catalysts were casted containing the appropriate concentration of acrylamide/bisacrylamide suitable for the size of the protein of interest (8%-15%). Separation gels were covered with stacking gels made from 5% acrylamide/bisacrylamide, Tris-HCl (pH 6.8), 10% SDS, APS and TEMED. SDS-gels were loaded with prepared protein samples and run at 100 V for sample condensation and later at 200 V for protein separation.

4.2.3.4. Immunoblot

To make proteins accessible for antibody detection, they were transferred onto a nitrocellulose membrane by electroblotting after SDS-PAGE. Gel and membrane were packed between filter papers in ice-cold western blot buffer and transferred into a blotting chamber. During the blotting process the setup was either cooled with an ice pack or transferred to an ice-containing polystyrene box. After electroblotting at 100 V for 1 h, the membrane was removed from the blotting setup and incubated in PonceauS solution for 3 min to visualize the transferred proteins. The membranes were then washed with TBST and blocked with blocking solution (1x Roti Block in distilled H$_2$O) for 1 h at room temperature. After two more washing steps with TBST, incubation with the primary antibody in TBST on a shaker was performed overnight at 4°C. Then, the membrane was washed again three times and the secondary antibody tagged with horseradish-peroxidase (HRP) was applied in concentrations according to table 4.5 in TBST and incubated on a shaker at room temperature for 1 h. The protein-antibody complexes were detected using the chemiluminescent reagents Lumi Light or Super Signal West Femto. The signals were detected with a chemiluminescence imaging system and semi-quantitatively analyzed.

4.3. Statistics

All results obtained were summarized in Graph Pad Prism and given as mean±SEM. For 2-group comparisons the t-test was used. Analyses and comparison of 3 or more groups was performed with one or two way analysis of variance (one or two way ANOVA). A one-sample t-test was used for statistical analysis of data sets in which the control was set 1.

5   Results

5.1   Influence of RhoA on the morphology of NRCF and on the Golgi apparatus

5.1.1   The lentiviral-induced knockdown is RhoA-specific

To investigate the role of RhoA in neonatal rat cardiac fibroblasts (NRCF) a lentiviral-induced knockdown was used. For this, a RhoA-specific small hairpin construct was identified. It was found that after selection with puromycin the RhoA expression was reduced by 50% on the mRNA level and by about 75% on the protein level (Figure 5.1 A, B). As RhoA shares up to 80% homology with its family members RhoB and RhoC possible effects of the shRNA construct on both isoforms were evaluated. However, neither RhoB nor RhoC were regulated by the shRNA construct, as could be shown by mRNA and immunoblot analyses, respectively (Figure 5.1 C).
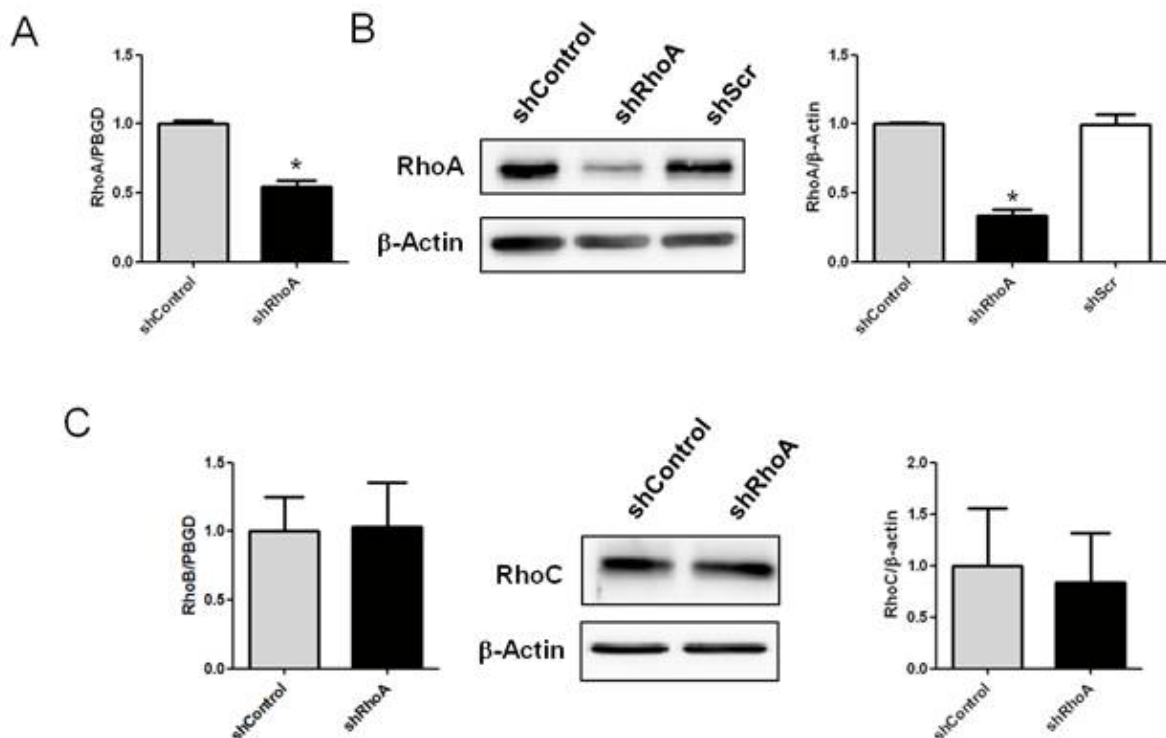

Figure 5.1: Analyses of RhoA, RhoB and RhoC expression in shControl and shRhoA NRCF *A) qPCR analysis of RhoA mRNA in shControl and shRhoA NRCF (means ± SEM, n = 6, values were normalized to PBGD and are given relative to shControl, *p < 0.05). B) Representative immunoblot of RhoA in shControl, shRhoA and shScr cells and quantitative*

analysis of RhoA expression normalized to β-actin (right). The relative changes in shRhoA and shScr to shControl are given (means ± SEM, n = 22, *p < 0.05). C) qPCR analysis of RhoB mRNA in shControl and shRhoA NRCF (means ± SEM, n= 6, values were normalized to PBGD and are given relative to shControl) (left). Representative immunoblot of RhoC and β-actin in shControl and shRhoA NRCF (middle) and quantitative analysis of RhoC expression normalized to β-actin (means ± SEM, n = 4) (right). The relative change in shRhoA to shControl is given.

To determine if the lentivirally infected fibroblasts still respond to an extracellular stimulus, a RhoA activity assay was performed. ShControl and shRhoA NRCF were stimulated with 100 nM angiotensin II (Ang II) for 30 sec or left untreated and the amount of RhoA-GTP was detected. It could be shown that in shControl NRCF RhoA was clearly activated by Ang II whereas in shRhoA NRCF no activation was detectable and the amount of total RhoA was strongly decreased.
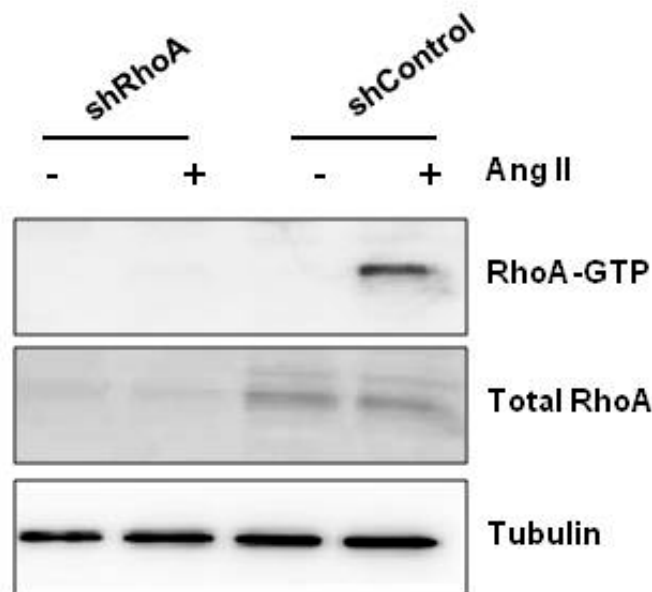

Figure 5.2: Angiotensin II-dependent RhoA activation in shRhoA and shControl NRCF
Serum-starved shControl and shRhoA NRCF were treated with 100 nM angiotensin II for 30 sec, lysed and RhoA-GTP was precipitated. Shown is the immunoblot analysis of RhoA-GTP, total RhoA and tubulin as loading control.

5.1.2   RhoA knockdown disrupts the cytoskeleton and changes cell morphology

In the next step the impact of the reduced RhoA expression on the cell morphology was analyzed. By staining of the actin cytoskeleton (Figure 5.3 A) and determination of the cell area and perimeter it was found that by 75% reduction in RhoA expression a 2-fold and 1.5-fold increase in area and perimeter, respectively, could be detected compared to shControl NRCF (Figure 5.3 B). To further validate whether this increase was due to general cell growth or to a change in adhesion low voltage field resistance measurement of detached cells were performed, however, no change could be detected in the volume of both cell types (Figure 5.3 B).
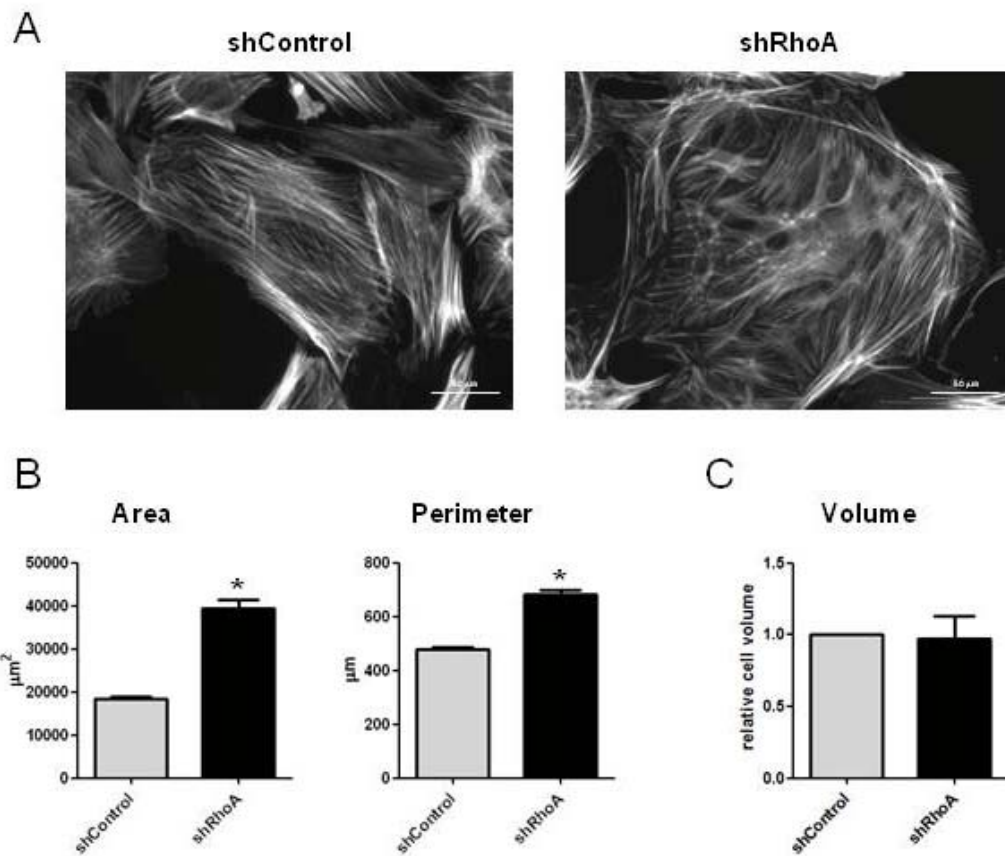
Figure 5.3: Evaluation of changes in cell morphology and volume of shControl and shRhoA NRCF *A) Representative actin stainings with TRITC-phalloidin of shControl (left) and shRhoA (right) cells. B) Quantification of cell area (left) and perimeter (right) of shControl and shRhoA NRCF were performed (means ± SEM; n = 3, at least 50 cells per condition and experiment were analyzed, *p < 0.05). C) Cell volume of detached shControl and shRhoA NRCF were measured by resistance in a pulsed low voltage field. The relative change of shRhoA NRCF volume compared to shControl is given (means ± SEM, n = 5).*

5.1.3   Reduction of RhoA influences cytoskeletal protein expression

Since RhoA is known to be a strong regulator of the cytoskeleton, the expression of proteins found in actin filaments, intermediate filaments and microtubules was investigated by immunoblot analyses (Figure 5.5 A).
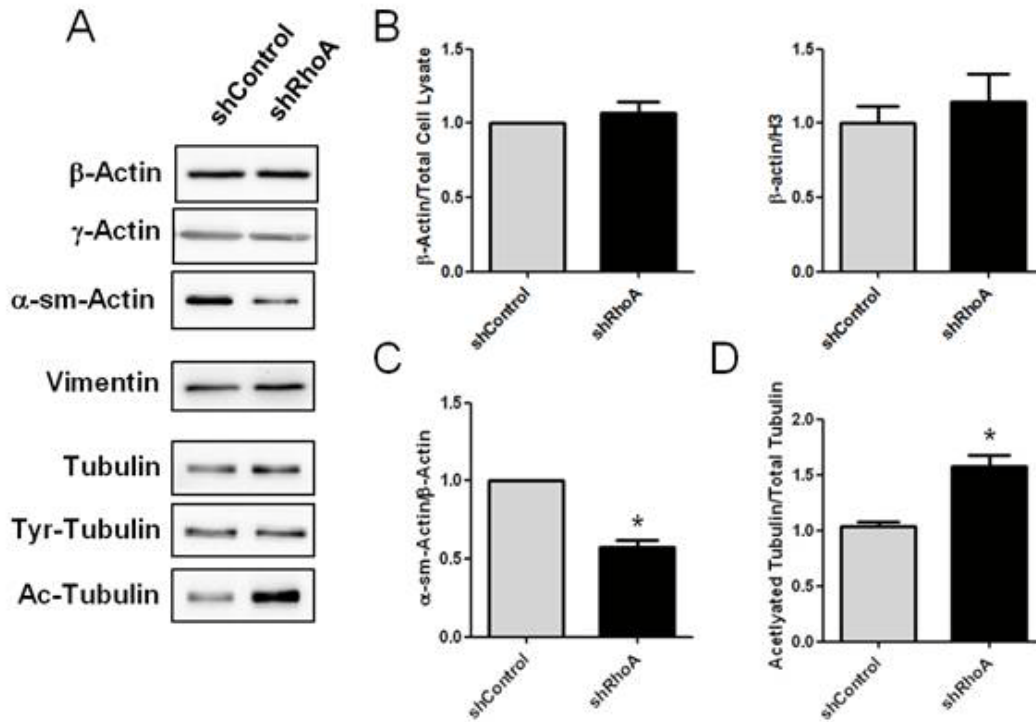

Figure 5.4: Immunoblot analyses of changes in cytoskeletal protein expression and modification A) *Representative immunoblots of cytoskeletal proteins in shControl and shRhoA NRCF lysates are shown. B) Quantification of β-actin expression in equal amounts of total cell lysates (left) and normalized to histone H3 (H3) (right) is shown. The relative changes in shRhoA versus shControl are given (means ± SEM, n = 7). C) Quantification of α-sm-actin expression in shRhoA NRCF normalized to β-actin and given relative to shControl NRCF is shown (means ± SEM, n = 7, *p < 0.05). D) Quantification of acetylated tubulin in shRhoA NRCF normalized to total tubulin and given relative to shControl NRCF is shown (means ± SEM, n = 12, *p < 0.05).*

First, it was determined whether β-actin is a proper loading control for immunoblot analyses by quantification of β-actin expression in relation to the total amount of analyzed cell lysates and by normalization to histone H3 expression. In neither case a change in β-actin expression in shRhoA NRCF could be detected (Figure 5.5 B). By using then β-actin as a

loading control, it could be shown that the myofibroblast marker α-smooth-muscle actin (α-sm-actin) was downregulated by 43% in shRhoA NRCF (Figure 5.5 C). In addition, the post-translationally modified acetylated tubulin was increased by 50% (Figure 5.5 D) while all other analyzed proteins like γ-actin, vimentin, tubulin and the tyrosine-modified tubulin were found unchanged (Figure 5.5 A).

To validate whether the increase in the acetylated tubulin fraction in shRhoA NRCF was due to a change in the expression of the main tubulin-deacetylase HDAC6, qPCR and immunoblot analyses were performed. In both cases changes could be detected neither on the mRNA nor on the protein levels (Figure 5.5).
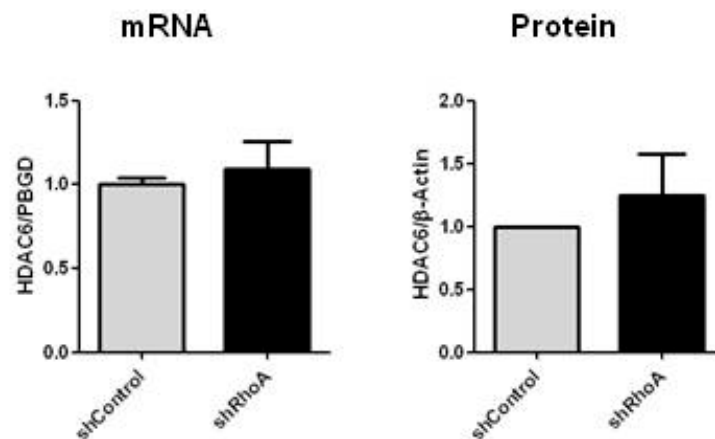
Figure 5.5: Evaluation of HDAC6 expression on in shRhoA and shControl NRCF *Left: qPCR analysis of HDAC6 mRNA in shControl and shRhoA NRCF (means ± SEM, n = 6, values were normalized to PBGD and are given relative to shControl). Right: Quantification of immunoblot analysis of HDAC6 protein normalized to β-actin in shRhoA NRCF compared to shControl is given (means ± SEM, n = 4).*

To determine whether other proteins showed a different acetylation level in shRhoA compared to shControl NRCF an immunoblot was performed using an anti-acetylated-lysine antibody. In this experiment both the cell lysates and the particulate fractions were analyzed. As shown in figure 5.6 no further differences between shControl and shRhoA NRCF could be found.

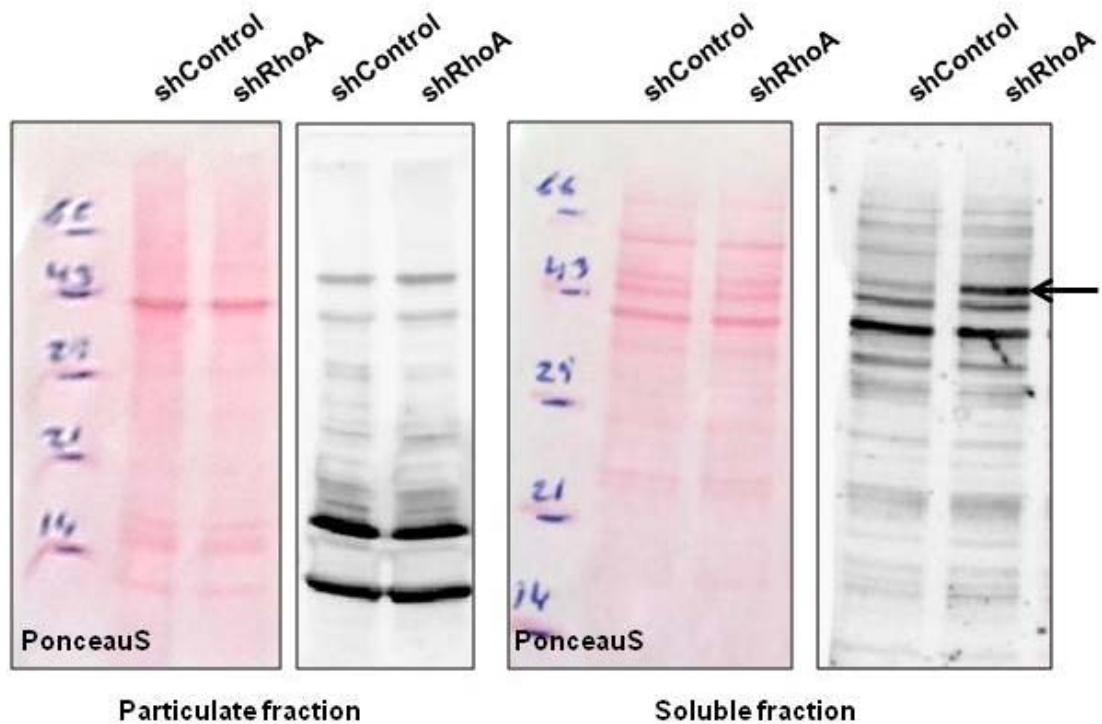**Figure 5.6: Analysis of protein acetylation in the particulate and soluble fractions of shRhoA and shControl NRCF** *Immunoblot analysis of the protein acetylation pattern in soluble and particulate fractions of whole cell homogenates from shControl and shRhoA NRCF were performed. Shown are the ponceauS stainings and the corresponding immunoblots using an anti-acetyl-lysine antibody. The arrow marks the size of tubulin.*

5.1.4   Actin structures of higher order are reduced in RhoA knockdown cells

In various cell types i.e. embryonic fibroblasts or HeLa cells, RhoA was connected to the assembly and turnover of cytoskeletal actin structures, especially stress fibers. In NRCF the knockdown of RhoA caused not only a reduction in stress fiber formation but also in other higher order actin structures like geodesic domes. Quantification of geodesic domes in shControl and shRhoA showed a significant lower number of cells carrying this highly complex actin networks (Figure 5.7).
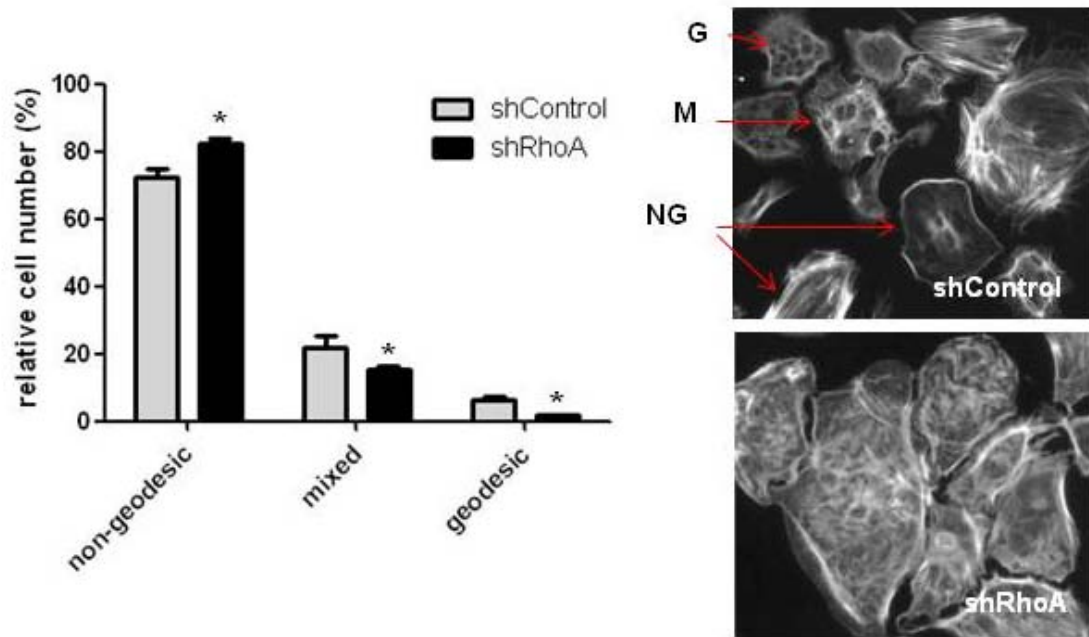
Figure 5.7: Evaluation of geodesic dome structures in shRhoA and shControl NRCF
Left: The numbers of geodesic (G), mixed (M) and non-geodesic (NG) cells were evaluated in shRhoA and shControl NRCF and are given as relative changes in percent of the total cell number (means ± SEM; n = 3, at least 50 cells per condition and experiment were analyzed, *p < 0.05). Right: Representative TRITC-phalloidin stainings of actin structures in shControl and shRhoA NRCF are shown.

5.1.5   Localization of cytoskeletal proteins is not altered in lentiviral-infected NRCF

To further analyze whether a rearrangement of the different actin isoforms could be detected in shRhoA NRCF, isoform-specific antibodies were used for immunofluorescence analysis. As shown in Figure 5.8 both β- and γ- actin showed a changed organization in shRhoA NRCF compared to shControl NRCF.
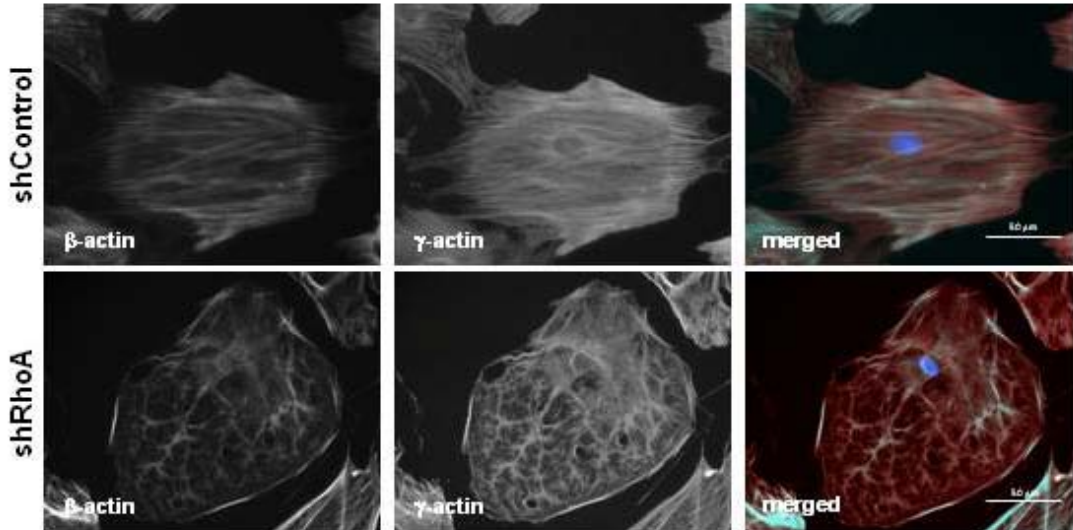
Figure 5.8: Immunostaining of β- and γ-actin isoforms in shRhoA and shControl NRCF
Detection of actin isoforms β- (green) and γ-actin (red) by immunofluorescence staining of shControl and shRhoA NRCF. In addition, the cell nuclei were stained with DAPI (blue) (320x).

As shown above by immunoblot analysis the NRCF express besides β- and γ-actin also α-sm-actin, which was found to be reduced in shRhoA NRCF. Detection of α-sm-actin by immunofluorescence showed that this actin isoform can be detected in the whole cell but with a higher accumulation in the cell middle. This was true for shControl as well as shRhoA NRCF (Figure 5.9).
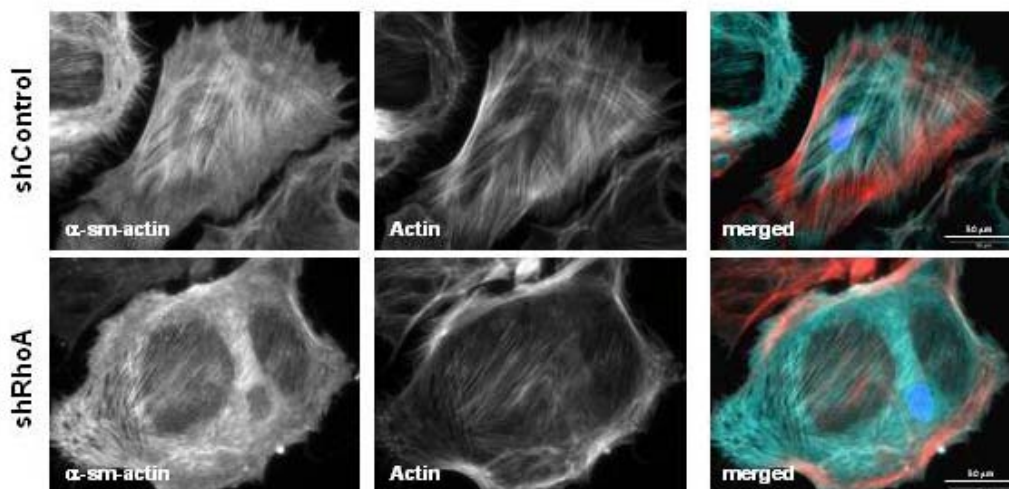
Figure 5.9: Immunostaining of α-sm-actin in shRhoA and shControl NRCF *Detection of α-sm-actin (green) by immunofluorescence staining and total actin by TRITC-phalloidin (red)*

of shControl and shRhoA NRCF. In addition, the cell nuclei were stained with DAPI (blue) (320x).

In addition to actin filament proteins, the intermediate filament protein vimentin and the microtubule protein α-tubulin were stained by specific antibodies in shRhoA and shControl NRCF. As shown in figure 5.10 no obvious changes could be detected in the distribution or integrity of both filaments.

Figure 5.10: Immunostaining of vimentin and α-tubulin in shRhoA and shControl NRCF *Detection of vimentin (upper two panels, green) and α-tubulin (lower two panels, green) by immunofluorescence staining and total actin by TRITC-phalloidin (red) of shControl and shRhoA NRCF. In addition, the cell nuclei were stained with DAPI (blue) (320x).*

In contrast to α-tubulin, the posttranslational modified acetylated tubulin was found significantly upregulated in immunoblot analysis. Interestingly, immunofluorescence staining of acetylated tubulin in shControl and shRhoA NRCF showed a condensed area of acetylated microtubules in the perinuclear region. In a co-staining of acetylated tubulin with wheat germ agglutinin (WGA) the condensed area was found to be in the area of the Golgi apparatus (Figure 5.11).
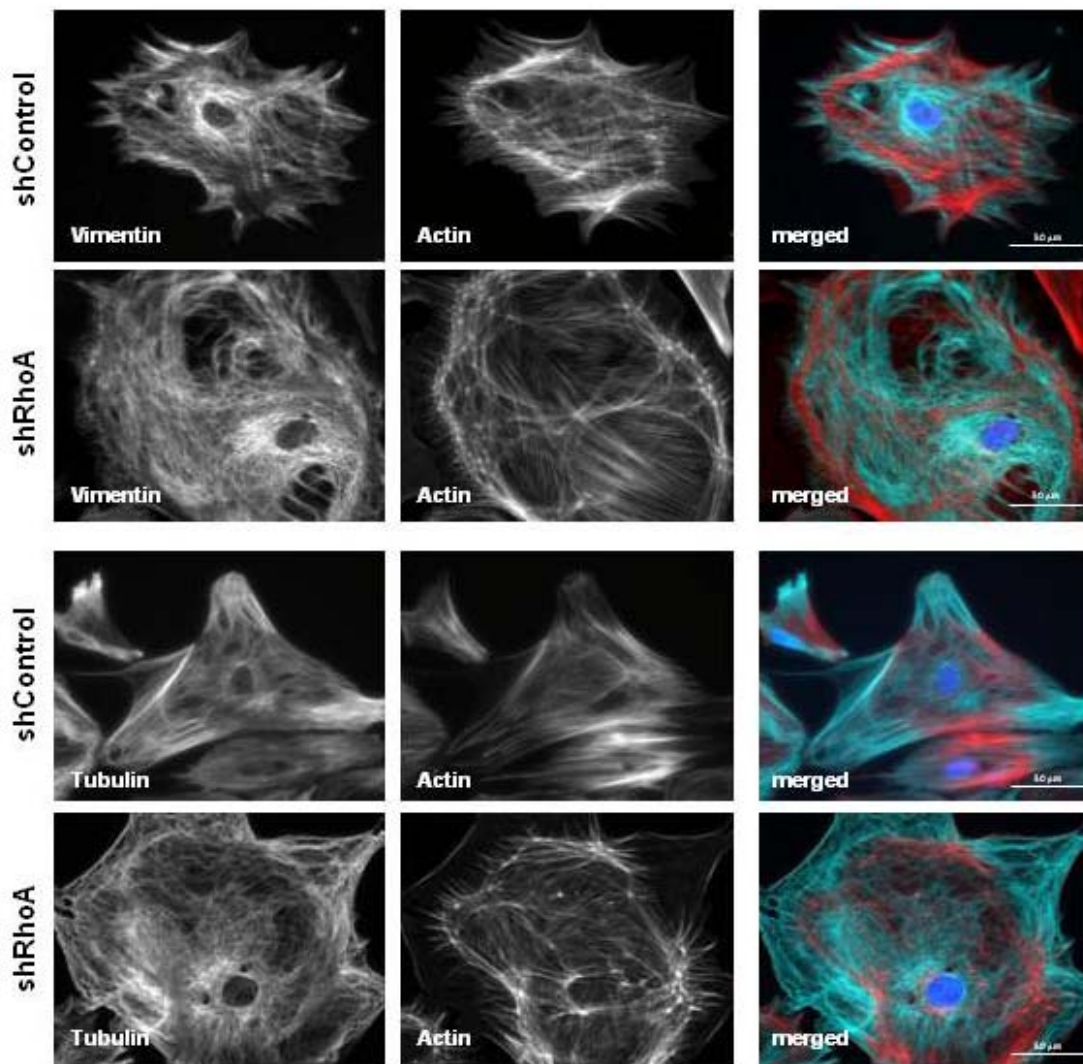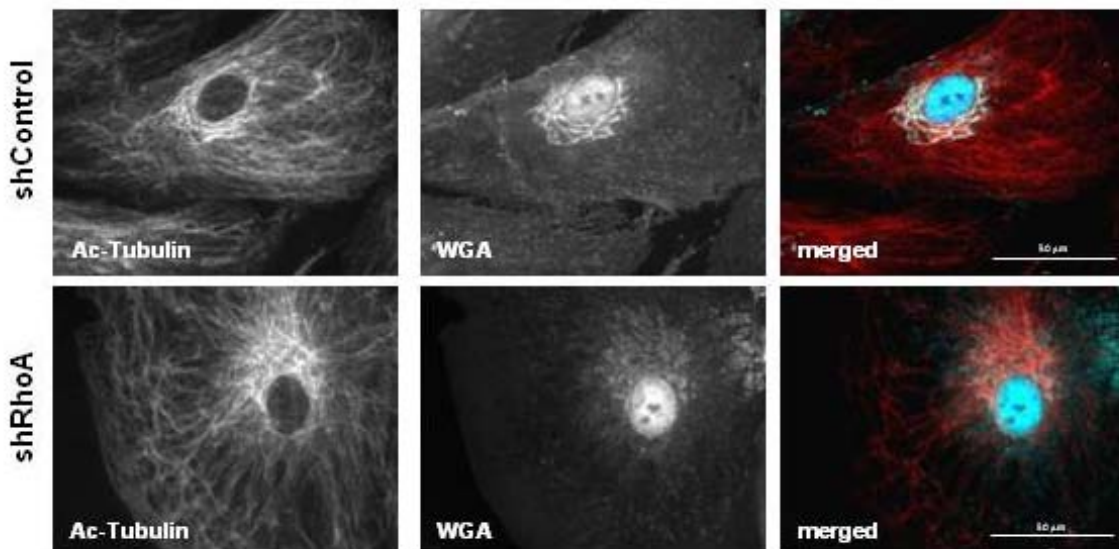

Figure 5.11: Co-staining of acetylated tubulin and the Golgi apparatus in shRhoA and shControl NRCF *Detection of acetylated tubulin (red) by immunofluorescence staining and of the Golgi apparatus by Alexa Fluor 488-labeled wheat germ agglutinin (green) in shControl and shRhoA NRCF. In addition, the cell nuclei were stained with DAPI (blue) (400x).*

5.1.6 The Golgi apparatus morphology is changed in lentiviral-infected NRCF

The condensed area of actylated tubulin below the Golgi apparatus led to the hypothesis that this tubulin modification is important for Golgi morphology and that Golgi size and density could be influenced by a change in acetylation level and thus by RhoA.

WGA-stainings of Golgi membranes in shControl and shRhoA NRCF showed a clear change in Golgi morphology. The morphometric analysis of Golgi size and density revealed that the area of Golgi membranes is not larger but significantly more condensed in shRhoA compared to shControl NRCF (Figure 5.12).
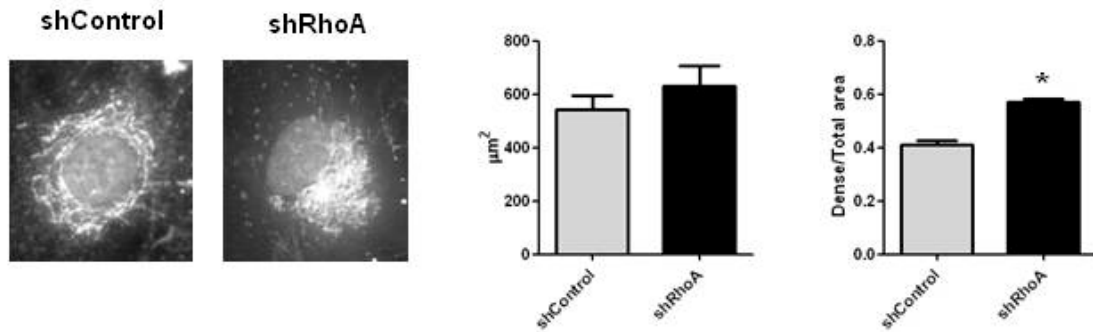
Figure 5.12: Evaluation of the Golgi apparatus size and density in shRhoA and shControl NRCF *Representative fluorescence stainings of the Golgi apparatus by Alexa Fluor 488-labeled WGA (640x) (left). Morphometric analysis of Golgi size (middle) and density (right) of shControl and shRhoA NRCF (means ± SEM; n = 3, at least 10 cells per condition and experiment were analyzed, *p < 0.05).*

5.1.7 Tubastatin A rescues the Golgi apparatus in RhoA knockdown cells

Upon treatment with the HDAC6 inhibitor tubastatin A (TubA), which induces an increase in acetylation of tubulin (see figure 5.13), it was found that this hyperacetylation stabilizes the Golgi membrane network in shRhoA NRCF. The increased density of the Golgi stacks in shRhoA NRCF could be reversed by application of TubA as assed by WGA-staining and morphometric analyses. Interestingly, TubA had no significant impact on the structure of the Golgi apparatus in shControl NRCF (Figure 5.13).
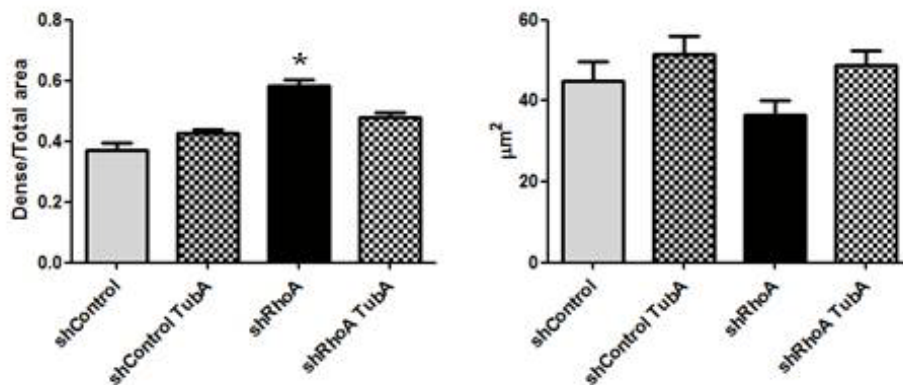
Figure 5.13: Analysis of the Golgi apparatus structure in shRhoA and shControl NRCF treated with TubA *Morphometric analysis of Golgi density (left) and size (right) of shControl and shRhoA NRCF in the absence and presence of 5 µg/mL TubA (means ± SEM; n = 3, at least 10 cells per condition and experiment were analyzed, *p < 0.05).*

5.1.8 Latrunculin A disrupts f-actin but does not change cytoskeletal protein expression in wild type NRCF

To investigate, whether the increase in tubulin acetylation is regulated by RhoA or a compensatory mechanism due to the loss of actin stress fibers or other actin structures, wild type NRCF were treated with the g-actin binding agent latrunculin A (LatA) to cause f-actin depolymerization. The concentration of LatA used created a mild phenotype similar to the RhoA knockdown.

Staining of total actin with TRITC-phalloidin showed a destabilized cytoskeleton with fragmented f-actin in LatA-treated cells after 4 h. At this early time point the collapse of the Golgi membrane network was detectable by WGA staining already (Figure 5.14 A). However, in immunoblot analyses neither a change in β- and α-sm-actin nor in total and acetylated tubulin was found even after treatment with 8.5 µM LatA for 24 h (Figure 5.14 B).
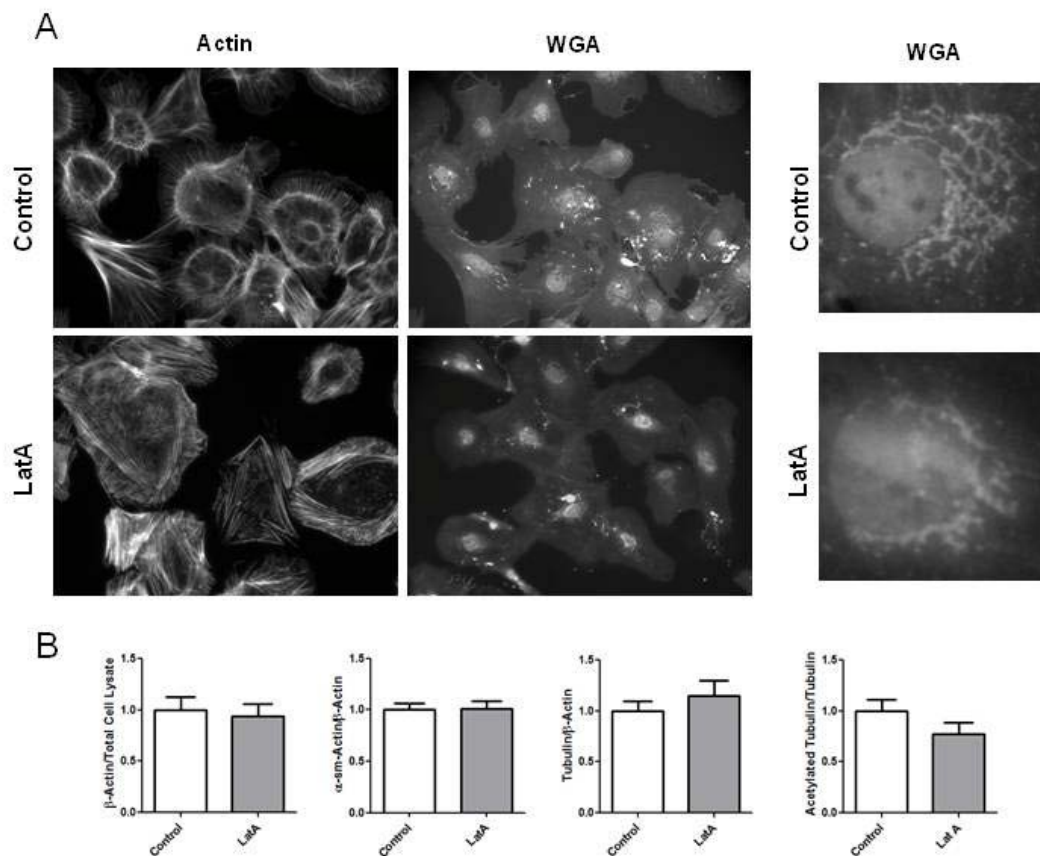
Figure 5.14: Impact of LatA on the cytoskeleton and the Golgi apparatus in NRCF *A) Representative stainings of total actin by TRITC-phalloidin and of the Golgi apparatus by Alexa Fluor 488-WGA in untreated cells and cells treated with 8.5 µM LatA for 4 h are presented (200x) (left). Representative magnified images of the Golgi for both conditions are shown in addition (640x)(right) B) Quantitative analysis by immunoblot of β-actin expression*

in equal amounts of total cell lysates (left), α-sm-actin expression (second from left) and tubulin expression (second from right) normalized to β-actin as well as expression of acetylated tubulin normalized to total tubulin (right) are shown. The relative changes in cells treated with 8.5 µM LatA for 24 h to untreated cells are given (means ± SEM, n = 7).

5.1.9   Inhibition of ROCK affects the cell morphology but not the Golgi structure or cytoskeletal protein expression in wild type NRCF

To identify the downstream effectors that mediate the impact of the RhoA knockdown on cell morphology, Golgi structure and protein expression, wild type NRCF were treated with ROCK and HDAC6 inhibitors. For ROCK inhibition 10 µM fasudil and 300 nM of the more specific H1152P, for HDAC6 inhibition 5 µg/mL TubA were used.

Fasudil- and H1152P-treated cells showed an increase in cell area by 100% and in perimeter by 25% compared to untreated control cells. In addition, stainings of the actin cytoskeleton revealed a loss of stress fibers, a disruption of actin structures and an epithelial-like phenotype very similar to the one found in shRhoA NRCF. The inhibition of HDAC6 by TubA on the other hand had no effect on cell morphology. The cells still showed prominent stress fibers and a myofibroblast-typical shape without any differences in area and perimeter compared to untreated control cells (Figure 5.15 A, B).
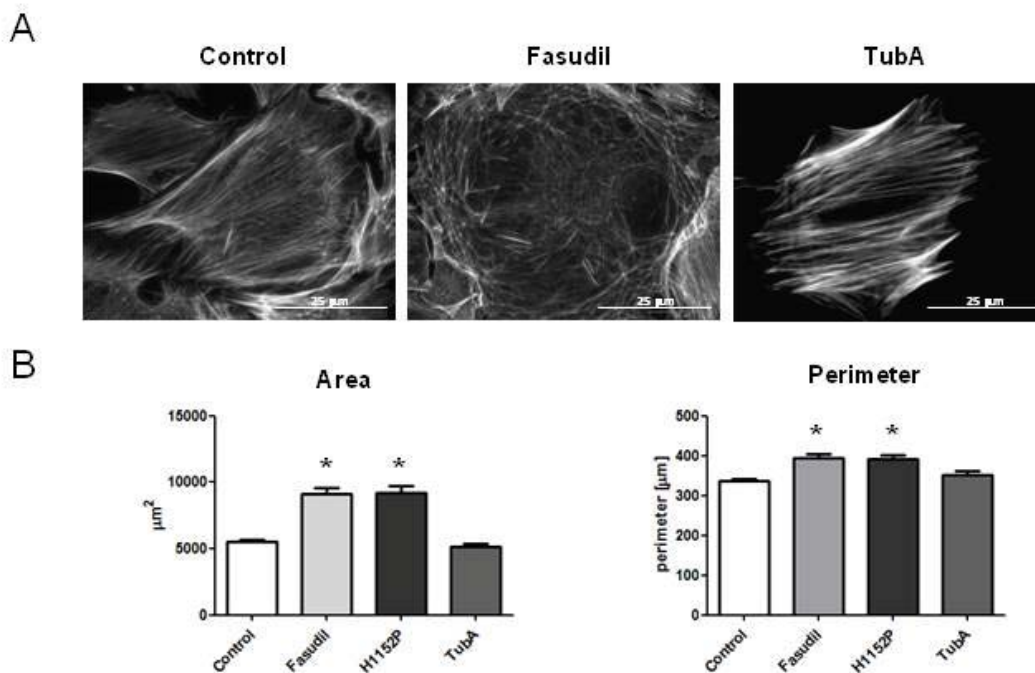
Figure 5.15: Morphometric analysis of fasudil-, H1152P- and TubA-treated wild type NRCF *A) Representative actin stainings with TRITC-phalloidin of untreated (control) (left) and fasudil- (10µM) (middle) or TubA- (5 µg/mL) (right) treated cells (400x). B) Quantification of cell area (left) and perimeter (right) of untreated or fasudil- (10 µM), H1152P- (300 nM) and TubA- (5 µg/mL) treated cells was performed (means ± SEM; n = 3, at least 50 cells per condition and experiment were analyzed, *p < 0.05).*

Morphological analysis of WGA-positive membranes showed, that neither the treatment with fasudil nor with TubA caused an increase in density or in size of the Golgi in wild type NRCF (Figure 5.16).
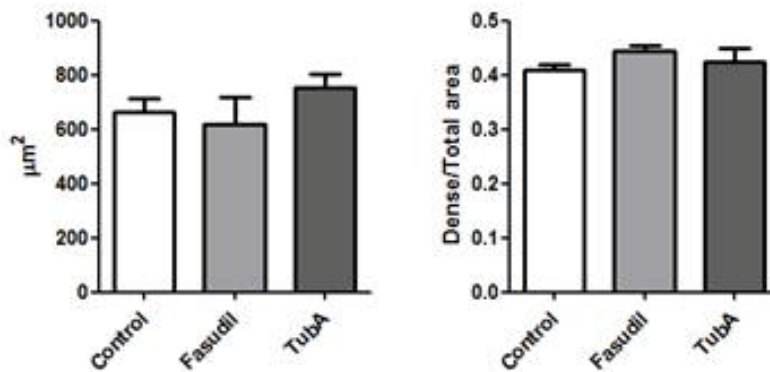
Figure 5.16: Morphometric analysis of the Golgi apparatus of wild type NRCF after fasudil and TubA treatment The *morphometric analysis of Golgi size (left) and density (right) of untreated (control), fasudil- (10 µM) and TubA- (5 µg/mL) treated cells is shown (means ± SEM; n = 3, at least 10 cells per condition and experiment were analyzed).*

In addition, the treatment of wild type NRCF with fasudil or TubA for 24 h as well as for 4 days did not influence the expression of α-sm-actin. Also, a change in acetylated tubulin in fasudil-treated cells could not be detected. The increase of acetylated tubulin by 4-fold in TubA-treated cells found, was caused by the inhibition of the HDAC6 activity (Figure 5.17).
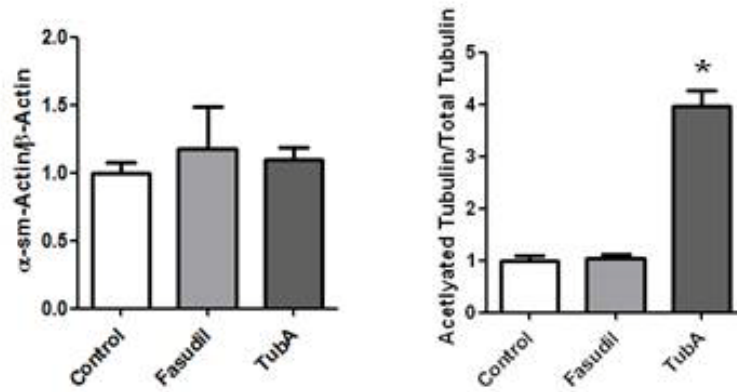
Figure 5.17: Analysis of protein expression in fasudil- and TubA-treated wild type NRCF *The quantification of α-sm-actin expression normalized to β-actin (left) and the acetylated tubulin expression normalized to total tubulin (right) in fasudil- (10 µM) and TubA- (5 µg/mL) treated cells relative to untreated (control) cells is shown (means ± SEM, n = 7).*

5.2 Influence of RhoA on the morphology of focal adhesion sites and on the adhesion velocity of NRCF

The observed changes in cell morphology and cytoskeletal arrangement in shRhoA NRCF led to the hypothesis that this could have an impact on the adhesion velocity and the arrangement of focal adhesion sites in these cells.

5.2.1 The RhoA knockdown leads to a random distribution and reduced length of focal adhesion sites

Vinculin, a protein associated with focal adhesion sites, was found to be unchanged in immunoblot analyses. However, immunofluorescence staining revealed a more random distribution of vinculin throughout shRhoA compared to shControl NRCF (Figure 5.18 A). The deviation from the cell axis and the length of focal adhesion sites was quantified in both cell types. In shRhoA NRCF focal adhesion sites were significantly shorter and had in average a higher angle of deviation from the cell axis compared to shControl NRCF (Figure 5.18 B).
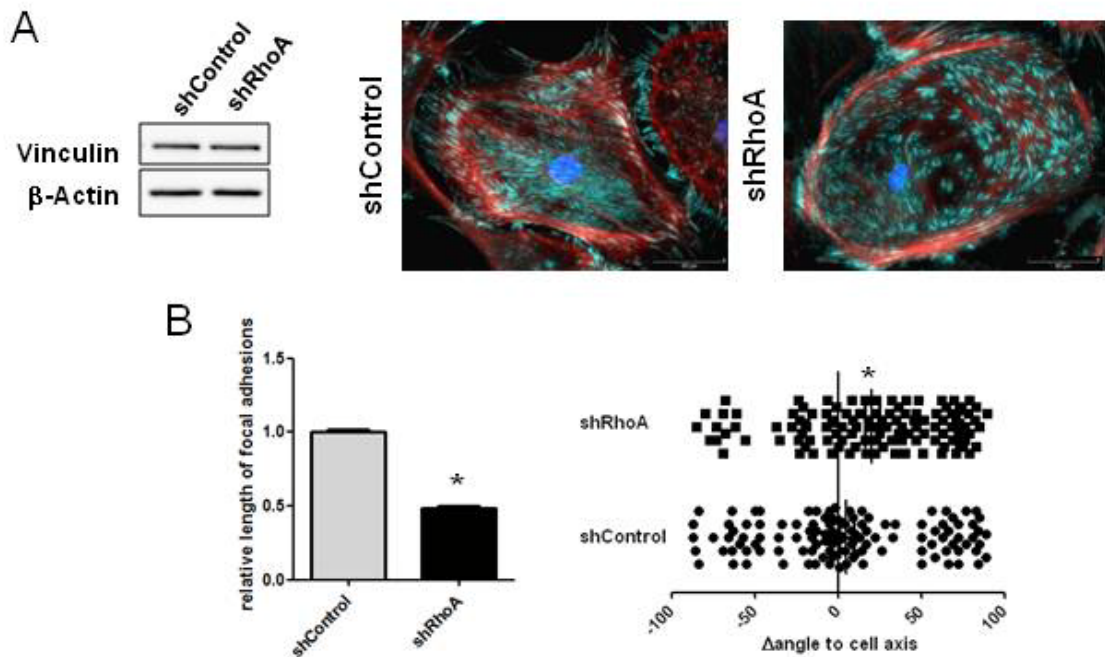
Figure 5.18: Analysis of focal adhesion site size and distribution in shRhoA and shControl NRCF *A) Representative immunoblots of vinculin and β-actin in shControl and shRhoA NRCF lysates are shown (left). Detection of vinculin (green) by immunofluorescence staining and total actin by TRITC-phalloidin (red) of shControl and shRhoA NRCF are presented. In addition, the cell nuclei were stained with DAPI (blue) (320x). B) Quantification of focal adhesion site length assessed by vinculin immunofluorescence staining in shRhoA NRCF relative to shControl NRCF is shown (means ± SEM; n = 3, at least 5 cells per condition and experiment were analyzed, *p < 0.05).*

5.2.2   The knockdown of RhoA increases the adhesion velocity

The knockdown of RhoA had also an impact on adhesion velocity. Both on a cell culture surface and on a collagen-coated surface more shRhoA NRCF were attached after 30 min compared to shControl NRCF (Figure 5.19). The overall difference between both cell types was higher when no collagen was used.
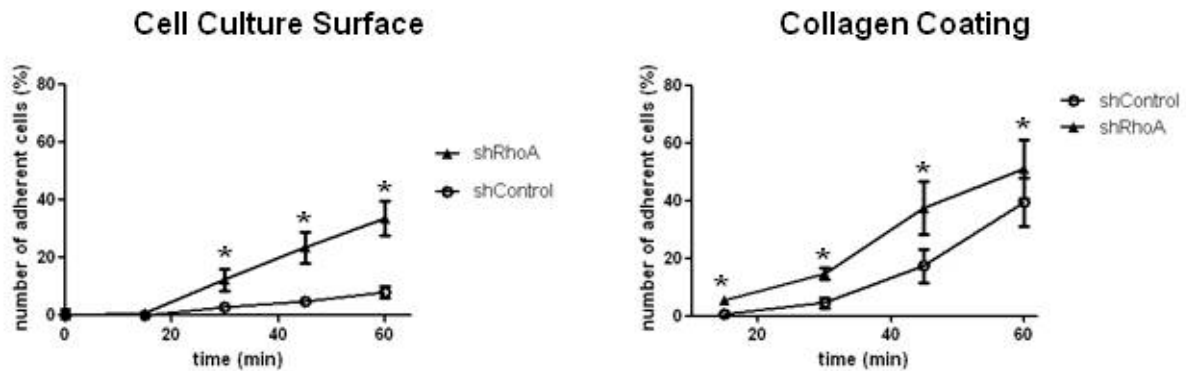
Figure 5.19: Analysis of the adhesion velocity of shRhoA and shControl NRCF
*Quantification of the number of adherent cells on cell culture-treated (left) and collagen-coated surfaces (right) is shown. The number of adherent shRhoA and shControl NRCF at each time point in percent is given (means ± SEM, n = 4, *p < 0.05).*

5.3   Influence of RhoA on the migration capacity of NRCF

Since shRhoA NRCF showed a random distribution of focal adhesion sites and a disruption of the cytoskeleton, it was investigated whether this could lead to impaired migratory performance. The same experiment was performed with fasudil- and TubA-treated wild type NRCF for comparison.

5.3.1   The knockdown of RhoA impairs the migration performance on a plane surface

The migration on a surface was assessed by tracking shControl and shRhoA as well as inhibitor-treated NRCF over 24 hours after visualizing the actin cytoskeleton with a GFP-tagged f-actin-binding polypeptide (LifeAct). ShRhoA NRCF showed a reduction in the migration velocity by 60% and a decreased absolute migration distance by 50% compared to shControl NRCF when tracked over a time course of 24 h (Figure 5.20 A). Similar findings were obtained by treating wild type NRCF with fasudil, which decreased the total distance by 60% and the migration velocity by 75%. TubA, on the other hand, reduced absolute distance and migration velocity only by about 15% and 20%, respectively (Figure 5.20 B).
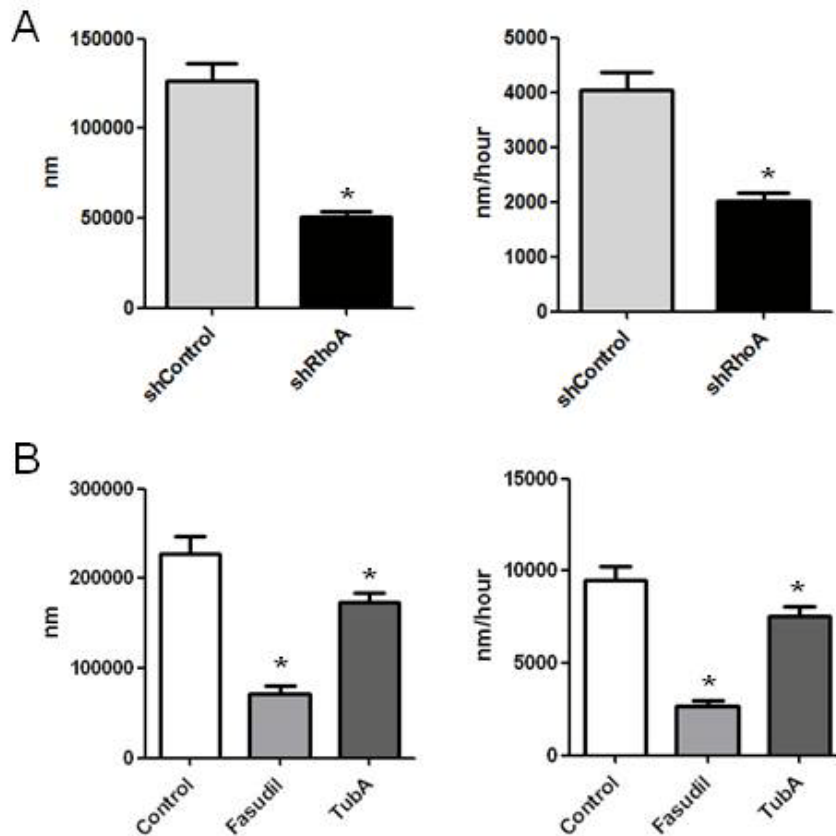
Figure 5.20: Analysis of the migration on a plane surface of shRhoA, shControl and inhibitor-treated NRCF *A) Quantification of the absolute distance migrated (left) and average migration velocity (right) of shControl and shRhoA NRCF on a cell culture surface over a time course of 24 h is shown (means ± SEM; n = 3, at least 14 cells per condition and experiment were analyzed, *p < 0.05). B) Quantification of the absolute distance migrated (left) and average migration velocity (right) of untreated (control), fasudil- (10 µM) and TubA- (5 µg/mL) treated cells on a cell culture surface over a time course of 24 h is shown (means ± SEM; n = 3, at least 14 cells per condition and experiment were analyzed, *p < 0.05).*

5.3.2   The invasive migration capacity is improved after RhoA knockdown but not after inhibitor treatment

The capacity of invasive migration through pores of lentiviral-infected and inhibitor-treated NRCF was assessed by seeding the cells on a porous membrane. The number of cells located inside the pores after a time course of 24 h was evaluated. All experiments were performed with and without a serum stimulus.

Under serum-reduced and high serum conditions shRhoA NRCF showed an improved invasive migration performance compared to shControl NRCF. In fact, the migration rate of

shRhoA NRCF without serum stimulation was already as high as the rate of shControl NRCF under high serum conditions (Figure 5.21 A).

The same experiment was performed with wild type NRCF and the indicated inhibitors. Cells treated with fasudil showed a 50% decrease in invasive migration in both reduced and high serum conditions compared to untreated cells. In addition, TubA decreased the number of cells inside the pores by 30% in serum-reduced conditions compared to control, however, this effect was diminished by a high serum stimulus (Figure 5.21 B).
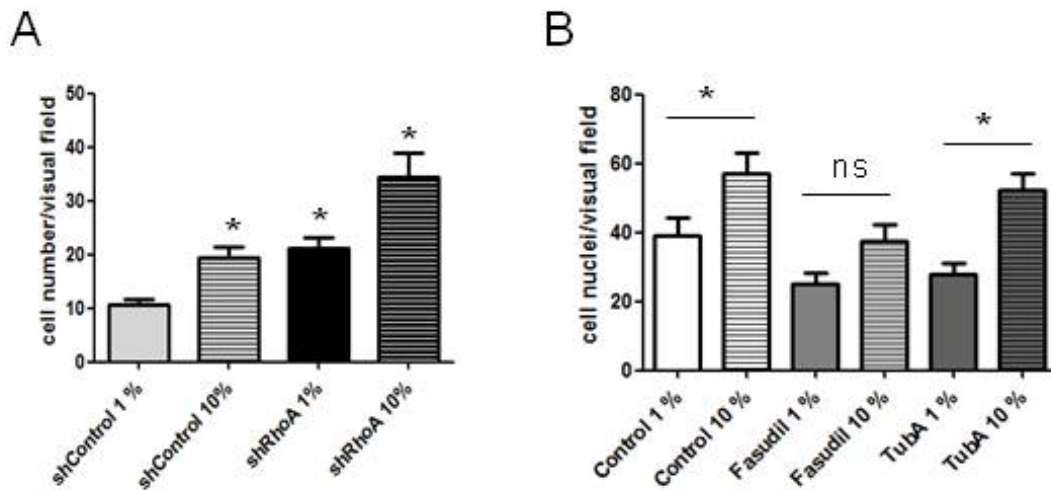
Figure 5.21: Analysis of the invasive migration of shRhoA, shControl and inhibitor-treated NRCF *A) Quantitative analysis of shControl and shRhoA NRCF inside a porous membrane (pore size: 8 µm) assessed by Hoechst staining in low serum (1%) and high serum (10%) conditions is presented. The absolute number of cells is given (means ± SEM, n = 5, *p < 0.05). B) Quantitative analysis of untreated (control), fasudil- (10 µM) and TubA- (5 µg/mL) treated cells inside a porous membrane (pore size: 8 µm) assessed by Hoechst staining in low serum (1%) and high serum (10%) conditions is shown. The absolute number of cells is given (means ± SEM, n = 5, *p < 0.05).*

5.4   Influence of RhoA on the proliferation of NRCF

The ability to proliferate is one of the typical myofibroblast characteristics that discriminates them from the quiescent fibroblasts. As the dynamics of the actin cytoskeleton and of microtubules are both essential for the process of cell division, it was investigated if the knockdown of RhoA as well as the inhibition of downstream effectors had an impact on the doubling time of NRCF.

5.4.1   The knockdown of RhoA increases the doubling time of NRCF as does HDAC6 inhibition

The doubling time of the lentiviral-infected or inhibitor-treated cells was evaluated by a proliferation-DAPI-assay with a serum stimulus over a time course of 4 days.

It was found that shRhoA NRCF had an increase in doubling time by 36% compared to shControl NRCF (Figure 5.22 A). Next, the number of apoptotic and necrotic cell in the cultures was evaluated to exclude an increase in cell death. In a co-staining of Annexin-V-FLUOS and propidium iodide no elevated levels and no difference between shRhoA and shControl NRCF were observed (Figure 5.22 B).
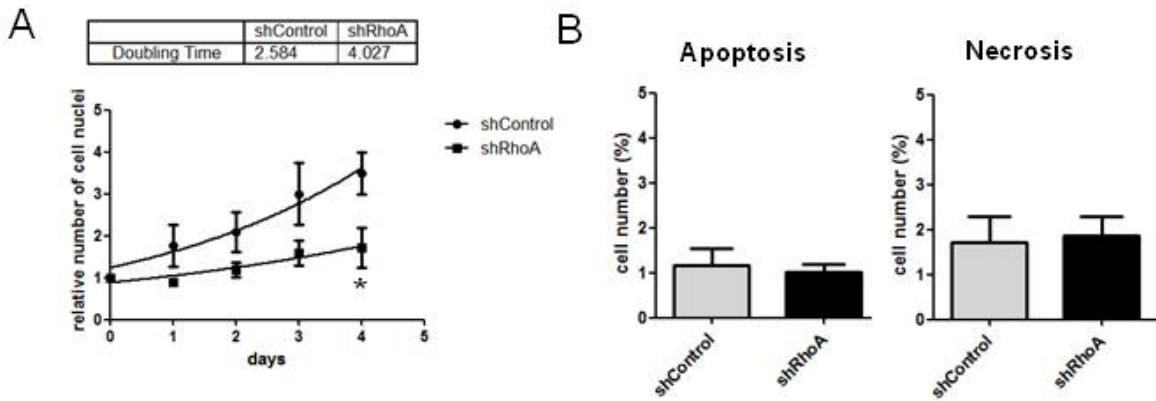
Figure 5.22: Analysis of proliferation and cell death of sRhoA and shControl NRCF *A) Shown is the quantitative analysis of the proliferation-DAPI assay of shControl and shRhoA NRCF with a serum stimulus (10% FCS) over a time course of 4 days. The absolute cell numbers at the different time points were assessed by DAPI staining. Given is the relative increase in cell number compared to day 0 (means ± SEM, n = 5, *p < 0.05). B) Quantification of apoptotic (left) and necrotic (right) shControl and shRhoA NRCF by Annexin-V-FLUOS and propidium iodide stainings is shown. The number of cells in percent is given (means ± SEM, n = 3)*

The found changes in cell doubling time were compared to wild type NRCF treated with fasudil, H1152P and TubA. First, ROCK inhibitors did not significantly change the doubling time of the cells compared to untreated cells. Second, the treatment of TubA was found to increase the cell doubling time by 48% (Figure 5.23).

	Control	Fasudil	H1152	Tub A
Doubling Time	1.659	1.307	1.291	3.186
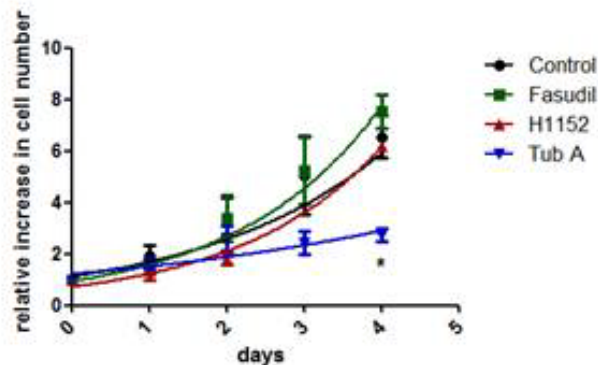
Figure 5.23: Analysis of the proliferation of NRCF treated with ROCK inhibitors and TubA *Shown is the quantitative analysis of the proliferation-DAPI assay of untreated (control), fasudil- (10µM), H1152P- (300nM) and TubA- (5µg/mL) treated NRCF with a serum stimulus (10% FCS) over a time course of 4 days. The absolute cell numbers at the different time points were assessed by DAPI staining. Given is the relative increase in cell number compared to day 0 (means ± SEM, n = 3, *p < 0.05).*

5.4.2 ROCK and HDAC6 inhibitors affect the actin cytoskeleton and the proliferation of normal adult human ventricular cardiac fibroblasts

Preliminary data about the effect of ROCK and HDAC6 inhibitors on normal adult human ventricular cardiac fibroblasts (NHCF-V) was obtained from actin stainings by TRITC-phalloidin and by a proliferation-DAPI-assay. A change in morphology to an epithelial-like phenotype after 24 hours of fasudil treatment was also observed in NHCF-V, while TubA had no effect on cell morphology (Figure 5.24 A). The proliferation-DAPI-assay was conducted with a serum stimulus over a time course of 4 days and the absolute cell number was determined at day 3 and 4. At both time points evaluated, TubA-treated NHCF-V showed a 50% lower absolute cell number, while with both ROCK inhibitors no change was observed compared to untreated cells (Figure 5.24 B).
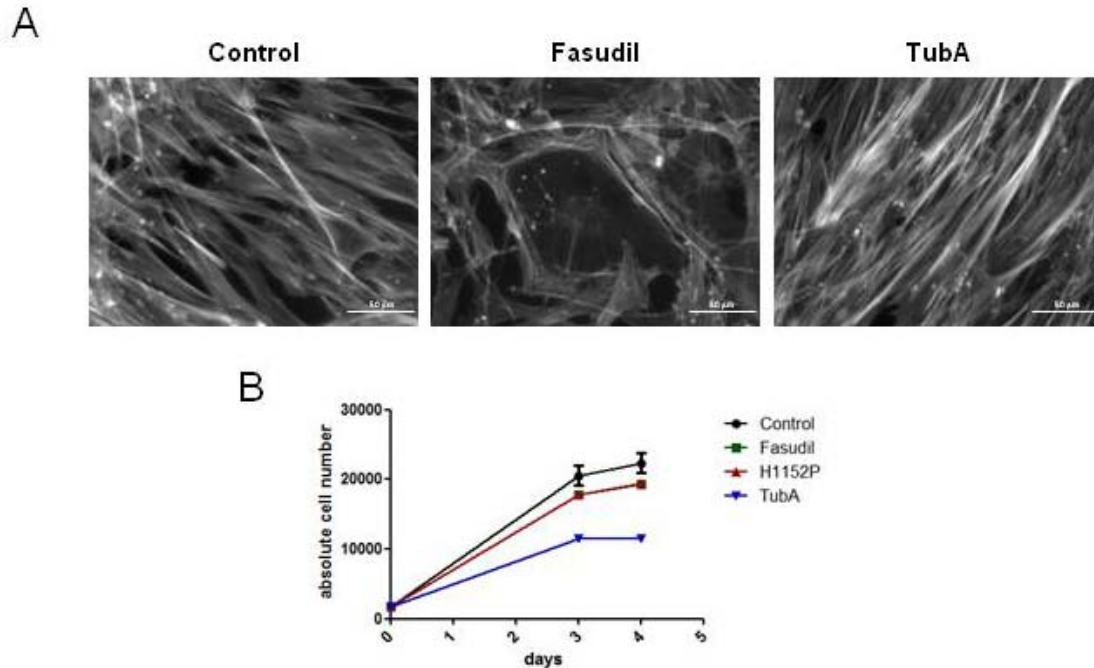
Figure 5.24: Analysis of the actin cytoskeleton and the proliferation after treatment with ROCK inhibitors and TubA in NHCF-V *A) Representative actin stainings with TRITC-phalloidin of untreated (control) (left), fasudil- (10µM) (middle) and TubA- (5 µg/mL) (right) treated NHCF-V is shown (320x). B) Shown is the quantitative analysis of a proliferation-DAPI assays of untreated (control), fasudil- (10µM), H1152P- (300nM) and TubA- (5µg/mL) treated NHCF-V with a serum stimulus (10% FCS) over a time course of 4 days. The absolute cell numbers at the different time points were assessed by DAPI staining (means ± SEM, n = 1, measured in 6 replicates).*

5.5   Influence of RhoA on the regulation of CTGF in NRCF

Due to the fact that RhoA has been shown to be involved in the secretion of matrix compounds and bioactive factors, it was hypothesized that the RhoA knockdown has also an impact on the secretion of the connective tissue growth factor (CTGF). CTGF is an intercellular signaling protein that was found to be secreted by cardiac fibroblasts as well as by cardiomyocytes and is elevated in fibrotic tissue [151].

5.5.1   CTGF co-localizes with the Golgi apparatus and acetylated tubulin

Immunofluorescence stainings for CTGF and acetylated tubulin as well as WGA stainings of the Golgi apparatus in shControl and shRhoA NRCF were performed. The staining revealed a co-localization of CTGF with the Golgi and in parts with the acetylated tubulin (Figure 5.25).
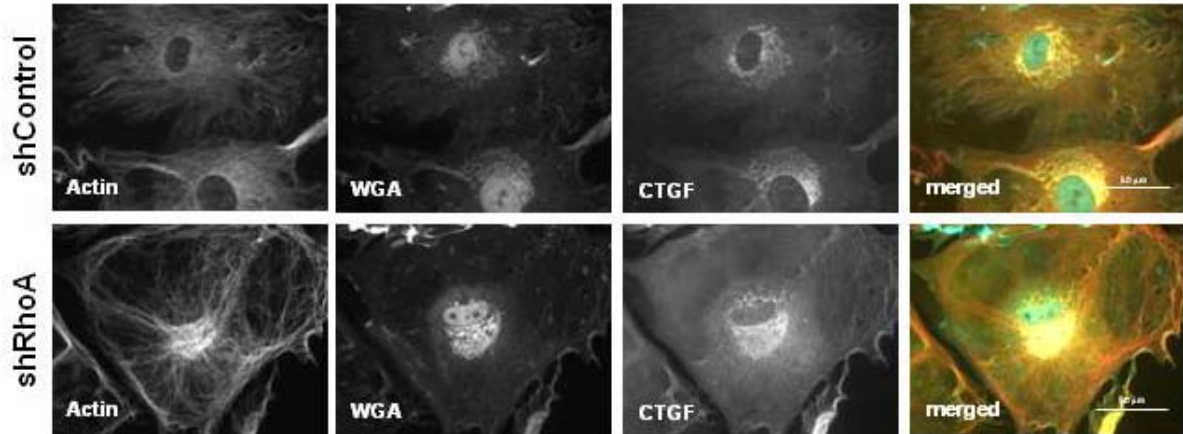
Figure 5.25: Co-stainings of acetylated tubulin, the Golgi apparatus and CTGF in shControl and shRhoA NRCF *Detection of acetylated tubulin (red) and CTGF (yellow) by immunofluorescence staining as well as staining of the Golgi apparatus by Alexa Fluor 488-labeled WGA (green) in shControl and shRhoA NRCF. In addition, the cell nuclei were stained with DAPI (blue) (320x).*

5.5.2   The knockdown of RhoA affects the expression and secretion of CTGF under low-serum conditions in NRCF

The co-localization of CTGF and the Golgi apparatus with the condensed area of acetylated tubulin led to the hypothesis that the knockdown of RhoA, which influenced the Golgi morphology and tubulin acetylation, could have an impact on the regulation of CTGF.

ShControl and shRhoA NRCF were cultured under serum-reduced (1%) or high serum (10%) conditions. The intracellular CTGF was then assessed by immunoblot analyses of the whole cell lysates, extracellular CTGF by the analysis of the culture medium, which revealed a decrease in intracellular CTGF by 30% and in extracellular CTGF by 40% in serum-reduced cultures of shRhoA compared to shControl NRCF (Figure 5.26).
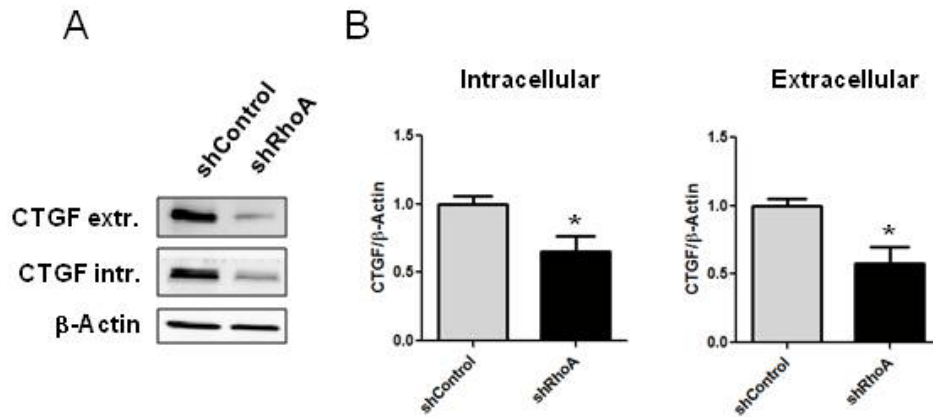
Figure 5.26: Analysis of CTGF expression and secretion in shRhoA and shControl NRCF under serum-reduced conditions *A) Representative immunoblots of extracellular (extr.) CTGF, intracellular (intr.) CTGF and β-actin from shControl and shRhoA NRCF cultured under serum-reduced conditions (1% FCS) are shown (left). B) Quantification of intracellular (middle) and extracellular (right) CTGF normalized to β-actin is shown. The relative changes in shRhoA versus shControl are given (means ± SEM, n = 7, *p < 0.05).*

In contrast to serum-reduced conditions, no change in the amount of the intracellular CTGF in shRhoA compared to shControl NRCF could be detected under high-serum conditions. Interestingly, the amount of extracellular CTGF was found to be increased by 30% in shRhoA NRCF (Figure 5.27).

Figure 5.27: Analysis of CTGF expression and secretion in shRhoA and shControl NRCF under high serum conditions *A) Representative immunoblots of extracellular (extr.) CTGF, intracellular (intr.) CTGF and β-actin from shControl and shRhoA NRCF cultured under high serum conditions (10% FCS) are shown (left). B) Quantification of intracellular*

(middle) and extracellular (right) CTGF normalized to β-actin is shown. The relative changes in shRhoA versus shControl are given (means ± SEM, n = 6, *p < 0.05).

5.5.3 Hyperacetylated tubulin increases extracellular CTGF solely in RhoA knockdown NRCF

Next the impact of acetylated tubulin on extracellular and intracellular CTGF was investigated. It was hypothesized that hyperacetylation of tubulin induced by TubA treatment can influence intracellular and extracellular CTGF amounts in lentiviral-infected cells.

To investigate this, shControl and shRhoA NRCF were treated with TubA for 24 h under high-serum conditions. First, it was found that TubA had no impact on the intracellular level of CTGF in shRhoA or shControl and on the extracellular CTGF in shControl NRCF. Second, the hyperacetylation of tubulin induced by TubA increased the extracellular CTGF in shRhoA NRCF up to 70% compared to shControl (Figure 5.28).

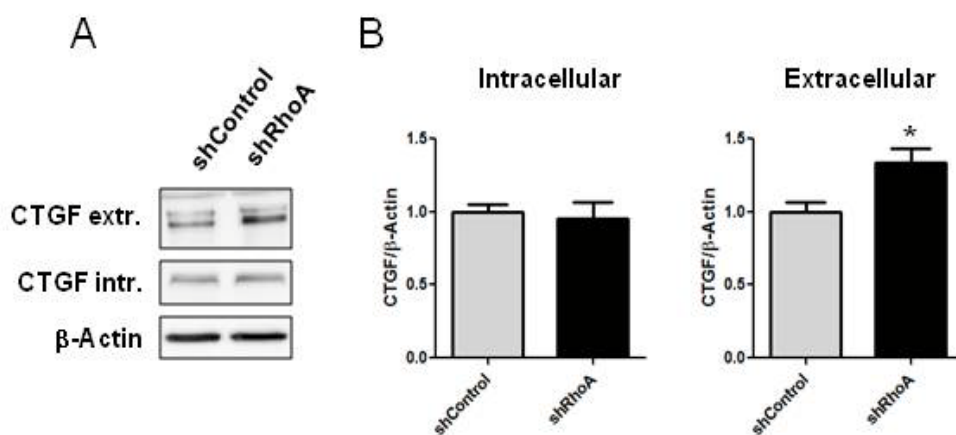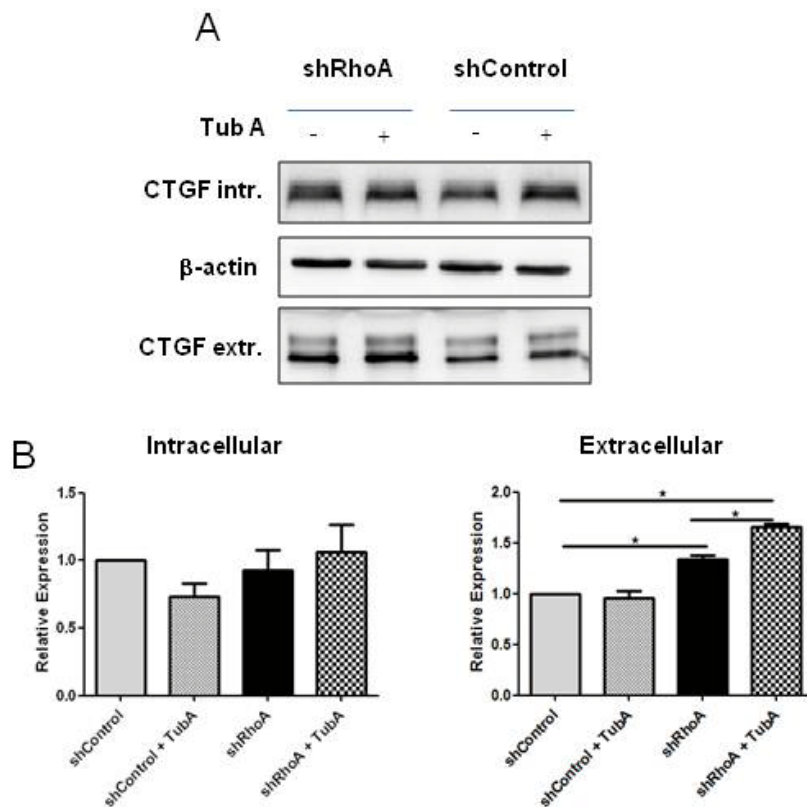**Figure 5.28: Analysis of CTGF expression and secretion in shRhoA and shControl NRCF under high serum conditions and additional TubA treatment** A) *Representative immunoblots of extracellular (extr.) CTGF, intracellular (intr.) CTGF and β-actin from shControl and shRhoA NRCF cultured under high serum conditions (10% FCS) and treated*

with 5 µg/mL Tub A as indicated are shown. B) Quantification of intracellular (left) and extracellular (right) CTGF normalized to β-actin is shown. The relative changes in shRhoA versus shControl are given (means ± SEM, n = 5, *p < 0.05).

5.6   Influence of RhoA on the contractile performance of engineered heart muscles

The analysis of engineered heart muscles (EHM) complemented with lentiviral-infected fibroblasts provided an insight into the function of these cells within a more "native" environment.

5.6.1   shRhoA NRCF complemented EHM develop less contractile force

Evaluation of the contractile parameters revealed that EHM complemented with additional shRhoA NRCF did not show a change in resting force (RF) compared to ones complemented with shControl NRCF. Interestingly, upon calcium stimulation shRhoA NRCF complemented EHM developed a force of contraction 40% lower than EHMs complemented with shControl NRCF at high calcium concentrations (Figure 5.29).
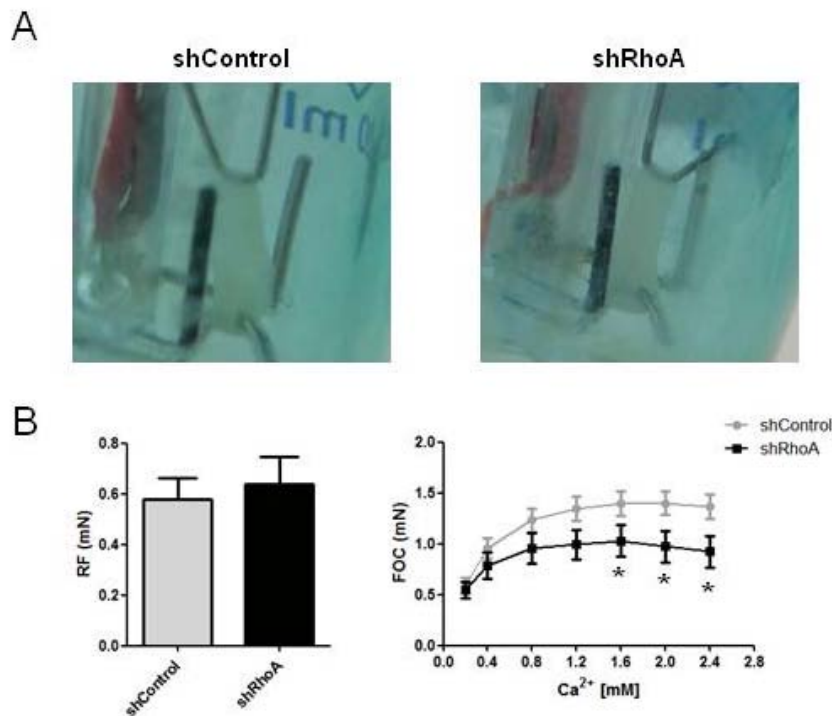
Figure 5.29: Contraction experiments of EHM complemented with shControl and shRhoA NRCF *Contraction experiments of engineered heart muscle (EHM) complemented with shControl and shRhoA NRCF. Evaluation of the resting force (RF, left) and the force of*

contraction (FOC) under increasing calcium concentrations (right) is shown (means ± SEM, n = 3, at least 2-4 EHMs per experiment and condition were analyzed, *p < 0.05).

5.6.2   EHM complemented with RhoA knockdown cells express less α-sm-actin and calsequestrin

After contraction experiments the final protein composition of the EHMs was assessed by immunoblot analyses. It was found that RhoA, β-actin, H3, tubulin and CTGF were unchanged in shRhoA NRCF complemented EHM compared to those containing shControl NRCF. An increasing trend in acetylated tubulin could be observed, however, was not found to be significant. Interestingly, expression levels of α-sm-actin and the cardiomyocyte marker calsequestrin were significantly decreased in shRhoA complemented EHM compared to shControl (Figure 5.30).
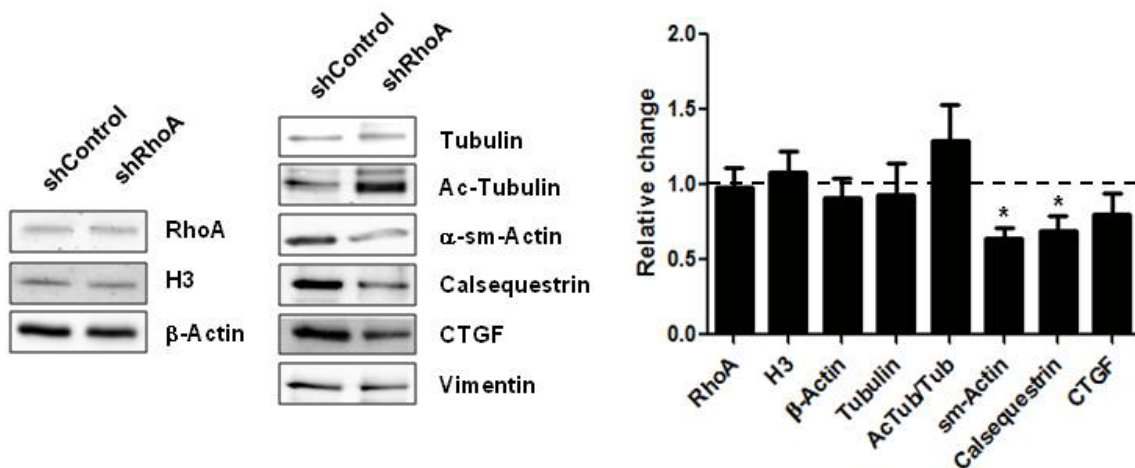
Figure 5.30: Analysis of protein composition of EHM complemented with shControl and shRhoA NRCF *Representative immunoblots of cytoskeletal proteins, calsequestrin, intracellular CTGF and histone H3 in cell lysates obtained from shControl and shRhoA NRCF complemented EHM are shown (left). Quantitative analysis of EHM protein composition normalized to vimentin is shown. The relative change of shRhoA NRCF complemented versus shControl NRCF complemented EHM is given (means ± SEM, n = 3, at least 2-4 EHMs per experiment and condition were pooled and analyzed, *p < 0.05) (right).*

5.7 Outlook

Generation of a BiFC-based biosensor plasmid to visualize RhoA activity in living cells

Based on the cloning strategy described in the chapter 3, a plasmid encoding for a fusion protein was generated containing the sequences for the N-terminus of venus-YFP, for RhoA with the Rho-binding domain of rhotekin (RBD) and for the C-terminus of venus-YFP. The plasmid was then transfected in HEK293A cells and the expression of the fusion protein was investigated by immunoblot analyses. Both the antibodies against RhoA and against YFP detected the sensor protein with an approx. molecular weight of 66 kDa (Figure 5.31).
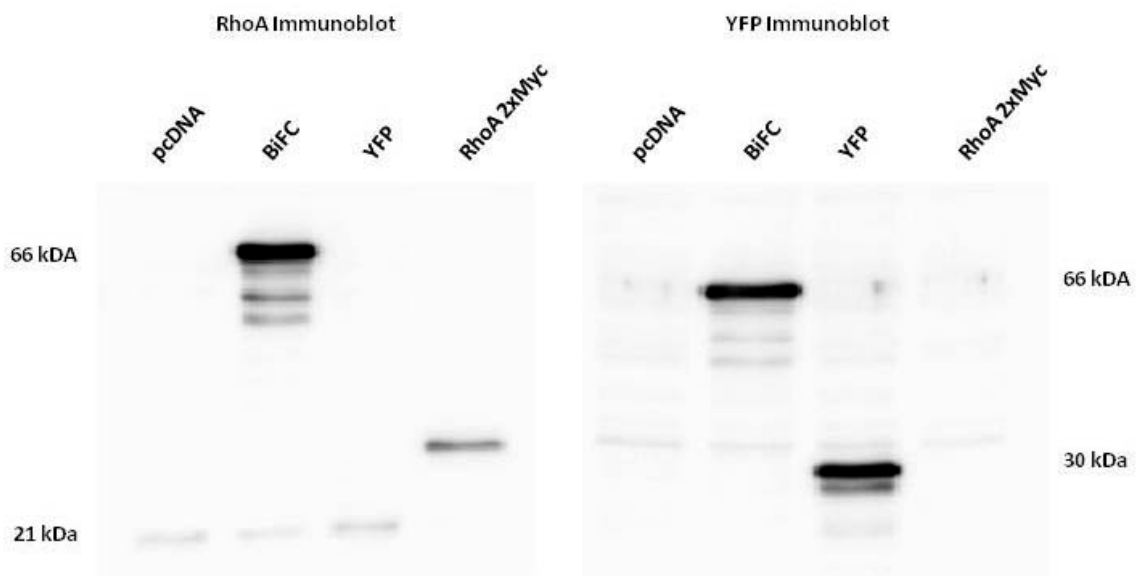
Figure 5.31: Analysis of the BiFC sensor protein expression in HEK293A cells by immunoblot *Immunoblot analysis of RhoA and YFP in whole cell lysates obtained from HEK293A cells transfected with pcDNA3.1(+)/Zeo (pcDNA), the BiFC sensor plasmid (BiFC), or two control plasmids coding for YFP and RhoA-2xMyc.*

The cells transfected with the sensor plasmid showed a fluorescence signal in the YFP channel and a mild rounded phenotype comparable with the cells transfected with wild type RhoA (Figure 5.32).
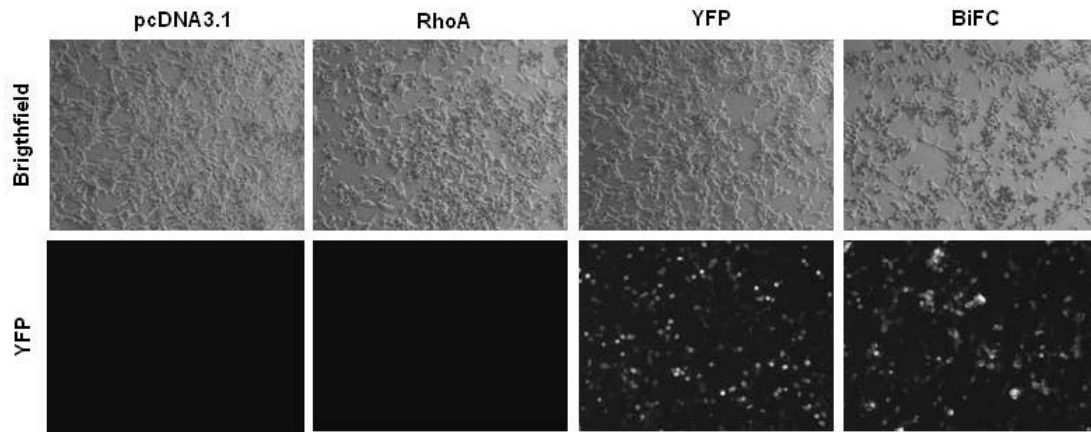
Figure 5.32: Analysis of the BiFC sensor expression in HEK293A cells by fluorescence microscopy *Representative bright field and fluorescence images of HEK293A cells transfected with pcDNA3.1(+)/Zeo ((pcDNA), the BiFC sensor plasmid (BiFC), or two control plasmids coding for YFP and RhoA-2xMyc.*

6. Discussion

During pathological remodeling the heart undergoes changes in function, shape and cellular composition. The transition of quiescent fibroblasts into myofibroblasts contributes to these changes by an increased ECM deposition creating interstitial and perivascular fibrosis or a scar tissue in case of myocardial infarction. The underlying signaling events inducing the transition of cardiac fibroblasts to myofibroblasts or controlling the typical myofibroblast characteristics like migration, proliferation or secretion are still not completely understood. Based on the well-known fact that in these processes the control of the actin cytoskeleton and microtubules is essential, a role of the monomeric GTPase RhoA, which is a prominent regulator of the cytoskeleton, was postulated. So far there is no systematic study on the function of RhoA in cardiac fibroblasts. Therefore, in this thesis a lentiviral-induced knockdown and small-molecule inhibitors were used to assess the impact of a reduction in RhoA expression as well as the inhibition of RhoA downstream effectors, respectively, on the cardiac myofibroblast.

6.1 RhoA influences the cytoskeleton, the cell morphology and the adhesion of NRCF

The knockdown of RhoA in NRCF by a small hairpin construct was shown to reduce the expression of RhoA on mRNA and protein level, while the two homolog family members RhoB and RhoC were not affected. Thus the knockdown and its outcome were considered to be specific.

In brief, the knockdown of RhoA resulted in a disruption of higher order actin structures, in an increase in the cell surface of adherent cell and a faster adhesion independent of the substratum. All this aspects are in line with the main postulated function of RhoA – its regulation of actin filaments. Although many of these features have not been assigned before to RhoA in cardiac fibroblasts, there is numerous literature demonstrating similar effects in other cell types.

For example, in this work the downregulation of RhoA led to a loss of geodesic actin dome structures in NRCF. These structures are rather rare and could not be observed in many other cells, but Malek et al. investigated in 2007 geodesic actin that forms from stress fibers in the perinuclear region of endothelial cells under hypertonic conditions. They could show

6. Discussion

that these complex actin structures are dependent on RhoA and ROCK as the use of C3T and the ROCK inhibitor Y-27632 completely suppressed their formation [152]. So far the function of these geodesic dome structures is not clear. Entcheva et al. postulated in 2009, that in NRCF geodesic actin is a precursor of stress fibers and gets transformed into those over time Furthermore, the authors showed that the nuclei in geodesic dome cells are more round-shaped and smaller, which is probably due to the lack of the intracellular tension as compared to stress fiber containing cells [153]. These findings might explain why in this work the shRhoA NRCF showed neither clear geodesic domes nor extensive stress fibers, but also why the knockdown of RhoA resulted in an increase in cell size. This is very likely due to the loss of the actin-dependent intracellular tension in case of stress fibers and the loss of the stability providing domes which are at least known from architecture to be highly resistant against tension and compression [154]. Moreover, the loss of these structures may also explain why the shRhoA NRCF display an increased adhesion velocity. Adhesion is a process which relays on the concerted activation of Rac1 and RhoA. Especially, in the early phase RhoA activation is counterproductive and inhibited by RhoGAPs like p190RhoGAP. Fibroblasts overexpressing a dominant negative variant of this GAP have been at least shown to display augmented cell spreading [155].

Mechanistically, the observed phenotype in shRhoA NRCF could be at least explained in parts. On the one hand, with respect to the actin cytoskeleton and the increased cell area similar results were obtained with the two ROCK inhibitors fasudil and H1152P indicating that the observed changes are ROCK-mediated. ROCK was already connected in 2007 by Harvey et al. to a morphological change in lung fibroblasts. The group demonstrated an increase in cell area after H1152P treatment and with a simultaneous reduction in stress fiber formation [156]. On the other hand, shRhoA NRCF displayed a reduction in the expression of the myofibroblast marker α-sm-actin [157-159] which is likely regulated by the MAL-induced activation of the SRF [76]. In this context, it has been shown that the integration of α-sm-actin in stress fibers leads to the formation of strong contractile fibrils and enables myofibroblasts to efficiently contract the ECM [93, 160] [161]. This process is especially of relevance after a myocardial infarction as a reduction in α-sm-actin levels in fibroblasts within the scarring area leads to poor wound closure and even to ventricular wall rupture [162].

Besides this, it is completely unclear what the role of the RhoA-dependent changes in the actin structures, in cell adhesion and spreading are within the native tissue. It can be assumed that in a heart, fibroblasts are neither of the pure stress fiber nor of the pure geodesic dome phenotype as the rigidity of the substratum, the tensile forces, the composition of the ECM and the paracrine environment is completely different than in a cell culture dish. However, the ability to react to changes in these parameters, as it occurs in

heart disease, very likely requires a response on the level of the actin cytoskeleton and thus requires RhoA. One of the processes which occur in heart disease and rely on such a response is cell migration.

6.2   RhoA influences NRCF migration

In this work, the knockdown of RhoA in NRCF led to decrease in cell migration on a plane surface which is easily explained by the disruption of the actin cytoskeleton and by the loss of cell polarity as demonstrated by vinculin staining. Similar data have been presented by different groups in various cell types and in accordance to the data presented in this thesis an involvement of ROCK has been discussed [163, 164] [165] [166].

More interestingly and probably more relevant in a tissue, the knockdown of RhoA in NRCF was found to improve the invasive migration. In pathological cardiac remodeling the invasive migration by myofibroblasts through the ECM is essential for the development of interstitial fibrosis and scar tissue and is enabled by secreting MMPs to degrade the scaffold in their path [80-83]. With the findings described in this thesis, RhoA can thus be connected to the invasive migratory performance of myofibroblasts. Mechanistically, it is not clear how RhoA regulates the invasive migration, especially, as an inhibition of ROCK led to the opposite effect, namely a reduction in migration. This discrepancy cannot be explained so far and has to be further investigated in the future.

6.3   RhoA controls myofibroblast proliferation by changes in tubulin stability

The ability to proliferate distinguishes the senescent fibroblast from its activated counterpart. The actin and tubulin cytoskeleton are known to be equally involved in the process of cytokinesis by forming the contractile cortical ring and separating the chromosomes. In this thesis, the proliferation rate was found to be decreased in shRhoA NRCF which could be shown to be dependent on the activity of HDAC6 ergo on an increase in tubulin acetylation. A direct link between RhoA and human atrial fibroblast proliferation was described by Porter et al. in 2004 where the reduction of active RhoA similarly reduced the proliferation rate [93]. The fact that HDAC6 inhibition and therefore stabile acetylated tubulin negatively regulate the proliferative capacity of cells was described before by Azuma et al. described in a mammary cancer cell line [167] and by Aguilar et al. in mouse fibroblasts [168]. The effect of

HDAC6 on proliferation in myofibroblasts has not been described so far. Nevertheless, the ability of myofibroblasts to proliferate is essential for pathological remodeling processes. In acute events, other myofibroblasts precursor from bone marrow like fibrocytes or endothelial cells undergoing EMT are recruited, however, the number of cells has to be increased similarly by proliferation of resident fibroblasts [103, 169].

Mechanistically, the link between RhoA and HDAC6 is not clear in cardiac fibroblasts. By this thesis at least the involvement of ROCK could be excluded as postulated before by Schofield et al. which demonstrated in HEK293 cells that ROCK can influence HDAC6 activity via the tubulin polymerization promoting protein 1 (TPPP1) [170]. Alternatively, mDia2 might be the mediator as shown before in osteoclasts [72]. Further studies have to clarify this issue to deepen the understanding of the mitogenic role of RhoA and HDAC6 in cardiac fibroblasts. Especially, as HDAC6 has been shown to plays a role in atrial fibrillation which is characterized by an activation and proliferation of atrial fibroblasts [93, 171, 172].

6.6   RhoA controls intracellular and extracellular CTGF and a change in Golgi morphology in NRCF

A quiescent fibroblast as found in the healthy cardiac tissue secretes ECM components just to maintain a slow constant matrix turnover. However, upon activation by a profibrotic stimulus or mechanic force myofibroblasts secrete a wide variety of cytokines and growth factors amongst them the connective tissue growth factor (CTGF). The downregulation of RhoA led in this thesis in serum-reduced conditions to a significant decrease in expression and secretion of CTGF. It was already shown before by Mun et al. and Laval et al. that RhoA [80] and ROCK inhibition [53] impaired CTGF expression in keloid fibroblasts and NRCF, respectively. In addition, the expression of CTGF was recently connected to the binding of the SRF [173]. To date, the RhoA mediated secretion of CTGF was not investigated in NRCF but was shown before to be processed through the Golgi in dermal fibroblasts [174]. Upon investigation, the Golgi membrane structure was found more condensed in shRhoA NRCF. The same effect on Golgi morphology was observed by Camera et al in neuronal cells after treatments with C3T [175] and by Lázaro-Diéguez et al. after treatment of vero cells with LatA [176] and therefore can be connected to RhoA activity and f-actin integrity. The downstream effector that mediated the condensation of the Golgi in shRhoA NRCF was not identified in this thesis but it was published before that the formin mDia1, which can be activated by RhoA, has a possible role in Golgi morphology [177]. The condensation of the Golgi structure was described by Ng et al. to induce a decrease, while a dispersion of the

membranes leads to an increase in secretory performance [178]. This could explain why the treatment with TubA that rescued the Golgi structure in shRhoA NRCF led to an improved secretion of CTGF. Whether the condensation of the Golgi or the knockdown of RhoA itself led to the decrease in intracellular and extracellular CTGF in shRhoA NRCF is not clear and needs further investigation. The role of CTGF in the heart is to date still obscure. It is considered a pro-fibrotic factor, while there is also growing evidence of its cardiomyocyte-protective function [179-182] in hypertrophic growth.

6.7   EHM complemented with shRhoA NRCF develop less contractile force and show signs of cardiomyocyte loss

In this these EHM were used a 3D tissue model to investigate the effect of a RhoA knockdown in NRCF on contractile force during calcium stimulation. It was found that shRhoA NRCF complemented EHMs showed no difference in resting tension, however, the contractile force with increasing stimulus was significantly reduced compared to shControl NRCF complemented EHM. The analyses of protein content revealed a significant reduction in cardiomyocyte marker calsequestrin as well as the myofibroblast marker α-sm-actin. The evaluation of contractile force development in EHMs complemented with RhoA knockdown fibroblasts has not been described before. Nevertheless, a comparable study was published by Mühlhäuser et al. in 2006. The group treated EHM with atorvastatin and performed contraction experiments using increasing concentrations of isoproterenol. It was found that atorvastatin had no effect on resting tension but decreased contractile force concentration-dependent up to 50% [183]. The reduction of the calsequestrin possibly illustrates a loss of cardiomyocytes in shRhoA NRCF complemented EHM which could explain the observed reduction in contractile force. Interestingly, a decreasing trend of the expression of CTGF was observed as well in shRhoA EMHs which gives a possible explanation for the loss of contractile cells. It was already described that CTGF has a pro-hypertrophic as well as an anti-apoptotic effect on cardiomyocytes and thus allow an adaptive growth response of the heart and therefore exerts a protective effect after increased workload [182, 184]. But also the changed regulation and secretion of other beneficial factors from cardiac fibroblasts is thinkable [185] Secretome analyses of cardiac fibroblasts with a regulation in RhoA expression will help in the future to further broaden the understanding of RhoA in the paracrine regulation of cardiomyocytes.

6.8   Conclusion

The data obtained in this thesis clearly argues for a major role of RhoA not only in myofibroblast characteristics but also in the maintenance of cell integrity and Golgi morphology. For the prominent downstream effectors of RhoA, investigated distinct functions and contributions to the myofibroblastic phenotype were identified. RhoA was therefore connected to the activation of cardiac fibroblasts seen in the induction of pathological remodeling, especially in cardiac fibrosis. Although the data collected in this thesis does not argue for RhoA as a potential drug target in the future, it increased the knowledge about its function in the cardiac fibroblasts and supports the already described beneficial effects of ROCK and HDAC6 inhibitors in the outcome of cardiovascular diseases including pulmonary arterial hypertension or atrial fibrillation, respectively.

7.   Literature

1.   Brown, J.H., D.P. Del Re, and M.A. Sussman, *The Rac and Rho hall of fame: a decade of hypertrophic signaling hits.* Circ Res, 2006. **98**(6): p. 730-42.
2.   Wennerberg, K., K.L. Rossman, and C.J. Der, *The Ras superfamily at a glance.* J Cell Sci, 2005. **118**(Pt 5): p. 843-6.
3.   F, C., *Arf GTPase-activating proteins and their potential role in cell migration and invasion.* Journal of Cell Adhesion and Migration, 2008. **2**(4): p. 258-262.
4.   Stenmark, H., et al., *Distinct structural elements of rab5 define its functional specificity.* Embo j, 1994. **13**(3): p. 575-83.
5.   Avis, J.M. and P.R. Clarke, *Ran, a GTPase involved in nuclear processes: its regulators and effectors.* J Cell Sci, 1996. **109 (Pt 10)**: p. 2423-7.
6.   Wennerberg, K. and C.J. Der, *Rho-family GTPases: it's not only Rac and Rho (and I like it).* J Cell Sci, 2004. **117**(Pt 8): p. 1301-12.
7.   Boureux, A., et al., *Evolution of the Rho family of ras-like GTPases in eukaryotes.* Mol Biol Evol, 2007. **24**(1): p. 203-16.
8.   Zong, H., K. Kaibuchi, and L.A. Quilliam, *The insert region of RhoA is essential for Rho kinase activation and cellular transformation.* Mol Cell Biol, 2001. **21**(16): p. 5287-98.
9.   Desrosiers, R.R., et al., *Modulation of Rho and cytoskeletal protein attachment to membranes by a prenylcysteine analog.* J Biol Chem, 2000. **275**(20): p. 14949-57.
10.   Faure, J. and M.C. Dagher, *Interactions between Rho GTPases and Rho GDP dissociation inhibitor (Rho-GDI).* Biochimie, 2001. **83**(5): p. 409-14.
11.   Triffo, S.B., et al., *Monitoring lipid anchor organization in cell membranes by PIE-FCCS.* J Am Chem Soc, 2012. **134**(26): p. 10833-42.
12.   Arbeloa, A., et al., *EspM2 is a RhoA guanine nucleotide exchange factor.* Cell Microbiol, 2010. **12**(5): p. 654-64.
13.   Jaiswal, M., et al., *Mechanistic insights into specificity, activity, and regulatory elements of the regulator of G-protein signaling (RGS)-containing Rho-specific guanine nucleotide exchange factors (GEFs) p115, PDZ-RhoGEF (PRG), and leukemia-associated RhoGEF (LARG).* J Biol Chem, 2011. **286**(20): p. 18202-12.
14.   Heo, J., R. Thapar, and S.L. Campbell, *Recognition and activation of Rho GTPases by Vav1 and Vav2 guanine nucleotide exchange factors.* Biochemistry, 2005. **44**(17): p. 6573-85.
15.   Cherfils, J. and M. Zeghouf, *Regulation of small GTPases by GEFs, GAPs, and GDIs.* Physiol Rev, 2013. **93**(1): p. 269-309.
16.   Scheffzek, K., et al., *The Ras-RasGAP complex: structural basis for GTPase activation and its loss in oncogenic Ras mutants.* Science, 1997. **277**(5324): p. 333-8.
17.   Wuertz, C.M., et al., *p63RhoGEF--a key mediator of angiotensin II-dependent signaling and processes in vascular smooth muscle cells.* Faseb j, 2010. **24**(12): p. 4865-76.
18.   Narumiya, S., M. Tanji, and T. Ishizaki, *Rho signaling, ROCK and mDia1, in transformation, metastasis and invasion.* Cancer Metastasis Rev, 2009. **28**(1-2): p. 65-76.
19.   Huelsenbeck, J., et al., *Cytoprotective effect of the small GTPase RhoB expressed upon treatment of fibroblasts with the Ras-glucosylating Clostridium sordellii lethal toxin.* FEBS Lett, 2012. **586**(20): p. 3665-73.
20.   Kwong, C.H., et al., *Regulation of the human neutrophil NADPH oxidase by rho-related G-proteins.* Biochemistry, 1993. **32**(21): p. 5711-7.
21.   Gomes, S.Z., et al., *Expression of NADPH oxidase by trophoblast cells: potential implications for the postimplanting mouse embryo.* Biol Reprod, 2012. **86**(2): p. 56.
22.   Gu, Y., Y. Zheng, and D.A. Williams, *RhoH GTPase: a key regulator of hematopoietic cell proliferation and apoptosis?* Cell Cycle, 2005. **4**(2): p. 201-2.

23.   Raftopoulou, M. and A. Hall, *Cell migration: Rho GTPases lead the way.* Dev Biol, 2004. **265**(1): p. 23-32.

24.   Chahdi, A. and J.P. Raufman, *The Cdc42/Rac nucleotide exchange factor protein beta1Pix (Pak-interacting exchange factor) modulates beta-catenin transcriptional activity in colon cancer cells: evidence for direct interaction of beta1PIX with beta-catenin.* J Biol Chem, 2013. **288**(47): p. 34019-29.

25.   Cuadrado, A., et al., *Transcription Factors NRF2 and NF-kappaB Are Coordinated Effectors of the Rho Family, GTP-binding Protein RAC1 during Inflammation.* J Biol Chem, 2014. **289**(22): p. 15244-15258.

26.   Miralles, F., et al., *Actin dynamics control SRF activity by regulation of its coactivator MAL.* Cell, 2003. **113**(3): p. 329-42.

27.   Boivin, D. and R. Beliveau, *Subcellular distribution and membrane association of Rho-related small GTP-binding proteins in kidney cortex.* Am J Physiol, 1995. **269**(2 Pt 2): p. F180-9.

28.   Madaule, P. and R. Axel, *A novel ras-related gene family.* Cell, 1985. **41**(1): p. 31-40.

29.   Yamamoto, K., et al., *Purification and characterization of a GTP-binding protein with a molecular weight of 20,000 in bovine brain membranes. Identification as the rho gene product.* J Biol Chem, 1988. **263**(20): p. 9926-32.

30.   Dias, S.M. and R.A. Cerione, *X-ray crystal structures reveal two activated states for RhoC.* Biochemistry, 2007. **46**(22): p. 6547-58.

31.   Chen, Z., et al., *Both farnesylated and geranylgeranylated RhoB inhibit malignant transformation and suppress human tumor growth in nude mice.* J Biol Chem, 2000. **275**(24): p. 17974-8.

32.   Zhao, Y., et al., *The role of RhoC in ovarian epithelial carcinoma: a marker for carcinogenesis, progression, prognosis, and target therapy.* Gynecol Oncol, 2013. **130**(3): p. 570-8.

33.   Koch, G., et al., *Role of Rho protein in lovastatin-induced breakdown of actin cytoskeleton.* J Pharmacol Exp Ther, 1997. **283**(2): p. 901-9.

34.   Wei, Y., et al., *Crystal structure of RhoA-GDP and its functional implications.* Nat Struct Biol, 1997. **4**(9): p. 699-703.

35.   Ihara, K., et al., *Crystal structure of human RhoA in a dominantly active form complexed with a GTP analogue.* J Biol Chem, 1998. **273**(16): p. 9656-66.

36.   Rossman, K.L., C.J. Der, and J. Sondek, *GEF means go: turning on RHO GTPases with guanine nucleotide-exchange factors.* Nat Rev Mol Cell Biol, 2005. **6**(2): p. 167-80.

37.   Xiang, S.Y., et al., *PLCepsilon, PKD1, and SSH1L transduce RhoA signaling to protect mitochondria from oxidative stress in the heart.* Sci Signal, 2013. **6**(306): p. ra108.

38.   Hirabayashi, T. and D. Saffen, *M1 muscarinic acetylcholine receptors activate zif268 gene expression via small G-protein Rho-dependent and lambda-independent pathways in PC12D cells.* Eur J Biochem, 2000. **267**(9): p. 2525-32.

39.   Walsh, C.T., D. Stupack, and J.H. Brown, *G protein-coupled receptors go extracellular: RhoA integrates the integrins.* Mol Interv, 2008. **8**(4): p. 165-73.

40.   Ritchie, B.J., et al., *Determinants at the N- and C-termini of Galpha12 required for activation of Rho-mediated signaling.* J Mol Signal, 2013. **8**(1): p. 3.

41.   Fukuhara, S., H. Chikumi, and J.S. Gutkind, *Leukemia-associated Rho guanine nucleotide exchange factor (LARG) links heterotrimeric G proteins of the G(12) family to Rho.* FEBS Lett, 2000. **485**(2-3): p. 183-8.

42.   Fukuhara, S., et al., *A novel PDZ domain containing guanine nucleotide exchange factor links heterotrimeric G proteins to Rho.* J Biol Chem, 1999. **274**(9): p. 5868-79.

43.   Hart, M.J., W. Roscoe, and G. Bollag, *Activation of Rho GEF activity by G alpha 13.* Methods Enzymol, 2000. **325**: p. 61-71.

44.   Momotani, K. and A.V. Somlyo, *p63RhoGEF: a new switch for G(q)-mediated activation of smooth muscle.* Trends Cardiovasc Med, 2012. **22**(5): p. 122-7.

45.   Kwon, A., et al., *SMURF1 plays a role in EGF-induced breast cancer cell migration and invasion.* Mol Cells, 2013. **36**(6): p. 548-55.

46.   Waheed, F., et al., *Central role of the exchange factor GEF-H1 in TNF-alpha-induced sequential activation of Rac, ADAM17/TACE, and RhoA in tubular epithelial cells.* Mol Biol Cell, 2013. **24**(7): p. 1068-82.

47.   Zhao, T.T., et al., *Lovastatin inhibits EGFR dimerization and AKT activation in squamous cell carcinoma cells: potential regulation by targeting rho proteins.* Oncogene, 2010. **29**(33): p. 4682-92.

48.   Balanis, N., et al., *beta3 integrin-EGF receptor cross-talk activates p190RhoGAP in mouse mammary gland epithelial cells.* Mol Biol Cell, 2011. **22**(22): p. 4288-301.

49.   Marcoux, N. and K. Vuori, *EGF receptor activity is essential for adhesion-induced stress fiber formation and cofilin phosphorylation.* Cell Signal, 2005. **17**(11): p. 1449-55.

50.   Ponik, S.M., et al., *RhoA is down-regulated at cell-cell contacts via p190RhoGAP-B in response to tensional homeostasis.* Mol Biol Cell, 2013. **24**(11): p. 1688-99, s1-3.

51.   Costa, P., et al., *Integrin-specific control of focal adhesion kinase and RhoA regulates membrane protrusion and invasion.* PLoS One, 2013. **8**(9): p. e74659.

52.   Anear, E. and R.W. Parish, *The effects of modifying RhoA and Rac1 activities on heterotypic contact inhibition of locomotion.* FEBS Lett, 2012. **586**(9): p. 1330-5.

53.   Lavall, D., et al., *The mineralocorticoid receptor promotes fibrotic remodeling in atrial fibrillation.* J Biol Chem, 2014. **289**(10): p. 6656-68.

54.   Paterson, H.F., et al., *Microinjection of recombinant p21rho induces rapid changes in cell morphology.* J Cell Biol, 1990. **111**(3): p. 1001-7.

55.   Kang, S., et al., *Dysfunction of vascular smooth muscle and vascular remodeling by simvastatin.* Toxicol Sci, 2014. **138**(2): p. 446-556.

56.   Maekawa, M., et al., *Signaling from Rho to the actin cytoskeleton through protein kinases ROCK and LIM-kinase.* Science, 1999. **285**(5429): p. 895-8.

57.   Lammers, M., et al., *Specificity of interactions between mDia isoforms and Rho proteins.* J Biol Chem, 2008. **283**(50): p. 35236-46.

58.   Hinz, B., et al., *Alpha-smooth muscle actin is crucial for focal adhesion maturation in myofibroblasts.* Mol Biol Cell, 2003. **14**(6): p. 2508-19.

59.   Lim, S.M., et al., *Extracellular matrix effect on RhoA signaling modulation in vascular smooth muscle cells.* Exp Cell Res, 2010. **316**(17): p. 2833-48.

60.   El-Sibai, M., et al., *RhoA/ROCK-mediated switching between Cdc42- and Rac1-dependent protrusion in MTLn3 carcinoma cells.* Exp Cell Res, 2008. **314**(7): p. 1540-52.

61.   Pettee, K.M., et al., *An mDia2/ROCK signaling axis regulates invasive egress from epithelial ovarian cancer spheroids.* PLoS One, 2014. **9**(2): p. e90371.

62.   Cao, J., et al., *Cortical actin dynamics facilitate early-stage centrosome separation.* Curr Biol, 2010. **20**(8): p. 770-6.

63.   Akhshi, T.K., D. Wernike, and A. Piekny, *Microtubules and actin crosstalk in cell migration and division.* Cytoskeleton (Hoboken), 2014. **71**(1): p. 1-23.

64.   Bartolini, F., N. Ramalingam, and G.G. Gundersen, *Actin-capping protein promotes microtubule stability by antagonizing the actin activity of mDia1.* Mol Biol Cell, 2012. **23**(20): p. 4032-40.

65.   Yoo, S.K., et al., *The role of microtubules in neutrophil polarity and migration in live zebrafish.* J Cell Sci, 2012. **125**(Pt 23): p. 5702-10.

66.   Asthana, J., et al., *Inhibition of HDAC6 deacetylase activity increases its binding with microtubules and suppresses microtubule dynamic instability in MCF-7 cells.* J Biol Chem, 2013. **288**(31): p. 22516-26.

67.   Ageta-Ishihara, N., et al., *Septins promote dendrite and axon development by negatively regulating microtubule stability via HDAC6-mediated deacetylation.* Nat Commun, 2013. **4**: p. 2532.

68.   ., W.J., *Rho GTPases at the crossroad of signaling networks in mammals: Impact of Rho-GTPases on microtubule organization and dynamics.* Small GTPases, 2014(5).

69.   Gundersen, G.G., et al., *Regulation of microtubules by Rho GTPases in migrating cells.* Novartis Found Symp, 2005. **269**: p. 106-16; discussion 116-26, 223-30.

70.   Palazzo, A.F., et al., *Localized stabilization of microtubules by integrin- and FAK-facilitated Rho signaling.* Science, 2004. **303**(5659): p. 836-9.

71.   Castro-Castro, A., et al., *ATAT1/MEC-17 acetyltransferase and HDAC6 deacetylase control a balance of acetylation of alpha-tubulin and cortactin and regulate MT1-MMP trafficking and breast tumor cell invasion.* Eur J Cell Biol, 2012. **91**(11-12): p. 950-60.

72.   Destaing, O., et al., *A novel Rho-mDia2-HDAC6 pathway controls podosome patterning through microtubule acetylation in osteoclasts.* J Cell Sci, 2005. **118**(Pt 13): p. 2901-11.

73.   Schofield, A.V., et al., *Tubulin polymerization promoting protein 1 (Tppp1) phosphorylation by Rho-associated coiled-coil kinase (rock) and cyclin-dependent kinase 1 (Cdk1) inhibits microtubule dynamics to increase cell proliferation.* J Biol Chem, 2013. **288**(11): p. 7907-17.

74.   Tsou, P.S., et al., *Cellular Mechanisms of Tissue Fibrosis. 8. Current and future drug targets in fibrosis: focusing on Rho GTPase regulated gene transcription.* Am J Physiol Cell Physiol, 2014.

75.   Arnaud, M., et al., *Interaction of the tyrosine phosphatase SHP-2 with Gab2 regulates Rho-dependent activation of the c-fos serum response element by interleukin-2.* Biochem J, 2004. **382**(Pt 2): p. 545-56.

76.   Tabuchi, A., et al., *Nuclear translocation of the SRF co-activator MAL in cortical neurons: role of RhoA signalling.* J Neurochem, 2005. **94**(1): p. 169-80.

77.   Machamer, C.E., *Accommodation of large cargo within Golgi cisternae.* Histochem Cell Biol, 2013. **140**(3): p. 261-9.

78.   Pathak, R. and C. Dermardirossian, *GEF-H1: orchestrating the interplay between cytoskeleton and vesicle trafficking.* Small GTPases, 2013. **4**(3): p. 174-9.

79.   Price, L.S., et al., *The small GTPases Rac and Rho as regulators of secretion in mast cells.* Curr Biol, 1995. **5**(1): p. 68-73.

80.   Mun, J.H., et al., *Simvastatin inhibits transforming growth factor-beta1-induced expression of type I collagen, CTGF, and alpha-SMA in keloid fibroblasts.* Wound Repair Regen, 2014. **22**(1): p. 125-33.

81.   Miklavc, P., et al., *Actin coating and compression of fused secretory vesicles are essential for surfactant secretion--a role for Rho, formins and myosin II.* J Cell Sci, 2012. **125**(Pt 11): p. 2765-74.

82.   Werner, M.E., et al., *Inversin modulates the cortical actin network during mitosis.* Am J Physiol Cell Physiol, 2013. **305**(1): p. C36-47.

83.   Pathak, R., et al., *The microtubule-associated Rho activating factor GEF-H1 interacts with exocyst complex to regulate vesicle traffic.* Dev Cell, 2012. **23**(2): p. 397-411.

84.   Uchinaka, A., et al., *Tissue inhibitor of metalloproteinase-1 and -3 improve cardiac function in an ischemic cardiomyopathy model rat.* Tissue Eng Part A, 2014.

85.   Turner, N.A., et al., *Simvastatin inhibits TNFalpha-induced invasion of human cardiac myofibroblasts via both MMP-9-dependent and -independent mechanisms.* J Mol Cell Cardiol, 2007. **43**(2): p. 168-76.

86.   Mehner, C., et al., *Tumor cell-produced matrix metalloproteinase 9 (MMP-9) drives malignant progression and metastasis of basal-like triple negative breast cancer.* Oncotarget, 2014.

87.   Xue, F., et al., *Blockade of Rho/Rho-associated coiled coil-forming kinase signaling can prevent progression of hepatocellular carcinoma in matrix metalloproteinase-dependent manner.* Hepatol Res, 2008. **38**(8): p. 810-7.

88.   Solinet, S., et al., *The actin-binding ERM protein Moesin binds to and stabilizes microtubules at the cell cortex.* J Cell Biol, 2013. **202**(2): p. 251-60.

89.   Yuce, O., A. Piekny, and M. Glotzer, *An ECT2-centralspindlin complex regulates the localization and function of RhoA.* J Cell Biol, 2005. **170**(4): p. 571-82.

90.   Nishimura, Y. and S. Yonemura, *Centralspindlin regulates ECT2 and RhoA accumulation at the equatorial cortex during cytokinesis.* J Cell Sci, 2006. **119**(Pt 1): p. 104-14.

91.   Rosenblatt, J., et al., *Myosin II-dependent cortical movement is required for centrosome separation and positioning during mitotic spindle assembly.* Cell, 2004. **117**(3): p. 361-72.

92.   Bement, W.M., H.A. Benink, and G. von Dassow, *A microtubule-dependent zone of active RhoA during cleavage plane specification.* J Cell Biol, 2005. **170**(1): p. 91-101.

93.   Porter, K.E., et al., *Simvastatin reduces human atrial myofibroblast proliferation independently of cholesterol lowering via inhibition of RhoA.* Cardiovasc Res, 2004. **61**(4): p. 745-55.

94.   Phrommintikul, A., et al., *Effects of a Rho kinase inhibitor on pressure overload induced cardiac hypertrophy and associated diastolic dysfunction.* Am J Physiol Heart Circ Physiol, 2008. **294**(4): p. H1804-14.

95.   Chevalier, L., et al., *Athlete's heart patterns in elite rugby players: effects of training specificities.* Arch Cardiovasc Dis, 2013. **106**(2): p. 72-8.

96.   Li, J., et al., *New frontiers in heart hypertrophy during pregnancy.* Am J Cardiovasc Dis, 2012. **2**(3): p. 192-207.

97.   Guellich, A., H. Mehel, and R. Fischmeister, *Cyclic AMP synthesis and hydrolysis in the normal and failing heart.* Pflugers Arch, 2014. **466**(6): p. 1163-75.

98.   Waterbolk, T.W., et al., *Pulmonary valve replacement with a mechanical prosthesis. Promising results of 28 procedures in patients with congenital heart disease.* Eur J Cardiothorac Surg, 2006. **30**(1): p. 28-32.

99.   Sabbah, H.N., et al., *Effects of ACE inhibition and beta-blockade on skeletal muscle fiber types in dogs with moderate heart failure.* Am J Physiol, 1996. **270**(1 Pt 2): p. H115-20.

100.   Kuwahara, K., T. Nishikimi, and K. Nakao, *Transcriptional regulation of the fetal cardiac gene program.* J Pharmacol Sci, 2012. **119**(3): p. 198-203.

101.   Buyon, J.P. and R.M. Clancy, *From antibody insult to fibrosis in neonatal lupus - the heart of the matter.* Arthritis Res Ther, 2003. **5**(6): p. 266-70.

102.   Lu, D. and P.A. Insel, *Cellular Mechanisms of Tissue Fibrosis. 6. Purinergic signaling and response in fibroblasts and tissue fibrosis.* Am J Physiol Cell Physiol, 2014. **306**(9): p. C779-88.

103.   Krenning, G., E.M. Zeisberg, and R. Kalluri, *The origin of fibroblasts and mechanism of cardiac fibrosis.* J Cell Physiol, 2010. **225**(3): p. 631-7.

104.   Naito, H., et al., *Optimizing engineered heart tissue for therapeutic applications as surrogate heart muscle.* Circulation, 2006. **114**(1 Suppl): p. I72-8.

105.   Boyer, A.S., et al., *TGFbeta2 and TGFbeta3 have separate and sequential activities during epithelial-mesenchymal cell transformation in the embryonic heart.* Dev Biol, 1999. **208**(2): p. 530-45.

106.   Lei, P.P., et al., *Fibrocytes are associated with the fibrosis of coronary heart disease.* Pathol Res Pract, 2013. **209**(1): p. 36-43.

107.   Chang, H.Y., et al., *Diversity, topographic differentiation, and positional memory in human fibroblasts.* Proc Natl Acad Sci U S A, 2002. **99**(20): p. 12877-82.

108.   Kanekar, S., et al., *Cardiac Fibroblasts: Form and Function.* Cardiovascular Pathology, 1998. **7**(3): p. 127-133.

109.   Lindner, D., et al., *Differential expression of matrix metalloproteases in human fibroblasts with different origins.* Biochem Res Int, 2012. **2012**: p. 875742.

110.   Camelliti, P., et al., *Fibroblast network in rabbit sinoatrial node: structural and functional identification of homogeneous and heterogeneous cell coupling.* Circ Res, 2004. **94**(6): p. 828-35.

111.   Reed, R.K., et al., *Blockade of beta 1-integrins in skin causes edema through lowering of interstitial fluid pressure.* Circ Res, 1992. **71**(4): p. 978-83.

112.   Zhan, H. and L. Xia, *Excitation-contraction coupling between human atrial myocytes with fibroblasts and stretch activated channel current: a simulation study.* Comput Math Methods Med, 2013. **2013**: p. 238676.

113.   Zhan, H.Q., et al., *Fibroblast proliferation alters cardiac excitation conduction and contraction: a computational study.* J Zhejiang Univ Sci B, 2014. **15**(3): p. 225-42.

7.   Literature

114.   Hou, L., B. Hu, and J. Jalife, *Genetically engineered excitable cardiac myofibroblasts coupled to cardiomyocytes rescue normal propagation and reduce arrhythmia complexity in heterocellular monolayers.* PLoS One, 2013. **8**(2): p. e55400.

115.   Ikeuchi, M., et al., *Inhibition of TGF-beta signaling exacerbates early cardiac dysfunction but prevents late remodeling after infarction.* Cardiovasc Res, 2004. **64**(3): p. 526-35.

116.   Ying, Z., et al., *Angiotensin II up-regulates the leukemia-associated Rho guanine nucleotide exchange factor (RhoGEF), a regulator of G protein signaling domain-containing RhoGEF, in vascular smooth muscle cells.* Mol Pharmacol, 2006. **69**(3): p. 932-40.

117.   McDowell, K.S., et al., *Susceptibility to arrhythmia in the infarcted heart depends on myofibroblast density.* Biophys J, 2011. **101**(6): p. 1307-15.

118.   Zhou, B. and W.T. Pu, *Epicardial epithelial-to-mesenchymal transition in injured heart.* J Cell Mol Med, 2011. **15**(12): p. 2781-3.

119.   Barresi, V., et al., *Immuno-expression of endoglin and smooth muscle actin in the vessels of brain metastases. Is there a rational for anti-angiogenic therapy?* Int J Mol Sci, 2014. **15**(4): p. 5663-79.

120.   He, J. and H.E. Bazan, *Epidermal growth factor synergism with TGF-beta1 via PI-3 kinase activity in corneal keratocyte differentiation.* Invest Ophthalmol Vis Sci, 2008. **49**(7): p. 2936-45.

121.   Miyasato, S.K., et al., *Caveolin-1 modulates TGF-beta1 signaling in cardiac remodeling.* Matrix Biol, 2011. **30**(5-6): p. 318-29.

122.   Sun, Y., et al., *Cardiac remodeling by fibrous tissue after infarction in rats.* Journal of Laboratory and Clinical Medicine, 2000. **135**(4): p. 316-323.

123.   Christia, P., et al., *Systematic characterization of myocardial inflammation, repair, and remodeling in a mouse model of reperfused myocardial infarction.* J Histochem Cytochem, 2013. **61**(8): p. 555-70.

124.   Kapoun, A.M., et al., *B-type natriuretic peptide exerts broad functional opposition to transforming growth factor-beta in primary human cardiac fibroblasts: fibrosis, myofibroblast conversion, proliferation, and inflammation.* Circ Res, 2004. **94**(4): p. 453-61.

125.   Porter, K.E., et al., *Tumor necrosis factor alpha induces human atrial myofibroblast proliferation, invasion and MMP-9 secretion: inhibition by simvastatin.* Cardiovasc Res, 2004. **64**(3): p. 507-15.

126.   Fredj, S., et al., *Role of interleukin-6 in cardiomyocyte/cardiac fibroblast interactions during myocyte hypertrophy and fibroblast proliferation.* J Cell Physiol, 2005. **204**(2): p. 428-36.

127.   Segura, A.M., O.H. Frazier, and L.M. Buja, *Fibrosis and heart failure.* Heart Fail Rev, 2014. **19**(2): p. 173-85.

128.   Bassett, E.G. and J.S. Wakefield, *Elastic fibers in myocardial scars in rats: development teraction with other components.* Connect Tissue Res, 2008. **49**(5): p. 321-7.

129.   Takemura, G., et al., *Role of apoptosis in the disappearance of infiltrated and proliferated interstitial cells after myocardial infarction.* Circ Res, 1998. **82**(11): p. 1130-8.

130.   Aoki, H., S. Izumo, and J. Sadoshima, *Angiotensin II activates RhoA in cardiac myocytes: a critical role of RhoA in angiotensin II-induced premyofibril formation.* Circ Res, 1998. **82**(6): p. 666-76.

131.   Boer, C., et al., *RhoA/Rho kinase and nitric oxide modulate the agonist-induced pulmonary artery diameter response time.* Am J Physiol Heart Circ Physiol, 2002. **282**(3): p. H990-8.

132.   Hunter, J.C., et al., *Nitric oxide inhibits endothelin-1-induced neonatal cardiomyocyte hypertrophy via a RhoA-ROCK-dependent pathway.* J Mol Cell Cardiol, 2009. **47**(6): p. 810-8.

133.   Kuwahara, K., et al., *The effects of the selective ROCK inhibitor, Y27632, on ET-1-induced hypertrophic response in neonatal rat cardiac myocytes--possible*

involvement of Rho/ROCK pathway in cardiac muscle cell hypertrophy. FEBS Lett, 1999. **452**(3): p. 314-8.

134. Sah, V.P., et al., *Cardiac-specific overexpression of RhoA results in sinus and atrioventricular nodal dysfunction and contractile failure.* J Clin Invest, 1999. **103**(12): p. 1627-34.

135. Takefuji, M., et al., *RhoGEF12 controls cardiac remodeling by integrating G protein- and integrin-dependent signaling cascades.* J Exp Med, 2013. **210**(4): p. 665-73.

136. Lin, G., et al., *Acute inhibition of Rho-kinase improves cardiac contractile function in streptozotocin-diabetic rats.* Cardiovasc Res, 2007. **75**(1): p. 51-8.

137. Satoh, S., et al., *Chronic inhibition of Rho kinase blunts the process of left ventricular hypertrophy leading to cardiac contractile dysfunction in hypertension-induced heart failure.* J Mol Cell Cardiol, 2003. **35**(1): p. 59-70.

138. Zou, C., et al., *Simvastatin activates the PPARgamma-dependent pathway to prevent left ventricular hypertrophy associated with inhibition of RhoA signaling.* Tex Heart Inst J, 2013. **40**(2): p. 140-7.

139. Li, Q., et al., *Inhibition of Rho-kinase ameliorates myocardial remodeling and fibrosis in pressure overload and myocardial infarction: role of TGF-beta1-TAK1.* Toxicol Lett, 2012. **211**(2): p. 91-7.

140. Del Re, D.P., S. Miyamoto, and J.H. Brown, *RhoA/Rho kinase up-regulate Bax to activate a mitochondrial death pathway and induce cardiomyocyte apoptosis.* J Biol Chem, 2007. **282**(11): p. 8069-78.

141. Rikitake, Y., et al., *Decreased perivascular fibrosis but not cardiac hypertrophy in ROCK1+/- haploinsufficient mice.* Circulation, 2005. **112**(19): p. 2959-65.

142. Okamoto, R., et al., *FHL2 prevents cardiac hypertrophy in mice with cardiac-specific deletion of ROCK2.* Faseb j, 2013. **27**(4): p. 1439-49.

143. Wei, L., et al., *Disruption of Rho signaling results in progressive atrioventricular conduction defects while ventricular function remains preserved.* Faseb j, 2004. **18**(7): p. 857-9.

144. Xiang, S.Y., et al., *RhoA protects the mouse heart against ischemia/reperfusion injury.* J Clin Invest, 2011. **121**(8): p. 3269-76.

145. Nasri, M., A. Karimi, and M. Allahbakhshian Farsani, *Production, purification and titration of a lentivirus-based vector for gene delivery purposes.* Cytotechnology, 2014.

146. Goto, T., M. Nakai, and K. Ikuta, *The life-cycle of human immunodeficiency virus type 1.* Micron, 1998. **29**(2–3): p. 123-138.

147. Szilluweit, R., et al., *HIV-1 Nef perturbs artificial membranes: investigation of the contribution of the myristoyl anchor.* Biophys J, 2009. **96**(8): p. 3242-50.

148. Boll, A., et al., *Mechanistic insights into the translocation of full length HIV-1 Tat across lipid membranes.* Biochim Biophys Acta, 2011. **1808**(11): p. 2685-93.

149. Riedl, J., et al., *Lifeact: a versatile marker to visualize F-actin.* Nat Methods, 2008. **5**(7): p. 605-7.

150. Krohn, R.I., *The colorimetric detection and quantitation of total protein.* Curr Protoc Cell Biol, 2011. **Appendix 3**: p. 3h.

151. Thakur, S., L. Li, and S. Gupta, *NF-kappaB-Mediated Integrin-Linked Kinase Regulation in Angiotensin II-Induced Pro-fibrotic Process in Cardiac Fibroblasts.* Life Sci, 2014.

152. Malek, A.M., et al., *Hypertonicity triggers RhoA-dependent assembly of myosin-containing striated polygonal actin networks in endothelial cells.* Am J Physiol Cell Physiol, 2007. **292**(5): p. C1645-59.

153. Entcheva, E. and H. Bien, *Mechanical and spatial determinants of cytoskeletal geodesic dome formation in cardiac fibroblasts.* Integr Biol (Camb), 2009. **1**(2): p. 212-9.

154. Simmel, S.S., P.C. Nickels, and T. Liedl, *Wireframe and Tensegrity DNA Nanostructures.* Acc Chem Res, 2014.

155. Arthur, W.T. and K. Burridge, *RhoA inactivation by p190RhoGAP regulates cell spreading and migration by promoting membrane protrusion and polarity.* Mol Biol Cell, 2001. **12**(9): p. 2711-20.

156. Harvey, K.A., et al., *Diverse signaling pathways regulate fibroblast differentiation and transformation through Rho kinase activation.* J Cell Physiol, 2007. **211**(2): p. 353-63.

157. Davis, J. and J.D. Molkentin, *Myofibroblasts: Trust your heart and let fate decide.* J Mol Cell Cardiol, 2014. **70c**: p. 9-18.

158. Driesen, R.B., et al., *Reversible and irreversible differentiation of cardiac fibroblasts.* Cardiovasc Res, 2014. **101**(3): p. 411-22.

159. Watson, C.J., et al., *Hypoxia-induced epigenetic modifications are associated with cardiac tissue fibrosis and the development of a myofibroblast-like phenotype.* Hum Mol Genet, 2014. **23**(8): p. 2176-88.

160. Copaja, M., et al., *Simvastatin induces apoptosis by a Rho-dependent mechanism in cultured cardiac fibroblasts and myofibroblasts.* Toxicol Appl Pharmacol, 2011. **255**(1): p. 57-64.

161. Hinz, B., et al., *Alpha-smooth muscle actin expression upregulates fibroblast contractile activity.* Mol Biol Cell, 2001. **12**(9): p. 2730-41.

162. Shimazaki, M., et al., *Periostin is essential for cardiac healing after acute myocardial infarction.* J Exp Med, 2008. **205**(2): p. 295-303.

163. Kato, K., et al., *The inositol 5-phosphatase SHIP2 is an effector of RhoA and is involved in cell polarity and migration.* Mol Biol Cell, 2012. **23**(13): p. 2593-604.

164. Yu, D., et al., *Murine missing in metastasis (MIM) mediates cell polarity and regulates the motility response to growth factors.* PLoS One, 2011. **6**(6): p. e20845.

165. Goulimari, P., et al., *LARG and mDia1 link Galpha12/13 to cell polarity and microtubule dynamics.* Mol Biol Cell, 2008. **19**(1): p. 30-40.

166. Buonomo, R., et al., *PED/PEA-15 controls fibroblast motility and wound closure by ERK1/2-dependent mechanisms.* J Cell Physiol, 2012. **227**(5): p. 2106-16.

167. Azuma, K., et al., *Association of estrogen receptor alpha and histone deacetylase 6 causes rapid deacetylation of tubulin in breast cancer cells.* Cancer Res, 2009. **69**(7): p. 2935-40.

168. Aguilar, A., et al., *alpha-Tubulin K40 Acetylation is Required for Contact Inhibition of Proliferation and Cell-Substrate Adhesion.* Mol Biol Cell, 2014.

169. Yi, X., et al., *Hepatocyte growth factor regulates the TGFbeta1induced proliferation, differentiation and secretory function of cardiac fibroblasts.* Int J Mol Med, 2014.

170. Schofield, A.V., R. Steel, and O. Bernard, *Rho-associated coiled-coil kinase (ROCK) protein controls microtubule dynamics in a novel signaling pathway that regulates cell migration.* J Biol Chem, 2012. **287**(52): p. 43620-9.

171. Rucker-Martin, C., et al., *Dedifferentiation of atrial myocytes during atrial fibrillation: role of fibroblast proliferation in vitro.* Cardiovasc Res, 2002. **55**(1): p. 38-52.

172. Zhang, D., et al., *Activation of histone deacetylase-6 induces contractile dysfunction through derailment of alpha-tubulin proteostasis in experimental and human atrial fibrillation.* Circulation, 2014. **129**(3): p. 346-58.

173. Haak, A.J., et al., *Targeting the myofibroblast genetic switch: inhibitors of myocardin-related transcription factor/serum response factor-regulated gene transcription prevent fibrosis in a murine model of skin injury.* J Pharmacol Exp Ther, 2014. **349**(3): p. 480-6.

174. Chen, Y., et al., *Connective tissue growth factor is secreted through the Golgi and is degraded in the endosome.* Exp Cell Res, 2001. **271**(1): p. 109-17.

175. Camera, P., et al., *Citron-N is a neuronal Rho-associated protein involved in Golgi organization through actin cytoskeleton regulation.* Nat Cell Biol, 2003. **5**(12): p. 1071-8.

176. Lazaro-Dieguez, F., et al., *Dynamics of an F-actin aggresome generated by the actin-stabilizing toxin jasplakinolide.* J Cell Sci, 2008. **121**(Pt 9): p. 1415-25.

177. Zilberman, Y., et al., *Involvement of the Rho-mDia1 pathway in the regulation of Golgi complex architecture and dynamics.* Mol Biol Cell, 2011. **22**(16): p. 2900-11.

178.   Ng, M.M., et al., *GOLPH3L antagonizes GOLPH3 to determine Golgi morphology.* Mol Biol Cell, 2013. **24**(6): p. 796-808.

179.   Campbell, S.E. and L.C. Katwa, *Angiotensin II stimulated expression of transforming growth factor-beta1 in cardiac fibroblasts and myofibroblasts.* J Mol Cell Cardiol, 1997. **29**(7): p. 1947-58.

180.   Lee, S.W., et al., *Snail as a potential target molecule in cardiac fibrosis: paracrine action of endothelial cells on fibroblasts through snail and CTGF axis.* Mol Ther, 2013. **21**(9): p. 1767-77.

181.   Koitabashi, N., et al., *Increased connective tissue growth factor relative to brain natriuretic peptide as a determinant of myocardial fibrosis.* Hypertension, 2007. **49**(5): p. 1120-7.

182.   Moe, I.T., et al., *CCN2 exerts direct cytoprotective actions in adult cardiac myocytes by activation of the PI3-kinase/Akt/GSK-3beta signaling pathway.* J Cell Commun Signal, 2013. **7**(1): p. 31-47.

183.   Muhlhauser, U., et al., *Atorvastatin desensitizes beta-adrenergic signaling in cardiac myocytes via reduced isoprenylation of G-protein gamma-subunits.* Faseb j, 2006. **20**(6): p. 785-7.

184.   Hayata, N., et al., *Connective tissue growth factor induces cardiac hypertrophy through Akt signaling.* Biochem Biophys Res Commun, 2008. **370**(2): p. 274-8.

185.   Abrial, M., et al., *Cardiac fibroblasts protect cardiomyocytes against lethal ischemia-reperfusion injury.* J Mol Cell Cardiol, 2014. **68**: p. 56-65.